Energy and Power Management of Hybrid Renewable Energy Systems for Remote Communities

by

Roshani Dilrukshi Peiris Kaluthanthrige

A Thesis submitted to the Faculty of Graduate Studies of
The University of Manitoba
in partial fulfillment of the requirements of the degree of

DOCTOR OF PHILOSOPHY

Department of Electrical and Computer Engineering
University of Manitoba
Winnipeg, Manitoba, Canada

Abstract

Incorporation of renewable sources and energy storage can contribute to reduce fuel consumption in diesel generation-based remote off-grid power systems. This thesis proposes methodologies for improved management of available generating and storage resources to reduce costs and emissions and investigates the coordination of energy management with power management functions essential for stable operation of the isolated power systems.

Firstly, a test system is developed considering a case of retrofitting an existing diesel power system with photovoltaic (PV) generation and battery energy storage. A sizing study conducted using HOMER software with weather and load data for Northern Canada resulted in a PV-Diesel-Battery topology with high PV penetration levels. Next, the energy management functions are developed incrementally in three steps. First, a computationally efficient energy management system (EMS) is implemented to optimize the system operation while incorporating multiple operational requirements essential to remote power systems. Then, a demand response (DR) model that requires minimal bi-directional interactions and therefore implementable without sophisticated communication infrastructure is developed and integrated with the EMS. Thirdly, a computationally efficient two-stage model predictive control process is developed to compensate for forecast uncertainties. Finally, the power management functions necessary to achieve a logical real-time operation are implemented and coordinated with the energy management functions in a hierarchical architecture. Also, an operation evaluation framework is suggested to assess the viability of the optimum operation routines under dynamic conditions.

After adding PV and energy storage to an existing diesel-only system and optimizing the operation with the DR integrated EMS, over 60% cost and emission reductions are achieved for a representative summer day compared to the diesel-only operation. The cost and emission reductions achieved for a representative winter day are 31% and 11%, respectively. During the intra-day operation, the proposed uncertainty management framework navigates the system judiciously and achieves cost and emission performance closer to that is obtainable when perfect forecast information is available in a

computationally efficient manner. Numerous tests verify the correct operation of the proposed power management strategies and the utility of the operation evaluation framework while demonstrating the importance of coordination of the energy and power management functions.

Use of Copyrighted Material

I like to confirm the approval from all the authors and hereby acknowledge the use of the following publications during the preparation of this thesis. Only the contents of the publications where I am the first author are included in this thesis.

Publications in Elsevier Journals

- **R. Kaluthanthrige** and A. D. Rajapakse, “Two-stage framework for optimizing the operation of remote off-grid power systems under uncertainties,” Int. J. Electr. Power Energy Syst., vol. 135, p. 107553, 2022, doi: https://doi.org/10.1016/j.ijepes.2021.107553.
- **R. Kaluthanthrige** and A. D. Rajapakse, “Evaluation of hierarchical controls to manage power, energy and daily operation of remote off-grid power systems,” *Appl. Energy*, vol. 299, no. June, p. 117259, 2021, doi: 10.1016/j.apenergy.2021.117259.
- **R. Kaluthanthrige** and A. D. Rajapakse, “Demand response integrated day-ahead energy management strategy for remote off-grid hybrid renewable energy systems,” *Int. J. Electr. Power Energy Syst.*, vol. 129, no. February, p. 106731, 2021, doi: 10.1016/j.ijepes.2020.106731.

Publication in Technology and Economics of Smart Grids and Sustainable Energy

- **R. Kaluthanthrige**, A. D. Rajapakse, C. Lamothe, and F. Mosallat, “Optimal Sizing and Performance Evaluation of a Hybrid Renewable Energy System for an Off-Grid Power System in Northern Canada,” *Technol. Econ. Smart Grids Sustain. Energy*, vol. 4, no. 1, pp. 24–26, 2019, doi: 10.1007/s40866-019-0061-5.

Publications in IEEE Conferences

- **R. Kaluthanthrige** and A. D. Rajapakse, "Operational Optimization of a Remote Off-Grid Hybrid Renewable Energy System in Northern Canada," *2019 IEEE 7th International Conference on Smart Energy Grid Engineering (SEGE)*, Oshawa, ON, Canada, 2019, pp. 268-273, doi: 10.1109/SEGE.2019.8859885.
- **R. Kaluthanthrige** and A. D. Rajapakse, "Use of Probabilistic Fuzzy Inference Systems to Model Demand Response in the Off-grid Power Systems of Northern

Canada," *2019 14th Conference on Industrial and Information Systems (ICIIS)*, Kandy, Sri Lanka, 2019, pp. 419-424, doi: 10.1109/ICIIS47346.2019.9063281.

Elsevier copyright policy:

"Authors can use their articles, in full or in part, for a wide range of scholarly, non-commercial purposes as outlined below:

- Use by an author in the author's classroom teaching (including distribution of copies, paper or electronic)
- Distribution of copies (including through e-mail) to known research colleagues for their personal use (but not for Commercial Use)
- **Inclusion in a thesis or dissertation (provided that this is not to be published commercially)**
- Use in a subsequent compilation of the author's works
- Extending the Article to book-length form
- Preparation of other derivative works (but not for Commercial Use)
- Otherwise, using or re-using portions or excerpts in other works

These rights apply to all Elsevier authors who publish their article as either a subscription article or an open-access article. In all cases, we require that all Elsevier authors always include a full acknowledgement and, if appropriate, a link to the final published version hosted on Science Direct."

Springer copyright policy:

"**Authors have the right to reuse their article's Version of Record, in whole or in part, in their own thesis.** Additionally, they may reproduce and make available their thesis, including Springer Nature content, as required by their awarding academic institution. Authors must properly cite the published article in their thesis according to current citation standards.
Material from: 'AUTHOR, TITLE, JOURNAL TITLE, published [YEAR], [publisher - as it appears on our copyright page]'"

IEEE copyright policy:

"**You may reuse your published article in your thesis or dissertation without requesting permission, provided that you fulfill the following requirements depending on which aspects of the article you wish to reuse.**

- Text excerpts: Provide the full citation of the original published article followed by the IEEE copyright line: © 20XX IEEE. If you are reusing a substantial portion of your article and you are not the senior author, obtain the senior author's approval before reusing the text.
- Graphics and tables: The IEEE copyright line (© 20XX IEEE) should appear with each reprinted graphic and table.
- Full text article: Include the following copyright notice in the references: "© 20XX IEEE. Reprinted, with permission, from [full citation of original published article].""

Acknowledgments

I would like to express my deepest gratitude to my advisor, Dr. Athula Rajapakse, for his invaluable guidance and encouragement during all stages of my graduate student life. I also wish to express my sincere gratitude to the examining committee members, Dr. Dharshana Muthumuni, Dr. Ngai Man (Carl) Ho, and Dr. Eric Bibeau as well as the external examiner Dr. Kankar Bhattacharya for their helpful comments and feedback which contributed to greatly improve the quality of the thesis.

I would like to acknowledge the financial support and valuable opportunities received through the NSERC CREATE: Sustainable Engineering in Remote Areas (SERA) program, NSERC Engage program, Research Manitoba program, and University of Manitoba in accomplishing my research goals. I also wish to express my deepest gratitude to the staff of Manitoba Hydro International and Solar Solutions Inc. who helped me in acquiring experience related to different aspects of Engineering and beyond. I also express my gratitude to all academic, administrative, and technical staff at the Department of Electrical and Computer Engineering for their assistance. Also, I like to acknowledge and thank all members of the power systems research group for their continuous support and encouragement.

Last but not least, I like to extend my deepest appreciation and respect to my beloved parents and my loving husband for being there for me always.

Roshani Kaluthanthrige

January 2022

Dedication

To my beloved mother, father, and husband.

Contents

List of Tables

List of Figures

List of Abbreviations

ANN	Artificial Neural Network
BESS	Battery Energy Storage System
CC	Cycle Charging
CPM	Consumer Price Model
CRM	Consumer Responsiveness Model
DER	Distributed Energy Resource
DOD	Depth of Discharge
DOM	Degree of Membership
DR	Demand Response
DRM	Demand Response Model
ECS	Energy Consumption Scheduler
EMPC	Economic Model Predictive Controller
EMS	Energy Management System
EMT	Electromagnetic Transients
EWH	Electric Water Heater
FDL	Final Decision Logic
GA	Genetic Algorithm
GAMS	General Algebraic Modeling System
HAN	Home Area Network
HEMS	Home Energy Management System
HOMER	Hybrid Optimization Model for Electric Renewables
HRES	Hybrid Renewable Energy System
IRR	Internal Rate of Return
LCOE	Levelized Cost of Electricity
LCS	Load Consumption Scheduler
LF	Load Following
MPC	Model Predictive Control

MPPT	Maximum Power Point Tracking
NPC	Net Present Cost
O&M	Operation and Maintenance
OMF	Output Membership Function
OPU	Operation Planning Unit
PDF	Probability Distribution Function
PFIS	Probabilistic Fuzzy Inference System
PLL	Phase Locked Loop
PMS	Power Management System
PSO	Particle Swarm Optimization
PV	Photovoltaic
PWM	Pulse Width Modulation
RAPSIM	Remote Area Power Supply Simulator
RF	Renewable Fraction
ROI	Return on Investment
RWS	Roulette Wheel Selection
SOC	State of Charge
SPP	Simple Payback Period
STC	Standard Test Conditions
VSC	Voltage Source Converter

Chapter 1

Introduction

1.1 Background

Many remote communities in the world are still served by off-grid power systems which rely on diesel as their primary energy resource [1]–[3]. Development of these remote territories, often characterized with limited accessibility, harsh weather conditions, or difficult terrains, has been impeded by several economic, environmental, and social constraints arising from the high reliance on diesel [1]–[3]. Increasing fuel prices and the adverse effects of increased carbon footprint have shifted the energy policies to favor more environmentally healthy approaches [4]. Renewable electricity, renewable heat, energy efficiency measures, and grid connections can be identified as few of the environmentally friendly pathways for diesel-reduction in these remote power systems [2]. The focus of this research is on the role of renewable electricity in the diesel reduction progress.

Among the available renewable electricity generation methods, intermittent sources such as solar photovoltaic (PV) and wind is gradually gaining a higher share over the past years [2]. When integrated with dispatchable storage technologies, they have emerged as viable candidates to compete with the conventional diesel-only generation facilities. However, given the remoteness and harsh weather conditions experienced by these remote power systems, system planners are advocating the availability of conventional generation infrastructure such as diesel units to ensure the reliability and continuity of energy supply [5]–[7]. Hence, the “Hybrid Renewable Energy Systems (HRESs)” discussed in this thesis will be devised with an energy mix having both conventional and renewable energy sources. An example of a typical HRES configuration is schematically shown in Figure

1.1. The conventional source in remote power systems is typically a diesel plant and the common renewable sources are solar PV, wind, small-hydro, or biomass generation. Energy storage is optional and may be integrated with a renewable source such as solar PV.

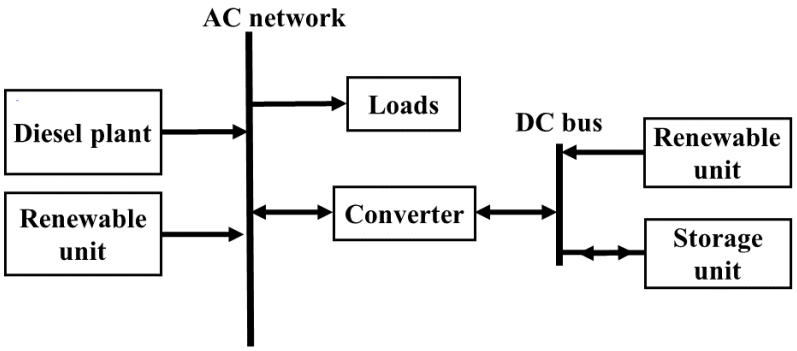

Figure 1.1 An example HRES configuration

Integration of significant amounts of intermittent, non-dispatchable, and inverter-interfaced resources to these smaller and weaker off-grid power systems can impose several challenges extending from the supervisory-level energy management to the system-level controls during actual deployment [8], [9]. Failure to properly integrate, manage, and control the available resources can result in economic losses, increased emissions, generation curtailment, load shedding, and even eventual infeasibility [9]. Therefore, the need of energy and power management become imperative to maximize the envisioned benefits while operating the power system in a secure, reliable, environmentally friendly, and cost-effective manner.

As the required control functions have different levels of criticalities, often a hierarchical control architecture is proposed to effectively integrate energy management and power management strategies to the system operation [10], [11]. A high-level representation of this control hierarchy is shown in Figure 1.2. The energy and power management controls are generally deployed to the tertiary (supervisory-level) and secondary (local-level) control layers, respectively, to provide references for the primary (unit-level) controls implemented at each system component [10], [12]. The respective response time scales of different control levels are also indicated on Figure 1.2. Specific functionalities of the energy management and power management control layers will be

introduced in the following sub-sections while highlighting the identified areas for improvement.

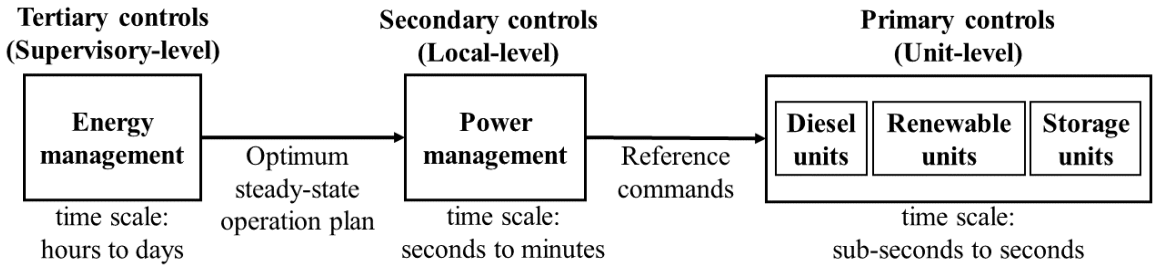

Figure 1.2 High-level control architecture of a remote power system

1.2 Energy Management

1.2.1 Energy management systems

To optimally integrate the intermittent renewable resources, specially under high penetration levels, energy management in both day-ahead and intra-day control horizons are being explored in the existing studies [9]. This task is further complicated in the presence of many supply and storage systems with different operational constraints. Once the load and resource forecasts are obtained, the primary role of a Energy Management System (EMS) is to attain a quantitative optimality over a pre-specified control horizon by either minimizing or maximizing a set of quantitative objectives such as cost reduction, loss reduction, emission reduction, improved utilization of renewable sources etc. [13], [14]. As shown in Figure 1.2, energy management is usually implemented as a supervisory-level control function. The existing energy management studies usually deploy mathematical models and rule-based control algorithms whereas the system variables are usually represented as averaged values [14]. Such problem formulation methods are effective in identifying the best candidates from a wide array of possibilities for longer control horizons, typically expanding hours to days.

While some interesting work has been carried out in this area, there are many more aspects to explore when deploying them in remote off-grid power systems, especially in

simplifying the problem formulation and including operational requirements related to remote power systems.

1.2.2 Integration of demand response strategies

Energy management systems can be combined with Demand Response (DR) strategies to add value for the energy providers and the consumers by modifying the electricity demand [15]. DR accommodates judicious interactions between the utility and the consumers and provides an extra degree of freedom for the energy management task.

When energy management is combined with DR, the accurate estimation of the modified load curve for a given incentive is crucial in arriving at realistic conclusions. Therefore, these schemes mostly use smart metering, advanced communication platforms, and Home Energy Management Systems (HEMSs) as essential technical drivers to estimate the modified load curve for a contracted incentive [16]–[18]. Also, in contexts where HEMSs are scarcely available, utility side depends on frequent consumer interactions to estimate changes to the load curve. Based on the targeted market model, these problems are mostly formulated as utility maximizations or as cost minimizations. The adopted solution methodologies highly rely upon the two-way interactive communication process either performed in day-ahead or intra-day time frames [16], [17].

Although these schemes that require frequent automated or human-in-the-loop bi-directional communication may work in urban settings, they are too complicated for practical implementation in a remote community where most of the electricity consumers fall into the residential category. Moreover, the investment on advanced control architecture in individual households may not be justifiable considering the limited load options available to participate in DR schemes both in variety and magnitude. If a DR scheme is underway, relying upon an automated HEMS is problematic due to lack of infrastructure and consumer unfamiliarity with the technology. A system that relies on the personal judgement to schedule their shiftable loads has more likelihood of succeeding in a remote community setting. In this context, utility side has to depend on frequent consumer interactions to estimate changes to the load curve. But, given the remoteness, atypical occupations of inhabitants, and possible harsh weather conditions, it is implausible

to expect the consumers in these remote communities to actively participate in an interactive process throughout the day.

Therefore, to realize the demand responsiveness of electricity consumers in a remote community lacking the infrastructure and consumer sophistication, a pathway that avoids intensive bi-directional communication is desirable.

1.2.3 Uncertainty management

The conventional operation optimization platforms adopted in the EMSs use a deterministic framework either in a day-ahead or an intra-day time frame [5], [19], [20]. Deterministic optimization strategies solve the underlying problem while assuming load and resource forecasts will hold for a given time horizon. However, when the control horizon progresses in real-time, the adopted certainty equivalence could make the EMS vulnerable towards unforeseen deviations occurring in the predicted load curve and the meteorological data. Such deviations can be critical when small and/or weaker power systems are integrated with high amounts of intermittent renewable energy like solar. Also, in cases where the energy management frameworks are unified with DR strategies, the consumer behavioural patterns add further uncertainty to the temporal power system demand. In addition, the remote power systems rely on past generation log data and historical meteorological data collected through distant weather stations in generating the forecasts, which further increases the associated uncertainty. Therefore, it is imperative to employ the EMSs with proper uncertainty management strategies to achieve the optimum scheduling of resources in a cost-effective, reliable, and safe manner.

Techniques employed in the academic literature to address the uncertainty issues in optimal multi-resource scheduling can be mainly categorized under robust optimization [21], closely-tracked deterministic optimization [22], stochastic optimization [23], [24], and chance-constrained optimization [25]. In the reviewed literature, the individual deployment of these approaches has resulted in several drawbacks such as computationally intractable solutions, inaccurate representation of the uncertainty spectrum, devising rather pessimistic and cost-prohibitive resource handling options etc. [12], [26]–[30]. Limited number of studies have proposed multi-layered and/or hybrid uncertainty management

methods to minimize the drawbacks of these individual approaches and to maximize computational feasibility, accuracy, robustness, and cost-effectiveness of multi-resource scheduling. These multi-layered and/or hybrid methodologies can be further improved while considering the operational requirements pertaining to remote off-grid power systems. Reduced dependency on frequently updated forecasts, feasibility to implement corrective control actions during actual deployment, simplicity, and absence of potential convergence issues can be highlighted as the identified areas for improvement.

1.3 Power Management

In contrast to EMSs, Power Management Systems (PMSs) operate in shorter time scales and prioritize in achieving a logical system operation within the imposed operational limits of the system and individual equipment [31]. As shown in Figure 1.2, power management is usually deployed as a secondary control function.

In studies focusing on secondary-level controls, emphasis is on achieving the dynamic stability through proper deployment of lower-level control functions (seamless transfer [32], voltage and frequency compensation [33], [34] etc.). In addition to such controls, power management of system components in a shorter time range is desired to effectively deploy the energy management set-points to the unit-level controls. Although operational strategies for interconnected power systems are well established, power management controls used in isolated HRESs must be envisioned based on the adopted energy resources, and operation requirements of individual equipment [35]. Also, the employed power management strategies must be able to integrate the reference commands derived by the upper-level energy management layer to the unit-level controls in a maximally permissive manner while only adapting to dynamic limitations with minimum required adjustments. Although power management and energy management strategies have been discussed before in their individual context, only few studies have focused on achieving a closely coordinated operation framework for the two control layers to ensure an optimal and logical operational trajectory.

1.4 Operation Evaluation

Most of the EMSs targeting longer (typically expanding hours to days) control horizons have introduced some form of simplification in the system representation to provide a computationally tractable dispatch solution. The simplified problem formulation is effective in identifying the best candidates from a wide array of possibilities [14]. However, the applicability of such dispatch commands and the competence of the underlying lower-level controls to navigate the suggested operational trajectory must be evaluated considering an accurate representation of the system and control layers [20]. To complete this dynamic performance validation, the need of a sophisticated Electromagnetic Transients (EMT) type simulation model becomes indispensable [36]. Also, such simulation models can be used to identify and verify necessary remedial actions for specific violation-prone events (zero-inertia grid forming, mode transitions, reactive power regulation, operating reserve violations, oscillation phenomenon, etc.) which would not have been revealed through the analysis of a steady state dispatch solution.

1.5 Problem Definition

Although the research on interconnected microgrids have shown a significant progress over the past decade, many issues remain unresolved or insufficiently discussed in the context of remote off-grid power systems as detailed in Section 1.2 to Section 1.4.

Although energy management is a well-researched and established subject area, improvements can be made in the problem formulation to combine several operational requirements related to remote power systems. Also, simplification of the basic operation optimization problem structure is desired to achieve effortless integration with other supervisory-level decision support systems.

The intended benefits can be further maximized when the EMSs are integrated with DR strategies. However, due to complexities associated with practical implementation of automated or human-in-the-loop bi-directional communication schemes, quantification of the consumer demand responsiveness has become a difficult task in the context of remote power systems. Therefore, there is a dearth of research that focus on an overall framework

where a DR scheme can be integrated with an EMS via utilizing a simplified communication platform with minimal consumer interactions.

Uncertainty management was also identified as an area for improvement in the context of remote off-grid power systems. The uncertainty management techniques used in the existing multi-resource scheduling studies are either computationally exhaustive or depend on frequently updated system conditions and/or forecasts.

During actual deployment, a coordinated control approach is required to integrate the reference commands derived through energy management strategies to the unit-level controls via the proper employment of power management strategies. Also, it is imperative to confirm whether the derived operation plan meets the logical criteria in maintaining a stable system operation. Therefore, close coordination and performance verification of the energy management and power management control layers is required to facilitate an optimized and logical operation trajectory. Although microgrid control is a highly researched topic, relatively few studies have addressed this specific issue.

1.6 Research Objectives and Scope

1.6.1 Objectives

The main goal of the proposed research is to develop appropriate models and methodologies to implement the energy and power management functions to optimize the operation of a remote off-grid HRES in terms of the operating costs and emissions while ensuring logical operation of the power system respecting both steady state and dynamic capabilities of individual equipment and the system as a whole. To achieve the main goal of this research, the following sub-objectives are proposed:

a) Development of a realistic test system for investigation of energy and power management algorithms.
b) Development of a computationally efficient operation optimization strategy to minimize operating costs and emissions while accommodating power system operational requirements related to remote off-grid HRESs.

c) Development of a DR estimation methodology less reliant on frequent two-way interactions and advanced communication platforms.
d) Development of a DR integrated day-ahead energy management framework by utilizing strategies developed in (b) and (c) to further maximize the intended benefits of operation optimization.
e) Development of a computationally efficient uncertainty management strategy which is less reliant on frequent forecast updates to maintain an optimal intra-day operation trajectory under deviations of load and resource profiles from the forecasts.
f) Development of power management strategies and coordinating them with energy management functions to follow an optimum operation trajectory while ensuring a logical system operation within the dynamic limitations of individual equipment and the overall system.
g) Development of an EMT simulation-based operation evaluation framework to assess the applicability of the derived optimum operation routines as well as to verify the competence of the lower-level controls.

The outcomes of the research are expected to contribute to reduce, optimize, or replace diesel-based generation with renewable sources while; increasing carbon-free generation capacity; promoting local energy resources; reducing system and customer energy costs; and enhancing power system energy security.

1.6.2 Scope

This thesis only focusses on the role of renewable electricity in contributing to the diesel reduction progress in remote communities. Therefore, other diesel reduction measures such as renewable heat and energy efficiency improvements are considered out of the scope. Among the renewable electricity generation methods, intermittent renewable sources such as solar PV has gained a higher energy share in the remote off-grid power systems over the past years [2]. Therefore, energy and power management methodologies will be developed focusing on the solar PV integration to these remote power systems.

In the energy management phase, main focus is on research areas such as operation optimization, DR integration, and uncertainty management. Therefore, load and solar

forecasting is considered out of the scope. Developed energy management controls will be demonstrated using historical data to represent the forecasts. Also, it is assumed that the existing diesel-only systems in these remote power systems can operate with high reliability and availability [2], [3], [7]. Therefore, unscheduled maintenance of diesel generators will not be considered.

In the power management and operation evaluation phase, focus is on achieving close coordination and performance verification between the energy and power management controls. Therefore, primary (unit-level) controls will be implemented using generic well-established methods and improvements to primary controls is considered out of the scope.

1.7 Thesis Overview

Chapter 1 provides the introduction giving the necessary background, objectives, scope, and organization of this thesis. The next five chapters address one or more objectives of the thesis as shown in Figure 1.3: Objective (a) is addressed in Chapter 2; Objective (b) is addressed in Chapter 3; Objectives (c) and (d) are addressed in Chapter 4; Objective (e) is addressed in Chapter 5; and Objectives (f) and (g) are addressed in Chapter 6. Each chapter consists of a focused literature review pertaining to the context addressed in it, and therefore the thesis does not contain a separate chapter dedicated for reviewing the literature, except for the overall background provided in Chapter 1. Contents of each chapter represent a major publication or a combination of several publications.

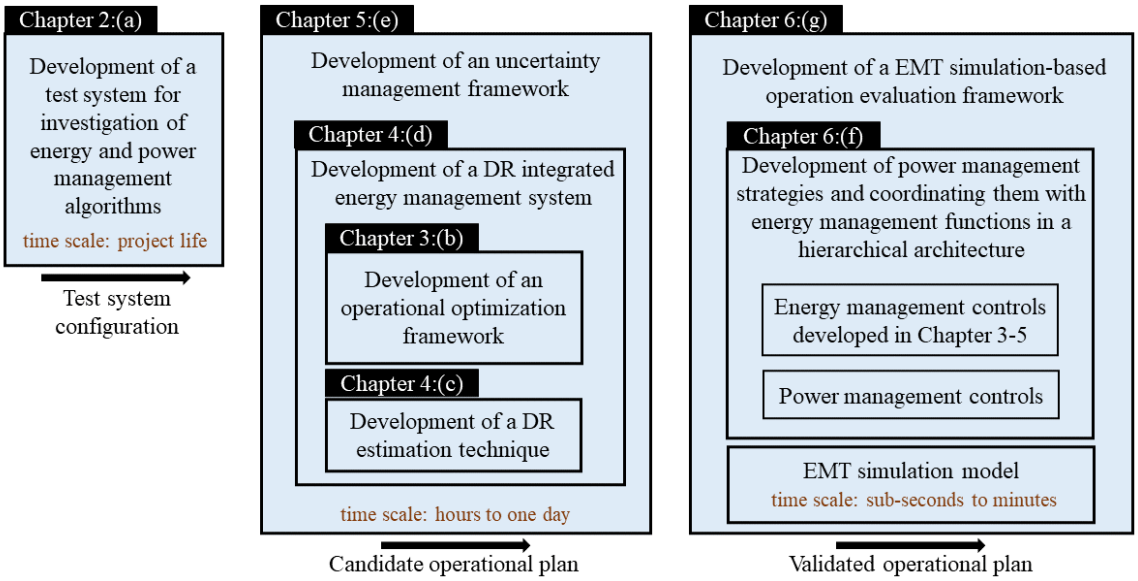

Figure 1.3 Flow of the thesis

Chapter 2 addresses the first objective of the thesis by developing a realistic test system to investigate the models and methodologies developed in the next four chapters.

The energy management control layer will be developed incrementally, starting with the formulation of an operational optimization scheme in Chapter 3. Next, in Chapter 4, a demand response estimation technique will be developed and integrated with operation optimization system from Chapter 3 to devise a DR integrated energy management scheme. In Chapter 5, an uncertainty management scheme will be developed to manage forecast uncertainties in the overall energy management layer. This energy management phase will eventually output a candidate optimum operation plan.

Next, to obtain an optimum and logical system operation, power management strategies will be developed and coordinated with the previously developed energy management functions in a hierarchical architecture in Chapter 6. Also, the developed lower-level control functions will be assessed in an EMT simulation-based operation evaluation framework to verify the applicability of the derived operation routines and to apply proper modifications to the energy managements set-points when required. Chapter 6 will provide a validated operation plan.

Chapter 7 presents the conclusions, main contributions, and future directions of the research.

Chapter 2

Development of a Test System for Energy and Power Management Studies

2.1 Introduction

In this chapter, an example of a remote HRES is developed to test and demonstrate the models and methodologies formulated in Chapter 3 to Chapter 6. The scope of this study is limited to retrofitting an existing diesel-only system by adding solar PV with or without battery energy storage. The resulting PV-Diesel and PV-Diesel-Battery test system configurations are sized using HOMER software under low, medium, and high PV penetration levels. Recommended test system is chosen considering costs, emissions, and reliability impacts of adding intermittent PV generation and battery storage to the existing diesel-based power systems.

2.2 Background and Literature Review

The design and assessment of HRES configurations dwell upon several factors. Among them, intermittent nature of renewable sources such as solar, climatic conditions, nonlinear response of system components, cost of equipment and sources, environmental risks etc. have made it a challenging task [37].

There are many techniques employed for sizing of HRES configurations. The simplest adopted technique involves the incorporation of worst-case scenarios [37]. Irrespective of the very low computational burden, systems designed using this method tends to be usually

oversized due to the low occurrence probability of the considered worst-cases. Therefore, incorporation of long time series data is preferred when sizing the power systems consisting of intermittent renewable energy sources [38]. To process the time series data considering a pre-defined set of objectives, several approaches have been explored, which can be primarily categorised into probabilistic, analytical, iterative, and hybrid methods [37]. Probabilistic methods, being the simplest of sizing techniques only take indicators such as loss of power supply probability and expected energy not served to assess the system performance after the construction of risk models. Due to less details involved both in modelling and assessment, these techniques are not considered to be highly accurate [37]. Iterative methods use a recursive assessment framework to find the best configuration. Recursive assessment is done by deploying optimization frameworks namely, Genetic Algorithm (GA), Particle Swarm Optimization (PSO) etc. Analytical methods use computational models to analyse the system performance for several system architectures in different sizing scales based on multiple performance indices. In the literature, such analytic assessments are conducted using either computer tools or numerical approximations of the system components. Evaluation of design options for variety of applications has been facilitated by simulation tools such as Hybrid Optimization Model for Electric Renewables (HOMER), RETScreen, HYBRID2, General Algebraic Modeling System (GAMS), TRNSYS, Remote Area Power Supply Simulator (RAPSIM), SOMES, INSEL etc. [39], [40].

Several sizing and assessment studies of off-grid HRES projects can be found in the literature. The remote off-grid sites considered in these studies are located all over the world: North-America [3], [41], Europe [42], Africa [43], Middle-East [44], [45], Asia [46], [47], and Australia [48]. Although the adopted design objectives and conclusions are highly case-specific, the reviewed literature provide valuable information on sizing and assessment of HRESs. HOMER as a simulation platform appears repeatedly in these studies confirming its competence in effectively handling large time series data associated with design and performance evaluation of HRESs [37]. Also, the availability of commercial equipment models, data sheets, cost data, and the integrated meteorological data makes HOMER an attractive tool for accurate configuration of the system components and the associated resources.

2.3 Test System Development

The test system was developed following the procedure discussed in the following sub-sections.

2.3.1 Formulation of planning objectives

As the first step of the design and assessment process, the issues of the existing power system which are expected to be either resolved or improved through the renewable addition is identified [38]. For remote off-grid power systems energized by diesel-based generation facilities, these objectives generally include increasing renewable generation capacity, reducing cost of energy supply, optimizing operation routine of the existing diesel generators, achieving a sustainable energy portfolio etc.

2.3.2 Setting-up candidate schemes and sizing

Candidate schemes, such as PV-Diesel and PV-Diesel-Battery, were considered in this study under low, medium, and high PV penetration scenarios.

For each candidate scheme, the newly added components sizes were determined using HOMER. HOMER takes Net Present Cost (NPC) as the basic assessment criteria in its grid-search algorithm. By simulating all possible configurations (derived pertaining to an user-defined search space), it determines the system configuration that meets the demand while satisfying the user-defined constraints at the lowest NPC as depicted in Figure 2.1 [42]. In Figure 2.1, NPC^{n} is the NPC of the n^{th} system, NPC^{opm} is the NPC of the last recorded optimum system, and N is the number of derived configurations.

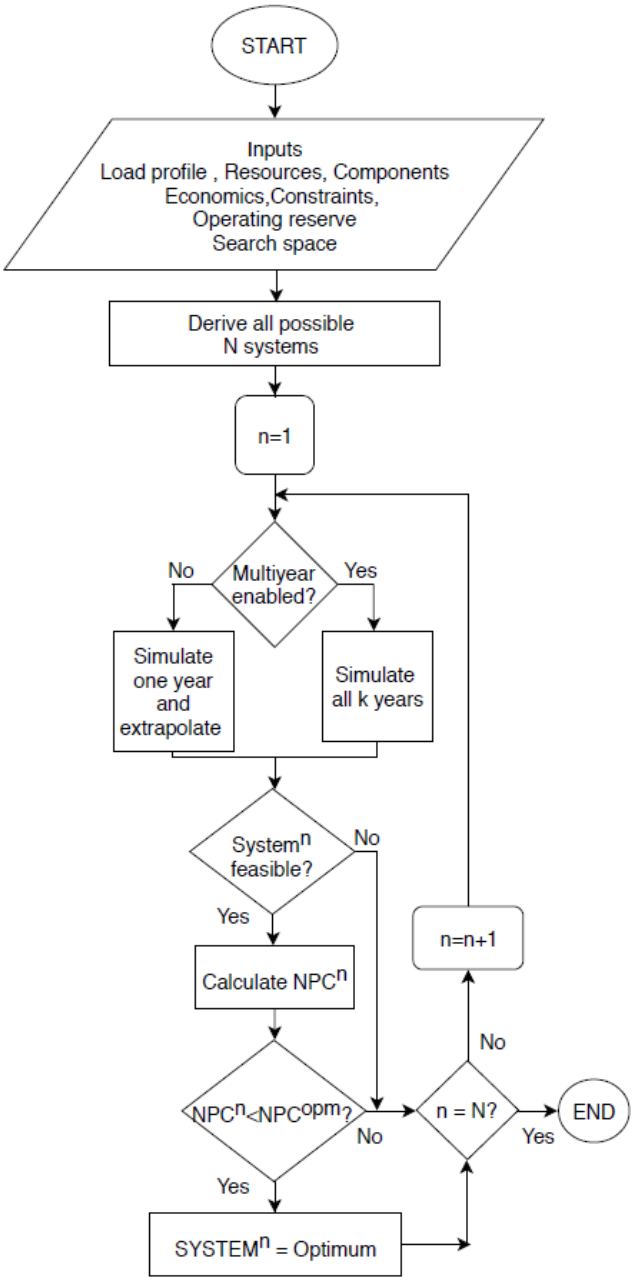

Figure 2.1 HOMER grid search algorithm

As this grid search selects the best system using NPC, system constraints and penalties can be incorporated as indirect measures to account for the reliability and environmental factors. Environmental factors can be indirectly considered by imposing penalties on the system emissions. To improve system reliability impacts due to integration of intermittent renewable sources, constraints can be applied on the annual capacity shortage to eliminate candidate configurations with capacity shortages more than a pre-specified value. Capacity

shortage is an indication of the system's inability to support the required operating capacity, including the system demand and the user-defined operating reserve. Operating reserve is the surplus operating capacity provided by the dispatchable sources such as diesel and battery units in operation. Therefore, it acts as a safety margin to compensate for the variations occurring in load and intermittent resources during actual operation. Usually, the required minimum operating reserve is defined as a weighted sum of the system demand, renewable resource outputs as well as the annual system peak demand as described in [3]. The selection of these weighting factors depends on the reliability requirements and uncertainties associated with the power system of choice as well as the intra-time-step variations associated with loads and resources [27].

HOMER by default runs the simulation for the first year and then extrapolates the results over the rest of the project life. Although this approach would result in a reduced computational burden, it deprives the user to account for the variations occurring in important system parameters during the planning period. Alternative method would be to use the HOMER Multiyear module. Through this approach, the important temporal variations occurring in critical system parameters can be incorporated in the result improving its credibility.

Also, it is worth mentioning that the sizing of the system configuration following this approach does not indicate that the selected system would perfectly match the expectations of the power system planner. It must be followed with series of power flow and short circuit calculations as well as security and stability analysis to ensure that the selected optimum system meets the standard grid codes and the stability criteria [38]. However, this step is considered out of the scope as the current study focuses only on providing a quantitative justification of the designed system performance over the considered project lifetime.

2.3.3 Evaluation and comparison of candidate schemes

After finalizing the system configuration under each candidate architecture, they will be assessed with reference to the existing diesel-only system using the economic, environmental, and reliability criteria related outputs available through HOMER.

The economic performance will be evaluated using both intrinsic and extrinsic parameters. Intrinsic parameters like NPC and Levelized Cost of Electricity (LCOE) assess the project independent of other alternatives. Extrinsic economic parameters such as Return on Investment (ROI), Internal Rate of Return (IRR), and Simple Payback Period (SPP) measure the associate performance between a given system and a predefined base case system.

CO_2 emissions and the Renewable Fraction (*RF*) as given by (2.1) are used to assess the environmental performance.

$$RF = 1 - \frac{nonrenewable\ electrical\ energy\ production}{Electricity\ load\ served} \tag{2.1}$$

Unmet electric load and capacity shortage were also observed to assess the capability to maintain a reliable operation after integrating intermittent renewable sources with or without battery storage.

2.4 Study System Background and Data Inputs

2.4.1 Study site and existing diesel-only power system

The hypothetical off-grid community example used in this study is modeled considering the typical characteristics of an isolated community in Northern Manitoba, Canada. This remote community is considered only accessible using small aircrafts, except when the winter roads are in operation. Typically, the winter roads operate only for one or two months in a year, therefore supplies for the entire year is transported and stored during this period.

For the considered study site, winter season has an elevated demand in comparison to summer. The annual demand of this community is around 2600 MWh and the average load is around 300 kW. The electric load does not reflect the heating/cooling energy demand due to the prevailing restrictions to use electricity for space heating/cooling applications. Often, this energy requirement is met either through wooden or oil furnaces. Therefore,

assuming no change in supply, current projections for annual load growth was assumed to be around 2% for this community.

The electrical power system incorporates a stand-alone diesel generating facility isolated from the transmission grid. The diesel plant consists of two diesel generators rated at 400 kW and 800 kW. An additional 400 kW generator remains as a back-up to be used in case one of the generators fails, since the delivery of spare parts and repair crews could take time. This type of configuration is typical for off-grid power systems in Northern Canada, and to ensure high reliability, million of litres of diesel are being shipped to these Northern communities every year [7]. Transportation of diesel is mostly done over winter roads which is costly and hazardous to both people and environment. Moreover, diesel storage facilities deployed in these settlements are susceptible to fuel tank leaks which can cause significant environmental damage by contaminating soil and groundwater. The highest impact to the environment is caused through the burning of large amount of diesel which contributes significantly to greenhouse gas emissions [3].

2.4.2 Data inputs

All the results were computed using HOMER Pro version 3.10. HOMER does not model electrical transients and other dynamic effects which requires a very small time-step. Therefore, an hourly time-step was used to adequately capture the important statistical aspects prevailing in the load and intermittent sources. This time-step also serves in reducing the computational burden of the optimization task. The main data used in modelling the system components are given in Appendix A, and the important aspects of input data are discussed below.

Solar irradiance data was obtained through the NASA surface meteorology and solar energy database for the considered study site [49]. The monthly averaged daily global solar irradiation levels for this site are shown in Figure 2.2 along with the average clearness index for each month.

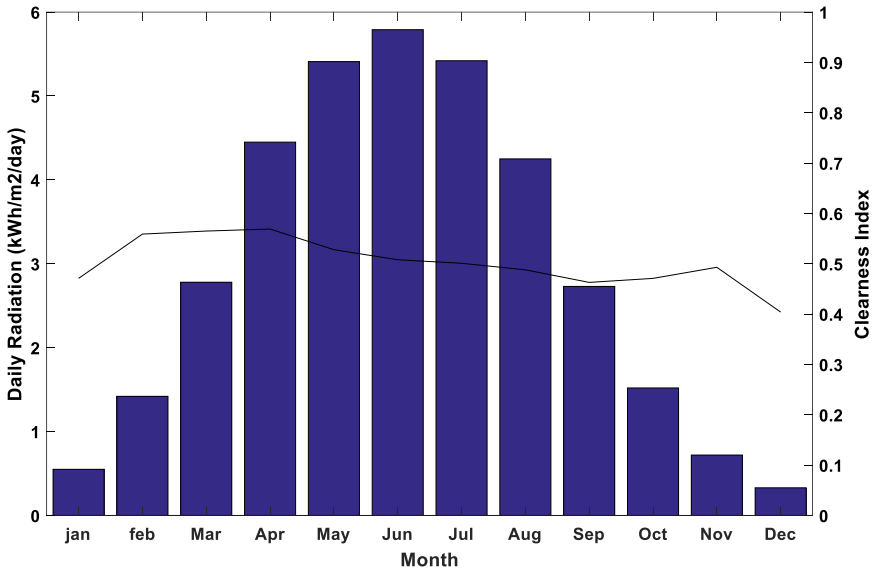

Figure 2.2 Global solar irradiation level

Also, following a preliminary Battery Energy Storage System (BESS) selection process, Li-ion was selected as the preferred battery technology for the study site [50].

To improve reliability, configurations with capacity shortages more than 0.01% were eliminated. A minimum operating reserve was defined as a weighted sum of the current time-step load demand, current time-step solar power output, and the annual peak demand whereas the corresponding weights were defined as 0.1, 0.4, and 0.05, respectively.

This study uses a project lifetime of 20 years. Canadian Dollar (C$) is used as the currency for all cost figures. A nominal discount rate of 6% and an expected inflation rate of 2% was considered [3], [7], [41], [51]. The landed cost of diesel was taken as 1.1 C$/litre subjected to a fuel price escalation rate of 1%. This was the wholesale market (rack) price in Winnipeg, Manitoba inclusive of a transportation cost of 0.24 C$/litre and other applicable discounts during the year of 2018. In addition, a penalty cost of 25 C$/tonne was imposed on the CO_2 emissions.

The three main cost figures used in modelling each system component and their lifetimes can be found in Table 2.1. Capital cost is the total installed cost of the component at the beginning of its lifetime. This mainly includes costs incurred for permits, purchasing, installation, and labor. As the existing diesel generators require no capital investment, their capital cost was taken as zero [42], [52]. Given the remoteness of the considered site, the

installation and labor costs for PV, converter, and battery were assumed to be significantly high compared to other parts of Canada as reflected in their capital costs. Operation and Maintenance (O&M) accounts for the costs associated with operating and maintaining a specific component and excludes the fuel cost. HOMER calculates fuel cost separately. The renewable addition accounts for reduced O&M costs as given in Table 2.1. However, O&M cost of the diesel plant was assumed considerably high given the maintenance requirements associated with diesel storage facilities as well as the high-priced material and labor cost prevailing in these remote areas. The replacement cost is incurred at the end of a component lifetime.

Table 2.1 Costs and lifetimes of system components

	Lifetime	Capital cost	O&M cost	Replacement cost
Solar array	25 years	6000 C$/kW	25 C$/kW/year	6000 C$/kW
Converter	15 years	1000 C$/kW	-	1000 C$/kW
Diesel generators	90,000 hours	0 C$/kW	60 C$/ hour	2500 C$/kW
Battery (Chemistry: Li ion)	6000 cycle life @ 100% DOD	7000 C$/unit	10 C$/unit/year	7000 C$/unit

2.5 Results and Discussions

2.5.1 Planning objectives

The objectives for the current study were formulated by first assessing the performance of the existing diesel-only power system. The operation of the two diesel generators was simulated in HOMER for the considered project lifetime. The results revealed a high LCOE of 0.5146 C$/kWh along with considerably elevated amounts of emissions associated with the diesel-only operation. No capacity shortages or unmet electric loads were detected during the project lifetime. However, the increased reliance on diesel-based electricity production will impose several constraints on its economic and environmental performance if the diesel-only operation were to be continued in the future. Moreover, emergencies like interruptions to the diesel supply chains and unexpected blackouts can increase energy

insecurity. Also, having the option of locally available resources bolster the ability of this power system to respond towards volatile and unpredictable market price fluctuations. Also, considering various environmental costs associated with the operation and maintenance of a diesel facility and diesel fuel transportation through winter roads, the need of integrating renewable generation got further heightened.

Thus, in the study that follows, it was expected to find the best retrofit for the existing diesel-only power system to enhance the economic and environmental performance while maintaining its reliability.

2.5.2 Candidate schemes and sizing

To retrofit the existing diesel-only system (Figure 2.3(a)), two electrical system architectures were investigated namely, 1) PV-Diesel, and 2) PV-Diesel-Battery as shown in Figure 2.3(b)-(c), respectively. For each candidate architecture, three scenarios were defined under low, medium, and high PV penetration levels. The newly added component sizes under each architecture were found using HOMER as detailed in Section 2.3.2.

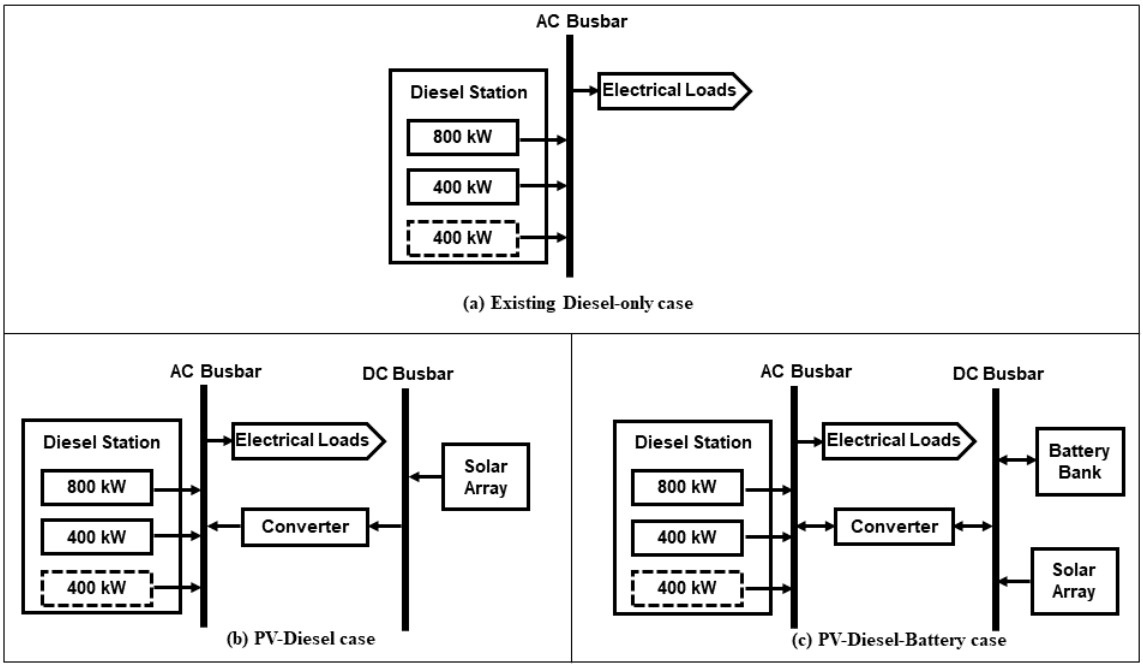

Figure 2.3 Different power system architecture: (a) Existing power system (Base case), (b) PV-Diesel system, and (c) PV-Diesel-Battery system

2.5.2.1. PV-Diesel case

The search spaces used for the three scenarios are given in Table 2.2. The system configurations with the lowest NPC were located at the lower bound of the defined search spaces for the low, medium, and high solar penetration scenarios as showed in Table 2.3.

Table 2.2 Search space for PV-Diesel case

Component		PV Penetration Scenario		
		S1 (Low)	S2 (Medium)	S3 (High)
Diesel Generators	800 kW	With or without 800 kW		
	400 kW	With or without 400 kW		
Solar PV	Range [kW]	25 – 200	200 – 400	400 – 700
	Step [kW/step]	25	25	25
Converter	Range [kW]	25 – 250	150 – 450	350 – 750
	Step [kW/step]	25	25	25

Table 2.3 PV-Diesel system with the lowest NPC as estimated by HOMER

Component	PV Penetration Scenario		
	S1 (Low)	S2 (Medium)	S3 (High)
Diesel Generators [kW]	800	800	800
	400	400	400
Solar PV [kW]	25	200	400
Converter [kW]	25	150	350

2.5.2.2. PV-Diesel-Battery case

The three scenarios defined in the PV-Diesel case were considered again with the addition of storage. To determine the method of charging the battery storage, the HOMER grid search algorithm also considers the dispatch strategy as a decision variable in this architecture. Two dispatch strategies were considered namely, Load Following (LF) and Cycle Charging (CC). Under CC, both diesel generators and renewable sources were committed to charge the battery bank whereas under the LF strategy only renewable sources were committed to charge the battery bank. The search spaces defined for each

scenario is given in Table 2.4 whereas the system configurations with the lowest NPC is shown in Table 2.5. For S1, the PV array and converter size for the system configuration with lowest NPC was located near the lower limit of the given search space. PV array was sized around the upper limit for S2 and in the middle range for S3. The battery storage also showed an elevated usage for the last two scenarios. Converter sizes were located at higher values to facilitate the battery operation as well as the increased solar penetration.

Table 2.4 Search space for PV-Diesel-Battery case

Component		PV Penetration Scenario		
		S1 (Low)	S2 (Medium)	S3 (High)
Diesel Generators	800 kW	With or without 800 kW		
	400 kW	With or without 400 kW		
Solar PV	Range [kW]	25 – 200	200 – 400	400 – 700
	Step [kW/step]	25	25	25
Converter	Range [kW]	25 – 250	150 – 450	350 – 750
	Step [kW/step]	25	25	25
Battery	Range [units]	0-50	0-150	0-200
	Step [units/step]	10	10	10
Dispatch		LF or CC		

Table 2.5 PV-Diesel-Battery system with the lowest NPC as estimated by HOMER

Component	PV Penetration Scenario		
	S1 (Low)	S2 (Medium)	S3 (High)
Diesel Generators [kW]	800	800	800
	400	400	400
Solar PV [kW]	25	400	625
Converter [kW]	25	450	600
Battery	10 units (76 kWh)	110 units (836 kWh)	120 units (912 kWh)
Dispatch	LF	CC	CC

2.5.3 Comparison and assessment

The existing diesel-only system was benchmarked to serve as a Base case. The performance of the system configurations as selected through HOMER was assessed and compared with that of the Base case system as shown in Table 2.6 under the criteria defined in Section 2.3.3.

Table 2.6 Results comparison

	Base case	PV-Diesel			PV-Diesel-Battery		
		S1	S2	S3	S1	S2	S3
LCOE [C$/kWh]	0.5146	0.5158	0.5235	0.5468	0.5167	0.5235	0.5121
NPC [C$]	21.31M	21.36M	21.68M	22.65M	21.40M	21.68M	21.21M
ROI [%]	-	0.2	0.5	-1.1	0.2	1.8	2.8
IRR [%]	-	1.3	0.9	N/A	0.5	2.9	4.1
SPP [years]	-	18.0	18.2	18.9	18.1	18.5	16.1
CO_2 emissions during project life [Mt]	0.0444	0.0441	0.0405	0.0388	0.0440	0.0382	0.0346
RF [%]	0	0.93	7.76	14.7	0.94	13.4	20.8
Unmet load [kW]	0	0	0	0	0	0	0
Unmet capacity [kW]	0	0	0	0	0	0	0

The system configurations found for the PV-Diesel case under low, medium, and high renewable penetration levels accounted for high economic costs with respect to the Base case operation. Also, with increasing renewable penetration levels, the associate economic performance of this topology further got deteriorated as presented in Table 2.6. Also, for the extrinsic economic parameters to make sense, the selected Base case system should have a comparatively lower initial capital value and a higher operating cost than the selected system. Violation of this criteria (indicated as “N/A”) was detected when calculating IRR for S3 of the PV-Diesel case. As PV is non-dispatchable, at least one diesel-unit has to be in operation to supply the required minimum operating reserve in a PV-Diesel power system. This lowers the achievable economic benefits even with higher PV penetration levels. Such technical constraints make it harder for the PV-Diesel topology to recover the associated high capital costs. Thus, this topology was considered unsatisfactory in achieving the design objectives for the considered study case.

The economic indices suggested no enhancement of economic performance for S1 of the PV-Diesel-Battery case. When increasing the PV penetration level and storage capacity, the PV-Diesel-Battery topology gained gradual enhancement in its associate economic performance with the Base case. Therefore, at increased penetration levels, when integrated with storage, the lower operating costs associated with renewables have gained the maximum advantage when deciding the system configuration. Converter size has also played a decisive task by facilitating the bi-directional energy transfer occurring between AC/DC buses. CC dispatch strategy was selected for the last two scenarios where both renewable generation and the diesel generators were used to charge the batteries. While extracting the excess renewable capacity, this control strategy allowed the diesel generators to achieve higher loading levels. The gradual reduction of greenhouse gas emissions in each scenario compared to the Base case operation heightens the environmental performance associated with the PV-Diesel-Battery topology. Among the three scenarios, S3 accounted for the lowest LCOE with 0.5% reduction to that of the diesel-only operation. For a renewable fraction of 21%, expected fuel savings are estimated to be around 22% with respect to the existing configuration.

Based on the overall analysis, PV-Diesel-Battery topology as suggested in S3 under high PV penetration levels would be a favourable alternative to the existing diesel facility and can be selected as the preferred test system to demonstrate the energy and power management algorithms developed in the following chapters. High environmental benefits were seen at reduced emission levels while providing a competitive economic performance to that of the Base case system. System reliability was also maintained comparable to the Base case system. Extrinsic economic indices assessing the economic performance of the selected HRES related to the Base case system also predicted positive return, although at lower rates. This observation is primarily influenced by the elevated capital costs associated with renewable integration at the selected remote location.

However, it must be noted that this study was primarily driven as a cost problem and externalities like environmental and legislative regulations were not directly accounted other than the carbon penalty price. It also excludes costs incurred due to spillage and emissions during the fuel transportation as well as soil and ground water contamination occurring inside diesel storage facilities. However, if those indirect costs were to be

accounted, the actual performance of the proposed HRES configuration would be much greater than that determined through this analysis. Also, with projected cost reductions in solar PV arrays, batteries, and converters, incorporation of renewable alternatives in off-grid power systems will gain increased momentum.

2.6 Concluding Remarks

This chapter presented the steps followed to design a realistic test system for the investigation of energy and power management algorithms developed in this thesis.

Electrical system architectures such as PV-Diesel and PV-Diesel-Battery were examined in HOMER software to find the best retrofit for a hypothetical diesel-only facility, while incorporating gradually increasing renewable penetration scenarios. Maximization of environmental benefits was identified at high solar penetration levels and increased battery and converter capacities in the PV-Diesel-Battery case. Under such conditions, the intrinsic economic indices remained competitive to the Base case scenario and extrinsic economic indices also predicted positive return, although at lower rates.

According to the overall analysis, the system configuration as derived under the PV-diesel-battery topology at high renewable penetration levels was selected as the preferred test system configuration.

Chapter 3

A Supervisory-level Operation Optimization Framework for Remote Power Systems

3.1 Introduction

In the presence of a hybrid architecture involving conventional generation, intermittent renewable generation and energy storage systems, deployment of an energy management system with an effective short-term operation optimization framework is imperative to enable efficient utilization of resources to achieve economic and environment goals. An EMS generates a short-term operational plan over a specified time horizon, which could extend from several hours to several days, and typically consists of a unit commitment and generation dispatch plan derived based on the forecasts of loads and generation resources.

Development of the energy management control functions is started in this chapter by formulating an operation optimization framework to derive the optimum power system operation plan with minimum costs and emissions over a user-defined control horizon. While energy management algorithms for isolated HRESs have been proposed before, an improved optimization problem formulation that achieves better computational efficiency is proposed in this chapter. This feature enables it to be efficiently integrated with other supervisory-level decision support applications such as DR integration and uncertainty management as that will be discussed in Chapter 4 and Chapter 5, respectively. Also, as a novel feature, in addition to minimizing operational costs and emissions, various operational requirements related to HRESs such as achieving optimized schedule for the

diesel generators with reduced start-stop cycles, reducing battery degradation, and minimizing energy spillage is addressed through the problem formulation.

3.2 Background and Literature Review

Once the load and resource forecasts are established, the objective of an operation optimization framework is to generate the power system operation plan while minimizing/maximizing a pre-defined objective or objectives. The derived operation plan includes the unit commitment and dispatch commands for the available dispatchable energy sources. A clear distinction can be identified between the centralized and decentralized methods as an implementation architecture for the operation optimization frameworks [53]. Given the high-level of coordination and critical demand supply balance required by isolated power systems, centralized architectures are usually preferred at the cost of reduced autonomy of Distributed Energy Resources (DERs) [26].

Usually, the optimum operation plan includes a set of operating points for the dispatchable energy resources. These set-points characterize the deployed objective function as well as the underlying optimization problem. For instance, continuous and/or discrete set-points result in a real, mixed integer or integer optimization problems, respectively [53]. According to [13], [14], the primary objectives targeting standalone systems include operation cost reduction, emission reduction, increased utilization of renewable sources, increased system stability etc. Also, when determining the optimal energy management, useful energy available from primary energy sources, associated operating costs, project economics, State of Charge (SOC) of storage devices, lifetime of components, and number of start-ups for generators are detailed as the critical parameters [9]. The deployed control functions do not consider the transient behaviour corresponding to fast system dynamics allowing the system operator to arrive at a steady state assumption on the system behaviour without much loss of accuracy [12].

Several authors have discussed the optimal operation of HRESs for standalone power generation [53]. In [54], authors have devised a operation optimization framework based on linear programming, equipped with a trust region. Every device is considered as a unit that can generate or absorb power within the imposed constraints whereas the objective

function comprises costs, penalties, and revenues. The optimization problem is devised in a generalized manner where the specific characteristics of individual resources are loosely integrated. In [55], authors have formulated a dispatch strategy for a PV-Diesel-Battery system based on set-point values of the system load and battery SOC to achieve lowered system costs. The results obtained under the proposed optimum plan has been compared with two other dispatch strategies. In [56], an optimal EMS is proposed for a standalone PV-Diesel-Battery application using the load-following dispatch strategy. The energy flows are discussed considering the impact of weekday, weekend, and seasonal changes in demand. In [5], the optimal operation plan is derived for a PV-Diesel-Battery power system to minimize the overall operation cost. The results are presented for two separate control strategies involving "continuous" and "ON/OFF" operation of the diesel generators. Both [5], [56] derive the optimum set-points by minimizing the diesel fuel costs and depend on commercial solvers to solve the underlying optimization problem. An EMS optimization model for a multi-source isolated microgrid is presented in [57]. The optimization problem is solved using PSO to primarily minimize the cost of energy production while maximizing the energy storage usage and the utilization of renewable resources. Authors in [19] develop the operation plan considering, battery life loss cost, O&M cost, fuel cost, and environmental cost of a standalone microgrid. The optimization problem is formulated as a multi-objective optimization and the set-points are derived using the genetic algorithm. A thorough review of other studies detailing operation optimization and control strategies for remote off-grid HRESs can be found in [58]. All these studies have used distinct problem formulation methods to optimize their respective objectives and confirm to the fact that there is no "one plan fits all" way of realizing the best operational strategy. However, many of the reviewed studies have mostly used least-cost based approaches when formulating the problem and thus can be improved to address operational requirements related to remote power systems.

Techniques generally used as the preferred optimization platforms for the underlying optimum energy management problems can be summarized as, dynamic programming, mixed integer linear/non-linear programming, and heuristics-based evolutionary computational approaches (genetic/swarm algorithms) as discussed in [17], [53]. Although being theoretically sound, optimization frameworks based on dynamic programming and

mixed integer linear programming can be computationally expensive in the presence of complexities associated with large number of variables [17]. Also, studies using mixed integer linear/non-linear programming often relies on their availability in commercial software packages, which can otherwise be omitted due to the shorter control span (< day) involved in daily operation optimization. In addition, when integrated with these complex solvers, the optimization problem gets conditioned, and the nature of the variables are sometimes forced to change to accomplish the requirements. On the other hand, many researchers have used heuristics-based evolutionary approaches to determine optimum or sub-optimum results with less computational complexity [17]. In the reviewed literature, genetic algorithms and many other swarm-based techniques have shown proven-competency to handle multiple objectives in a robust manner [53]. However, even when deploying techniques based on heuristics, the reviewed problem formulation strategies can be further improved to achieve fast convergence times. This will be advantageous when integrating the operation optimization framework with other supervisory-level decision support systems.

3.3 System Set-up

In this section, the objectives and constraints of operational optimization related to remote off-grid PV-Diesel-Battery power systems are discussed first. Then, the outputs related to individual system components as well as the costs and emission figures required to define the final objective function used in operation optimization are formulated based on existing approaches.

3.3.1 Objectives and constraints

PV-Diesel-Battery layout as shown in Figure 3.1 represents a power system configuration frequently deployed/proposed in the context of small remote off-grid power systems. However, the outputs from various generation sources and storage units need to be coordinated and optimized to realize their full benefits, which is the main task of an operation optimization framework.

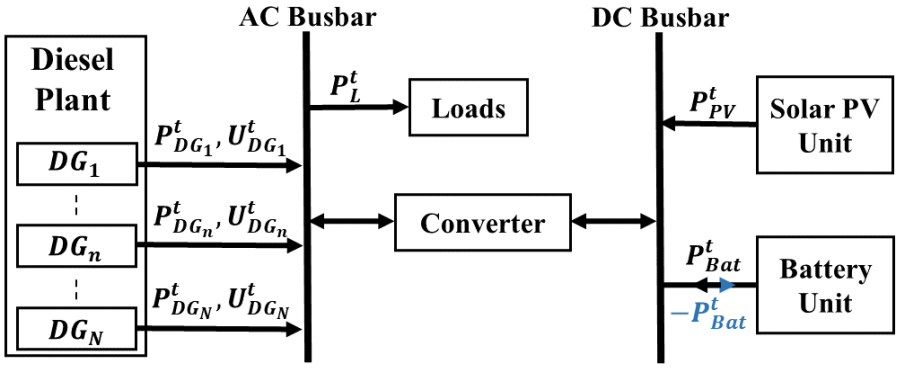

Figure 3.1 Layout of a PV-Diesel-Battery HRES

It is desired to regulate the output power of the non-dispatchable generation units, such as the PV array, based on the optimal operating condition considering its primary energy source [35]. Therefore, the operation plan only constitutes set-points for the dispatchable energy sources. For example, for the system layout shown in Figure 3.1, these include the diesel generator power outputs ($P^t_{DG_n}$) along with their on/off status ($U^t_{DG_n}$), and the power commands for the battery unit (P^t_{Bat}) for a specified control horizon. For remote power systems, usually the main objectives of an operation optimization framework deployed in an EMS is to minimize the operation cost and emissions by optimally manipulating the identified set-points. However, this task is complicated by the operational limits associated with individual equipment as well as the system as a whole.

The constraints involving individual equipment mainly ensures their operation within the rated power/energy limits. As an additional feature, the EMS can be equipped with measures to increase the operational efficiency of the over-sized diesel generation facilities. Also, BESS degradation can be reduced to enhance the longevity of their operating lifespan. Constraints involving the entire system operation mainly ensures stability, reliability, and security of energy supply. At all times, the generated power must be equal to that consumed to maintain the power system stability. Also, the EMS usually functions on a deterministic framework while assuming predictions will hold for the specified time horizon. Therefore, to ensure reliable operation of the power system, it is advocated to maintain a minimum operating reserve as detailed in Section 2.3.2.

3.3.2 Individual system models

3.3.2.1. PV unit

The PV array output (P_{PV}^{t}) is usually controlled independent of the other units (grid-noninteractive strategy) using the power reference provided by the unit-level Maximum Power Point Tracking (MPPT) strategy [35]. Therefore, in each time-step, the power produced by the solar array at the DC bus is calculated as in (3.1) [59]:

$$P_{PV}^{t} = P_{PV}^{Rated} \times F_{PV} \times \frac{G^{t}}{G_{STC}} \times \left(1 + \alpha_{P}(C^{t} - C_{STC})\right) \tag{3.1}$$

where P_{PV}^{Rated} is the rated DC power of the PV array, F_{PV} is the PV derating factor, G^{t} is the incident solar irradiance in the current time-step, G_{STC} is the incident solar irradiance in the Standard Test Conditions (STC), α_{P} is the temperature coefficient of power, C^{t} and C_{STC} are the PV cell temperature in the current time-step and in STC, respectively.

The associated costs of operation are usually assumed negligible for the PV array. However, remote power systems can undergo scenarios with low loading and high solar penetrating conditions. If the power system experiences a prolonged energy surplus period under such conditions, the excess of PV power will have to be spilled (P_{Spill}^{t}), specially in the absence of dump loads. Therefore, to reduce the curtailed solar energy, in each time-step the spilled energy is penalised as given in (3.2):

$$Cost_{spill} = \sum_{t=1}^{T} ((P_{Spill}^{t} \times dt) \times c_{spill}) \tag{3.2}$$

where c_{spill} is the imposed penalty rate, dt is the length of a timeslot, and T equals the considered total number of timeslots.

3.3.2.2. Battery unit

Being a dispatchable energy source, battery power command is considered as an optimizable set-point in the operation plan. Thus, battery power command at each time-step is received through the optimization algorithm and can be used to calculate the SOC variations in that time-step. However, the power commands generated by the optimization

algorithm would require modifications in order to maintain the SOC level within the pre-specified limits. This can be achieved by limiting the received power command as shown in (3.3)-(3.5) preceding the SOC calculation as given in (3.6) [60]:

$$P_{Bat}^{t} = U_{d}^{t} \times [\min(P_{maxd}^{t}, P_{Bat}^{t})] + (1 - U_{d}^{t}) \times [\max(-P_{maxc}^{t}, P_{Bat}^{t})] \quad (3.3)$$

$$P_{maxc}^{t} = \min(P_{Bat}^{Rated\_max}, Bat_{cap} \times (SOC_{max} - SOC^{t})/(100 \times dt \times \eta_{c})) \quad (3.4)$$

$$P_{maxd}^{t} = \min(P_{Bat}^{Rated\_max}, Bat_{cap} \times \eta_{d} \times (SOC^{t} - SOC_{min})/(100 \times dt)) \quad (3.5)$$

$$SOC^{t+1} = SOC^{t} + \frac{(1 - U_{d}^{t}) \times (|P_{Bat}^{t}| \times dt \times 100 \times \eta_{c})}{Bat_{cap}} - \frac{U_{d}^{t} \times (P_{Bat}^{t} \times dt \times 100)}{Bat_{cap} \times \eta_{d}} \quad (3.6)$$

where U_{d}^{t} is the battery mode of operation (1 → discharging and 0 → charging), SOC^{t} is the SOC of the current time-step, SOC_{min} is the minimum SOC limit, SOC_{max} is the maximum SOC limit, $P_{Bat}^{Rated\_max}$ is the maximum allowable charging/discharging power without considering the SOC limits, Bat_{cap} is the battery energy capacity, η_{c} and η_{d} are the efficiencies of the charging and discharging modes, respectively.

Although the direct operating costs associated with BESS operation is negligible, it is necessary to approximate the battery degradation in the cost model of BESS. There can be many operational and non-operational factors affecting battery degradation, among which, number of cycles, discharge levels, and amount of energy throughput are considered as the most critical [61]. Therefore, to indirectly minimize the effects of battery aging, two types of battery degradation costs were considered, namely the calendar life degradation cost ($Cost_{calender}$) and the cycle life degradation cost ($Cost_{cycle}$).

It is assumed that the battery would need a replacement once its total throughput exceeds its lifetime throughput. From that perspective, the cost of energy circulated through the battery bank for the considered control horizon is calculated as in (3.7) [61]:

$$Cost_{calender} = \sum_{t=1}^{T} \frac{U_{d}^{t} \times P_{Bat}^{t} \times dt \times c_{rep}}{\sqrt{\eta_{bat}} \times E^{tot}} \quad (3.7)$$

where c_{rep} is the battery replacement cost, and η_{bat} is the battery roundtrip efficiency, and E^{tot} is the battery lifetime throughput.

$Cost_{cycle}$ is also incurred during a discharging stage of a cycle. Therefore, the cycle aging caused by a full cycle is considered to be similar to that caused by a discharging half-cycle of the same Depth of Discharge (DOD). The Rainflow Cycle Counting Algorithm [62] as presented in Appendix B is used to count the full cycles and discharging half-cycles occurring in ten different DOD segments from 0%-90% at gaps of 10%. $Cost_{cycle}$ is defined using the cost function given in (3.8) [63]:

$$Cost_{cycle} = \sum_{d=1}^{D} c_{cyc} \times Cycles_d \times (DOD_d)^2 \tag{3.8}$$

where c_{cyc} is a penalty cost factor, DOD_d and $Cycles_d$ are the number of subjected cycles and their respective DOD levels in each segment *d*, respectively.

3.3.2.3. Diesel generators

Diesel generators are usually considered as the preferred choice for grid-forming. These dispatchable units provide optimizable set-points for the operation plan in terms of their commitment and power outputs. In the proposed method, the power outputs of the online diesel units are defined as dependent optimization variables as detailed in Section 3.4.

Constraints involving the diesel generators maintain the number of starts under a user-specified value and ensure their operation within the permissible loading margins. The minimum loading requirement reduces inefficient operating conditions for the diesel generators whereas the maximum loading limit provides them with an extra operational margin to perform the grid-forming task irrespective of the intra-time-step variations during the actual system operation. For the derived power outputs in each time-step, diesel fuel consumption ($fuel^t_{DG_n}$) and the CO_2 emissions (E_{DG_n}) of n^{th} diesel unit is deduced using (3.9) and (3.10), respectively [19], [42]:

$$fuel^t_{DG_n} = (F_{0_n} \times DG_n^{Rated} + F_{1_n} \times P^t_{DG_n}) \times U^t_{DG_n} \times dt \tag{3.9}$$

$$E_{DG_n} = \sum_{t=1}^{T} \left(fuel^t_{DG_n} \times f_{CO_2} \right) \tag{3.10}$$

where F_{0_n} is the generator fuel curve intercept coefficient, F_{1_n} is the generator fuel curve slope, DG_n^{Rated} is the rated capacity, and f_{CO_2} is the CO_2 emission factor for diesel fuel.

The total operating cost of an online diesel generator was represented using the fuel cost, O&M cost, start-up cost [64], and the carbon penalty cost incurred at each time-step as given in (3.11) - (3.15):

$$Cost_{DG_n} = \sum_{t=1}^{T} (Cost_{fuel_n}^t + Cost_{O\&M_n}^t + Cost_{start_n}^t + Cost_{cp_n}^t) \tag{3.11}$$

$$Cost_{fuel_n}^t = fuel_{DG_n}^t \times c_{fuel} \tag{3.12}$$

$$Cost_{O\&M_n}^t = \left(U_{DG_n}^t \times dt\right) \times c_{O\&M} \tag{3.13}$$

$$Cost_{start_n}^t = \alpha_n + \delta_n \times \left(1 - e^{-\frac{T_{off_n}^t}{\tau_n}}\right) \tag{3.14}$$

$$Cost_{CP_n}^t = E_{DG_n}^t \times c_{cp} \tag{3.15}$$

where c_{fuel} is the fuel cost rate, $c_{O\&M}$ is the O&M cost rate, α_n is the hot start-up cost, δ_n is the cold start-up cost, τ_n is the cooling time constant, $T_{off_n}^t$ is the duration between last shutdown and current start, and c_{cp} is the CO_2 penalty rate.

3.4 Proposed Operation Optimization Framework

In this section, the proposed optimization problem formulation method is discussed. As depicted in Figure 3.2, it consists of an optimizer algorithm (ex: PSO or GA) to generate the candidate solutions in each iteration, a plant model, and the objective function, where F_{obj} is the objective function, $x^{t..T}$ denotes the set of independent optimization variables, and $x_{dependent}^{t..T}$ represents the dependent variables. The current system status and the updated load and resource forecasts for the projected control horizon ($t..T$) are obtained as the main inputs. The plant model consists of a pre-processing unit and the individual component models developed in Section 3.3. The inclusion of the pre-processing unit is a novel feature which serves two main purposes, reducing the optimization problem size and bringing the diesel generators' loading to their optimum range.

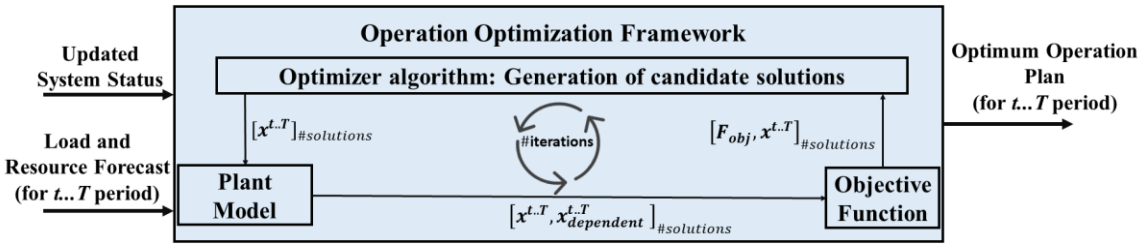

Figure 3.2 Operation optimization framework

To achieve this, for all the candidate optimization solutions ($\#solutions$) in an iteration, only the battery power commands for the considered control horizon ($P_{Bat}^{t..T}$) is defined as an independent optimization variable while maintaining the rest of the system variables as dependents based on steady state power balance, conversion stage efficiencies, capacity limits, and the adopted dispatch strategy. Also, to derive the diesel commitment while achieving optimum loading levels, the pre-processing unit is equipped with the algorithm shown in Figure 3.3. This method allows the optimization problem to be formulated with only continuous optimization variables while omitting discrete optimization variables such as the diesel commitment commands, which reduces the complexity of the optimization task.

1 ***Start***
2 $P_{DG_1}^t,..,P_{DG_n}^t,..,P_{DG_N}^t = 0$
3 $U_{DG_1}^t,..,U_{DG_n}^t,..,U_{DG_N}^t = 0$
4 $P_{net}^t = P_L^t - P_{PV_{AC}}^t - P_{Bat_{AC}}^t$
5 ***For*** $n = 1\ to\ N$ ***Do***
6 $DG_{\max_n}^{Cap} = DG_n^{Rated} + \eta_{inv} \times \min[(B_{maxd}^t - U_d^t \times P_{bat}^t), R_{inv}] - P_{Limit}^t$
7 ***If*** $\left(P_{net}^t \le DG_{max_n}\right)$ & $\left(P_{net}^t > DG_{min_n}\right)$ & $\left(P_{net}^t \le DG_{max_n}^{Cap}\right)$
8 $U_{DG\,n}^t = 1,\ P_{DG_n}^t = P_{net}^t$
9 ***Go to*** *Step* 12
10 ***End If***
11 ***End For***
12 ***Stop***

Figure 3.3 Proposed algorithm for derivation of diesel generator set-points for a given time-step

In Figure 3.3, the available N number of diesel units are evaluated in the ascending order of their rated capacity (DG_n^{Rated}). Also, it is assumed that the net generation required from the diesel plant (P_{net}^t), as derived in Step 4 in Figure 3.3, can be adequately met by

the operation of a single generator, which is generally true for the remote power systems. In Step 4, $P_{PV_{AC}}^{t}$ and $P_{Bat_{AC}}^{t}$ stand for the available solar power and battery power referred to the AC side in time-step *t*, respectively. In Step 6, $DG_{max_n}^{Cap}$ derives the maximum loading level that can be safely supplied by a given diesel unit while accounting for its own rated capacity, required minimum operating reserve level (P_{Limit}^{t}), and the dispatchable reserve supplied by the battery unit. In Step 6, η_{inv} and R_{inv} stands for the inverter efficiency and rated power, respectively. In Step 7, DG_{min_n} and DG_{max_n} are the minimum and maximum loading margins of the diesel unit, respectively. Thus, only the lowest rated generator that can supply P_{net}^{t} while satisfying the system constraints is committed. This algorithm can also be generalized for multiple PV and storage units via appropriately deriving the respective power outputs delivered to the AC side in Step 4 and accounting for the dispatchable operating reserve available from each storage unit in Step 6.

The objective function formulated in this thesis is unique in the sense that it incorporates multiple operational requirements related to remote power systems such as reducing operating costs, emissions, diesel generator starts, battery degradation, and renewable energy spillage. The objective function is defined using the weighted sum method to convert the multiple objectives to a single objective problem as shown in (3.16) [65]:

$$F_{obj} = (w_C \times \frac{Cost_{tot}}{B_C} + w_E \times \frac{E_{tot}}{B_E}) \times PF \tag{3.16}$$

where $Cost_{tot}$ is the total system costs, E_{tot} is the total CO_2 emissions, B_C and B_E are the average values used to normalize each term whereas w_C and w_E define their relative significance to the overall objective function, and *PF* is the imposed penalty factor.

E_{tot} is assumed to be entirely due to the operation of online diesel units as calculated in (3.10). $Cost_{tot}$ is defined as given in (3.17):

$$Cost_{tot} = Cost_{DG} + Cost_{Bat} + Cost_{spill} + Cost_{SOC}^{penalty} \tag{3.17}$$

where $Cost_{DG}$ is the diesel plant operation cost, $Cost_{Bat}$ is the battery degradation cost, and $Cost_{spill}$ is the lost income due to energy spillage which is defined as a penalty

cost. $Cost_{SOC}^{penalty}$ is a penalty cost imposed to keep the battery SOC value at the end of the control horizon higher than a pre-defined margin by penalizing scenarios violating this condition as in (3.18):

$$Cost_{SOC}^{penalty} = U_{SOC}^{Boundary} \times (c_{SOC}^{penalty} \times \left(1 - \frac{SOC^T}{SOC^B}\right)) \tag{3.18}$$

where SOC^T is the SOC at the end of control horizon, SOC^B is the SOC margin, $c_{SOC}^{penalty}$ is the imposed penalty cost rate, and $U_{SOC}^{Boundary}$ identifies the scenarios violating the assigned SOC margin.

The penalty factor used in (3.16) penalizes the violations detected by the plant model for the current control horizon, considering steady state power balance, minimum operational reserve, and the maximum number of starts of diesel units. In the presence of violations, *PF* will differ from unity to a positive value and its magnitude depend on the severity of the detected violations as given in (3.19)-(3.22):

$$PF = PF_{PB} \times PF_{OR} \times PF_{starts} \tag{3.19}$$

$$PF_{PB} = \prod_{t=1}^{T} (1 + c_{PB} \times \left|\frac{P_L^t - P_G^t}{P_L^t}\right|) \tag{3.20}$$

$$PF_{OR} = \prod_{t=1}^{T} (1 + c_{OR} \times \frac{P_{Limit}^t - P_{Rsr}^t}{P_{Limit}^t}) \tag{3.21}$$

$$PF_{starts} = \prod_{n=1}^{N} \left(1 + c_{starts} \times \frac{starts^{DG_n} - starts_{max}^{DG_n}}{starts_{max}^{DG_n}}\right) \tag{3.22}$$

where c_{PB}, c_{OR}, and c_{starts} represent the applied penalty rates. The power balance violation penalty (PF_{PB}) is defined in (3.20) where P_G^t stands for the total generation in time-step *t*. In (3.21), PF_{OR} defines the operating reserve violation penalty where P_{Rsr}^t represents the available operating reserve. PF_{starts} in (3.22) represents the penalty for violating the maximum number of generator starts permitted, where $starts^{DG_n}$ and $starts_{max}^{DG_n}$ represent the actual starts and maximum permitted starts for DG_n.

PSO [66] algorithm is used as the preferred optimizer to generate the candidate optimization solutions, although any other evolutionary computational technique can be applied. PSO uses a randomly initialised swarm of particles in a user-specified solution space to search for the optimum solution by updating their position in each iteration based on personal and cognitive knowledge of the particles. Its well demonstrated competence in handling large set of variables with adequate accuracy and speed, which is evident from the large body of literature that use PSO as the optimization engine for energy management related applications [67], support adopting PSO as the optimization algorithm.

3.5 Study System Description and Data Inputs

To illustrate the applicability of the proposed method, studies were performed on the PV-Diesel-Battery test system derived in Chapter 2. The main external data inputs required for testing the algorithm are the hourly forecasts of load, direct and diffuse solar radiation, and the temperature for the next day. Load forecast was created using sample days taken from historical data. The incident solar irradiation and temperature data for the same sample days were taken through HOMER to create the resource forecast. The minimum operating reserve was defined similar to Section 2.3.2 whereas the corresponding weights were defined as 0.05, 0.1, and 0.3, for the annual peak demand, current time-step load demand and solar power output, respectively. Rest of the main input data used in modelling the system components can be found in Table 3.1. The costs and penalty rates used in the optimization framework is given in Table 3.2. The cost incurred to produce one unit of PV energy was used to charge the spilled energy as given by c_{spill}. For DG_2, $c_{O\&M}$ was set higher than that of DG_1, to ensure that commitment of DG_2 is not a preferred option.

Table 3.1 Input data used in modelling the system components

Renewable energy system	
P_{PV}^{Rated} [kW]	625
F_{PV} [%]	88
α_P [% / °C]	-0.41
R_{inv} [kW]	600
η_{inv} [%]	96
$P_{Bat}^{Rated\_max}$ [kW]	± 600

Bat_{cap} [kWh]	912
SOC_{min} [%]	10
SOC_{max} [%]	100
SOC^{B} [%]	30
Initial SOC [%]	Summer: 50, Winter: 30
E^{tot} [kWh/unit]	45600
η_{bat} [%]	90
Dispatch strategy	Cycle Charging
Diesel generators	
DG_n^{Rated} [kW]	DG_1: 400, DG_2: 800
DG_{min_n} [%]	30
DG_{max_n} [%]	95
$starts_{max}^{DG_n}$	5
F_{0_n} [Liters/hour/kW_{rated}]	DG_1: 0.0299, DG_2: 0.0271
F_{1_n} [Liters/hour/kW]	DG_1: 0.2325, DG_2: 0.2334
τ_n [h]	DG_1: 0.3, DG_2: 0.4
f_{CO_2} [kg/liter]	2.64

Table 3.2 Input values used in the optimization framework

Parameter	Value
c_{spill} [$/kWh]	0.35
c_{rep} [$/unit]	7000
c_{cyc} [$]	100
c_{fuel} [$/liter]	1.1
$c_{O\&M}$ [$/h]	DG_1: 40, DG_2: 100
α_n [$]	DG_1: 20, DG_2: 30
δ_n [$]	DG_1: 20, DG_2: 30
c_{cp} [$/tonne]	25
c_{PB} [$]	20
c_{OR} [$]	15
c_{starts} [$]	10
$c_{SOC}^{penalty}$ [$]	500
w_C [%]	80
w_E [%]	20
B_C [$]	Summer: 1800, Winter: 4000
B_E [kg]	Summer: 2200, Winter: 6400

All the simulated results were computed using the software package MATLAB R2021a considering an hourly time-step and a daily control horizon.

3.6 Results and Discussions

3.6.1 Study cases

Prior to each day, a new set of optimum hourly set-points were generated for the next day 24-hour horizon, based on the forecasts and status of the power system. Simulation experiments were conducted considering three exemplary days in summer and winter seasons. The load and solar power forecasts used for the studied cases considering summer and winter season are shown in Figure 3.4 and Figure 3.5, respectively. For summer, the daily load profiles showed similar trends for the three days and the load varied in the 180 kW-375 kW region. Also, the solar power forecast suggested high availability for the first two days followed by a limited output for the third day. For winter, the load demand showed relatively high values (250 kW – 485 kW) and the forecasted solar power output was significantly lower compared to summer.

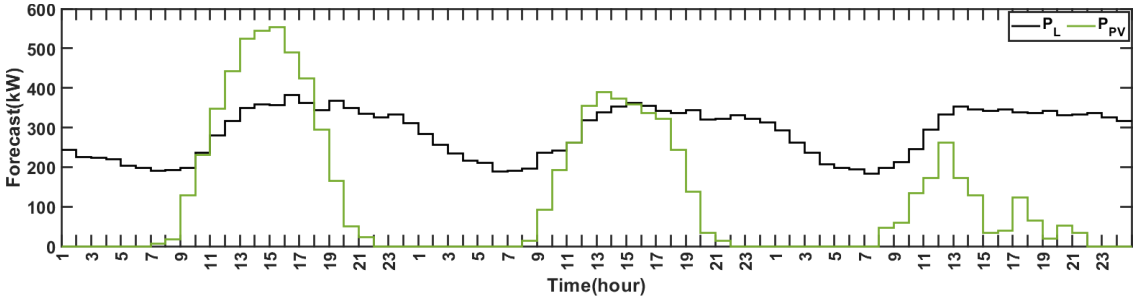

Figure 3.4 Summer: Load and solar power forecasts

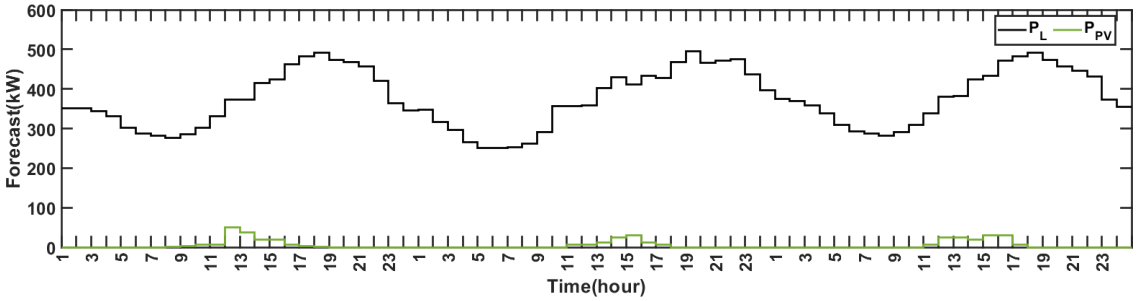

Figure 3.5 Winter: Load and solar power forecasts

3.6.1.1. Existing diesel-only operation

The operation of the existing diesel-only system under the forecasted load demand was analyzed first and the results were used as a source of reference to assess the proposed method. For the existing power system, the commitment of the two diesel generators is assumed to be derived based on engineering judgement. Factors such as the typical diurnal/seasonal load variations, peak demand, and the minimum/maximum diesel loading margins are taken into consideration during the decision-making process and no efforts are made to optimize the system operation.

Due to the prevailing low load demand for summer season, the parallel operation of the diesel generators is usually omitted to alleviate scenarios violating the minimum loading margin for the diesel generators. As given in Figure 3.6, for off-peak period the average-sized generator (DG_1-400 kW) is used to supply the load demand whereas for the peak period the over-sized generator (DG_2-800 kW) is committed. However, in the presence of high load demand in the winter season, parallel operation of the diesel generators is usually exercised for the peak load period, which often results in light-loading conditions for the two diesel generators as shown in Figure 3.7.

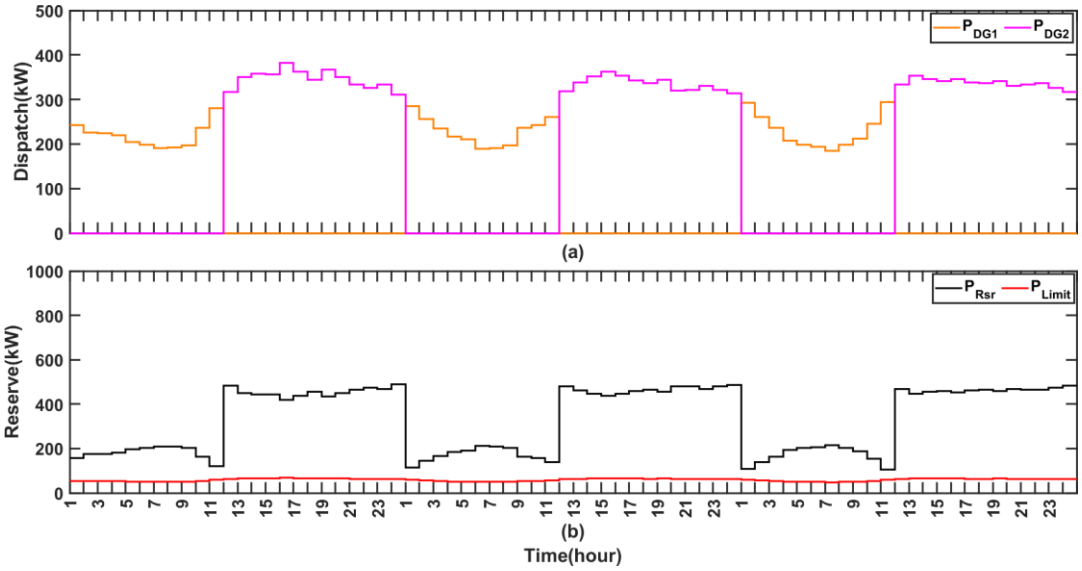

Figure 3.6 Summer - Operational routine for the existing diesel-only operation: (a) Operational routine and (b) Available operational reserve (P_{Rsr}) and minimum requirement (P_{Limit})

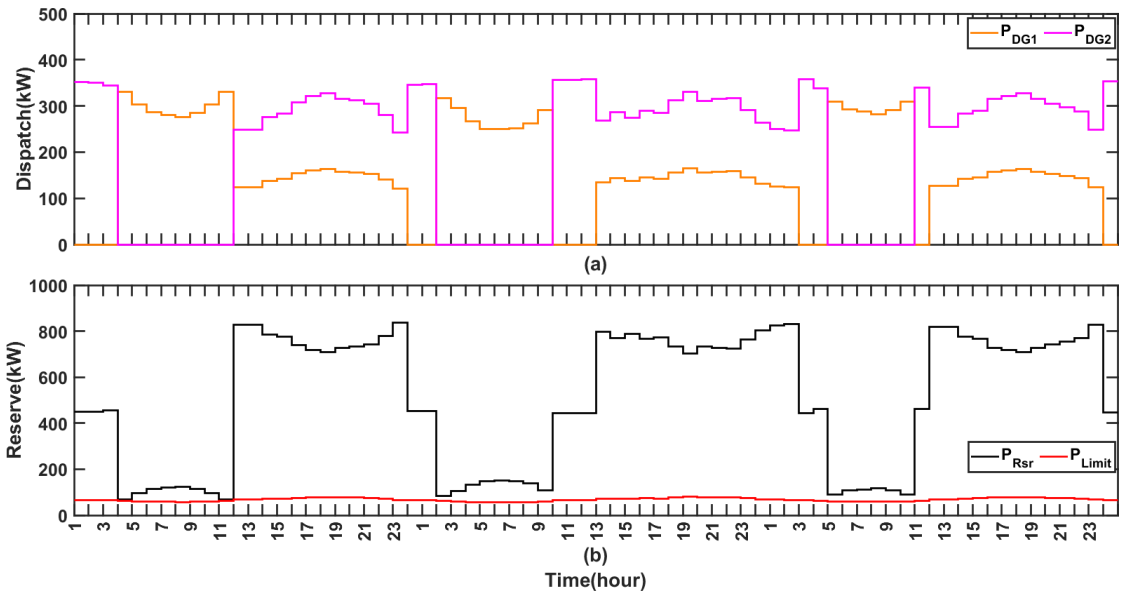

Figure 3.7 Winter - Operational routine for the existing diesel-only operation: (a) Operational routine and (b) Available operational reserve and minimum requirement

Overall, the existing diesel-only operation associated with high daily operational costs and emissions as given in Table 3.3 proved to be highly inefficient for both seasons. In the discussion that follow, the competence of the energy management methods proposed in this chapter in reducing the daily operational costs and emissions as well as in improving the operational efficiency of the system components is examined.

Table 3.3 Results obtained for the existing diesel-only operation

Case	Summer			Winter		
	Day 1	Day 2	Day 3	Day 1	Day 2	Day 3
Total costs [$]	4156	4190	4197	5625	5645	5960
Total CO_2 emissions [kg]	5339	5324	5340	7081	7035	7296

3.6.1.2. Modified diesel-only operation

The applicability of the algorithm demonstrated in Figure 3.3 in enhancing the operational efficiency of the existing diesel-only operation was also examined. The aim was to show how the diesel-only operation can be improved by the reduction of light-loading events, even without the inclusion of renewable components and/or operational

optimization frameworks. Such improvements can be useful for no-sun periods and during events where the renewable energy system is taken out for maintenance.

The modified operational routines derived for the summer and winter season are given in Figure 3.8 and Figure 3.9, respectively. The reduction in daily costs and emissions associated with the modified diesel-only operation compared to the reference case is presented in Table 3.4. For summer season, the modified operation routine was mostly similar to that of the existing diesel-only operation. However, if the power system can be energized pertaining to the operational reserve margin, the 400-kW generator was committed even during the peak load period, as showed in the derived operational routines. For the winter cases, the modified operational routine, successfully derived the commitment of the diesel generators omitting the parallel operation. Due to reduced light-loading events, this operational routine will result in higher efficiency for the diesel generators in contrast to the existing diesel-only operation.

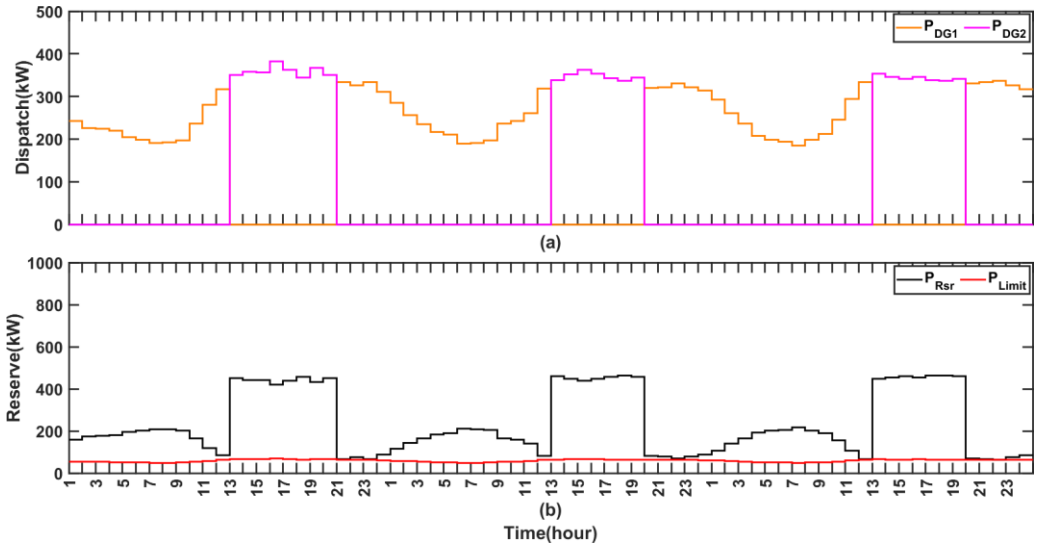

Figure 3.8 Summer – Modified operational routine of the existing diesel-only operation: (a) Operational routine and (b) Available operational reserve and minimum requirement

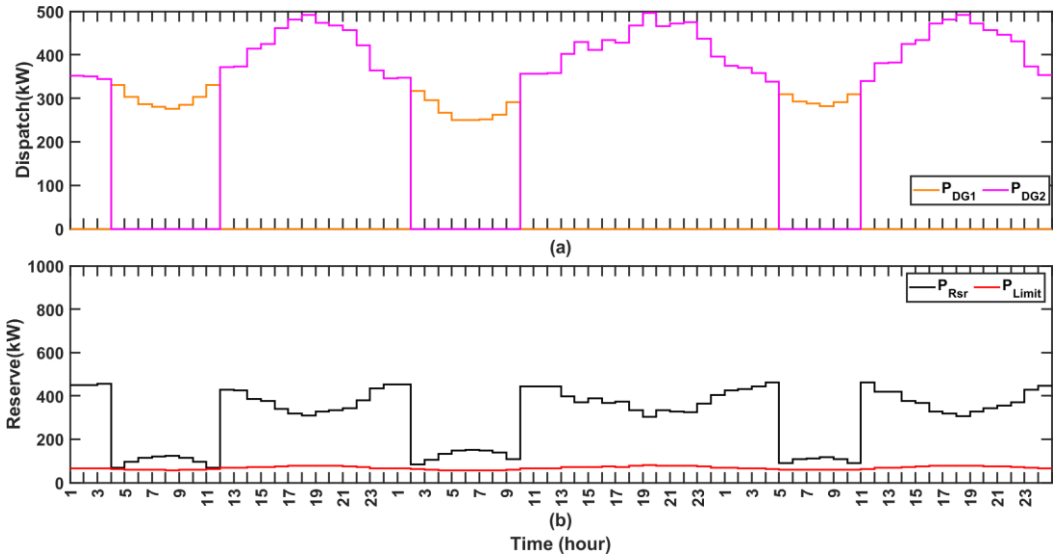

Figure 3.9 Winter – Modified operational routine of the existing diesel-only operation: (a) Operational routine and (b) Available operational reserve and minimum requirement

Table 3.4 Results obtained for the modified diesel-only operation

Case	Summer			Winter		
	Day 1	Day 2	Day 3	Day 1	Day 2	Day 3
Total costs [$]	3838	3759	3767	4980	4960	5167
Total CO_2 emissions [kg]	5207	5165	5181	6706	6660	6859

3.6.1.3. HRES operation under the proposed operation optimization method

Figure 3.10 and Figure 3.11 depict the optimized operation routines derived for the PV-Diesel-Battery configuration for summer and winter seasons, respectively. The PV power forecasts for the considered summer and winter cases are showed in Figure 3.4 and Figure 3.5, respectively. The incurred daily operational costs and CO_2 emissions are given in Table 3.5. A breakdown of energy supplied by each applicable system component in supplying the AC load as well as to charge the battery is presented in Table 3.6.

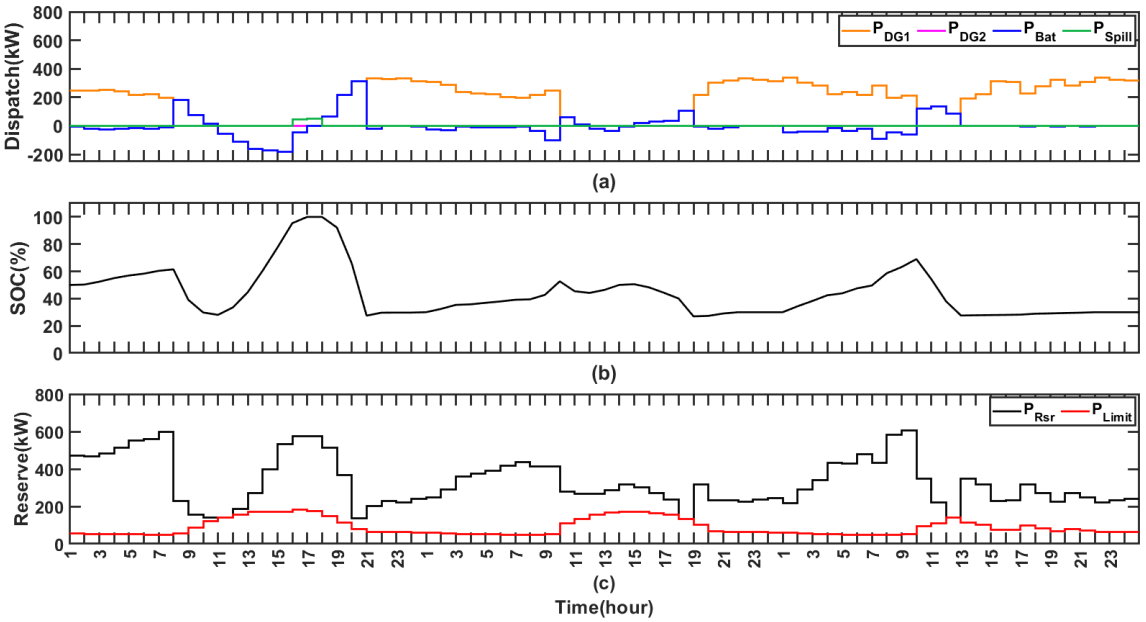

Figure 3.10 Summer - Optimum operational routine of the HRES: (a) Operational routine, (b) SOC, and (c) Available operational reserve and minimum requirement

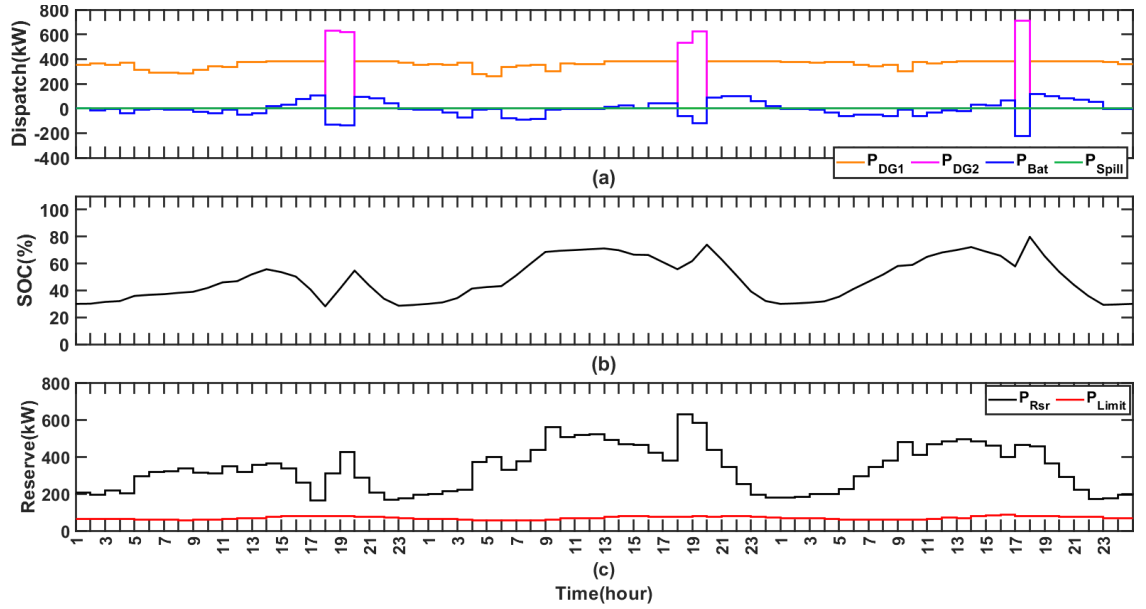

Figure 3.11 Winter - Optimum operational routine of the HRES: (a) Operational routine, (b) SOC, and (c) Available operational reserve vs minimum requirement

Table 3.5 Results obtained for the optimized HRES operation

Case		Summer			Winter		
		Day 1	Day 2	Day 3	Day 1	Day 2	Day 3
Total costs [$]		1680	1973	2804	4066	4084	4085
Total CO_2 emissions [kg]		2146	2900	4177	6335	6334	6434
Diesel costs [$]		1427	1920	2724	3977	3976	3959
Battery degradation costs [$]		220	53	80	89	108	126
Energy spillage penalty costs [$]		33	0	0	0	0	0
Penalties		-	-	-	-	-	-
Reduction compared to the existing diesel-only system	Costs [%]	59.5	52.9	33.2	27.7	27.6	31.5
	Emissions [%]	59.8	45.5	21.7	10.5	9.96	11.8

Table 3.6 Breakdown of energy supplied by each component

Case		Summer			Winter		
		Day 1	Day 2	Day 3	Day 1	Day 2	Day 3
AC load contribution from each source [kWh]	DG_1	2808	3818	5412	7557	7401	8074
	DG_2	0	0	0	965	963	482
	PV	3255	2801	1161	45	83	85
	Battery	835	253	326	423	467	511
Battery charging energy at the DC bus [kWh]	DG_1	115	124	290	172	405	387
	DG_2	0	0	0	268	184	216
	PV	757	200	129	103	12	54
Spilled solar energy [kWh]		94	0	0	0	0	0

After integrating PV and energy storage and optimizing the system operation, significant cost and emission reductions were achieved compared to the existing diesel-only power system for the considered distinct summer days as given in Table 3.5. For example, for the first summer day, these cost and emission reductions were estimated to be

59.5% and 59.8%, respectively. Large amount of solar energy was optimally utilized with the aid of BESS and the optimum initiation of transitions in between diesel-in (Gensup) and diesel-out (Isolated) modes of operation. For days with high solar power availability, the operation routine suggested longer periods of Isolated mode, which helped in reducing minimum loading violations for the diesel generators as well as in minimizing the spilled energy. During the suggested Gensup modes, power system was energized using DG_1 while omitting the light-loading events for DG_2. The system costs mainly comprised of the diesel costs for all three days. An energy spillage penalty cost was detected for the first day due to a prolonged energy excess period.

After integrating PV and energy storage and optimizing the system operation, the considered winter days also showed reduced costs and emissions compared to the reference diesel-only case as given in Table 3.5. For example, for the first winter day, these cost and emission reductions were estimated to be 27.7% and 10.5%, respectively. However, the reductions were not that promising due to the lower availability of freely-available solar energy during winter. Thus, the observed costs and emission reductions were mainly due to the optimized operation of the diesel generators facilitated by the battery unit. For the considered study cases, the operating hours for DG_1 got increased while reducing the light-loading operations of DG_2. Also, compared to results obtained in Section 3.6.1.1 and Section 3.6.1.2, both generators have showed high loading levels allowing them to operate with increased efficiency. The required operating reserve has been mostly supplied through the BESS, energy of which will be consumed at the end of the day within the imposed operational constraints confirming the optimum operation plan. Similar to summer, major part of the daily system costs was incurred due to the diesel generator operation. Battery degradation costs also showed relatively higher values due to their increased utilization in optimizing the diesel generator schedule.

Based on the overall analysis, it was observed that the proposed operation optimization framework is competent in achieving the intended quantitative objectives of energy management. For all the analysed scenarios, the daily costs and emissions were minimized while adhering to power balance, operational reserve margins, and individual component limits. Also, the optimum commitment of diesel generators while alleviating their light-

loading events and the careful utilization of the BESS as revealed by the presented results would result in strengthening their efficiency and longevity of operation.

In winter, as the peak load ranges near the regular-sized generator capacity (400 kW), even small reductions in peak load could be useful to operate the power system without using the 800 kW generator. Thus, reduction of peak loading events is desired. For summer, the correlation between demand and the available solar resource can be increased to further minimize the energy spillage.

3.6.2 Validating predictive operation optimization compared to a non-predictive energy balance approach

To demonstrate the benefits of predictive energy management, a comparison was made with a non-predictive energy balance approach for a summer day with high solar power availability and relatively lower load demand as shown in Figure 3.12(a). HOMER software, which is a tool used for design optimization, derives set-points of individual equipment through power balance in each time-step. Therefore, the set-points generated by the proposed operation optimization framework was compared with the set-points derived in HOMER software for the considered PV-Diesel-Battery power system as shown in Figure 3.12(b) and Figure 3.12(c), respectively. The operation optimization achieved around 25% operating cost reductions and 35% emission reductions compared to the hourly energy balance approach. With the knowledge of future operating conditions, the day-ahead operation optimization effectively managed the available resources to minimally commit the diesel units with reduced starts and to lessen the energy spillage within the imposed operational constraints. These measures aided to the observed benefits compared to the non-predictive energy balance approach.

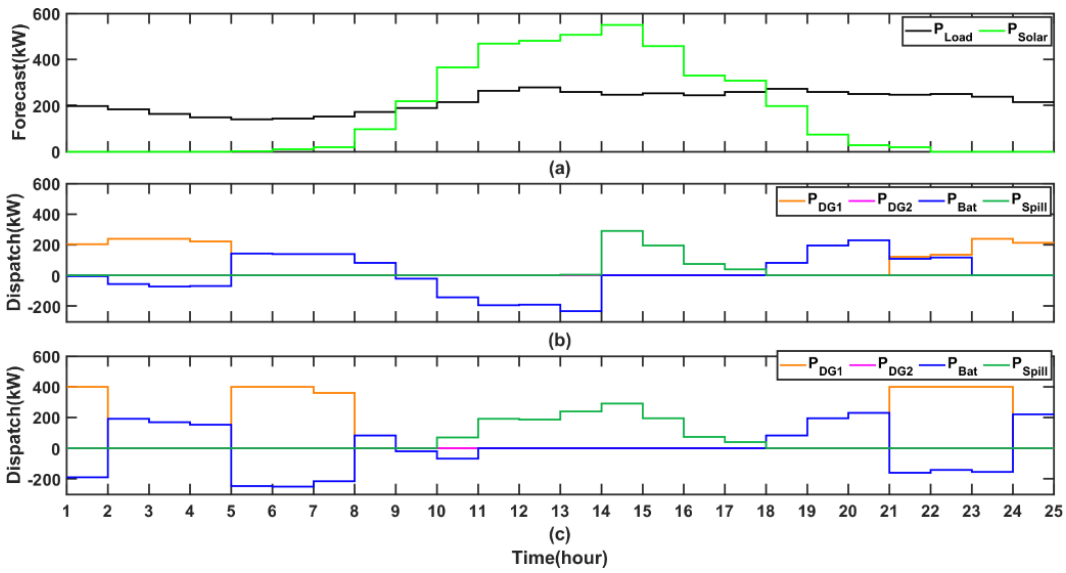

Figure 3.12 Operation routine: (a) Forecasts, (b) Dispatch solution through predictive day-ahead operation optimization, and (c) Dispatch solution through hourly energy balance

3.6.3 Computational efficiency

The optimization framework was modelled as a minimization problem with continuous optimization variables. To evaluate its computational performance, it was solved using the PSO optimization algorithm in a computer with AMD Ryzen 3600 CPU @ 3.6 GHz base (4.2 GHz boost) and 32GB DDR4 RAM @ 3600 MHz. For this set-up, the average computational time taken for a daily control horizon with hourly time-steps was estimated to be around 12.8 s. The computation time taken for a problem formulation deploying both discrete and continuous optimization variables was also assessed. In order to do this, battery power command and the unit commitment commands for the diesel generators were defined as independent optimization variables and the problem was solved using Binary PSO [68] method. When considering the same system set-up, it took an average computational time of 31.3 s to solve the optimization problem under this approach.

The detected improvement of computation efficacy demonstrated by the proposed method can be highly beneficial when integrated with other decision support systems (i.e., incentive optimization in demand response systems, model predictive control algorithms). In such systems, the optimization problem is solved iteratively with varying input

conditions in either day-ahead or intra-day time frame. Also, it might require reducing the duration of control steps in coming to more realistic conclusions. Hence, the lower computation time taken for one trial would benefit the system operator's capability in making decisions promptly and implementing corrective control actions when required.

3.7 Concluding Remarks

This chapter presented an operation optimization framework to achieve a quantitatively optimized operation trajectory minimizing system costs and CO_2 emissions while adhering to multiple operational requirements related to remote off-grid HRESs. The optimization framework was modelled as a minimization problem with continuous optimization variables reducing the computational requirements. The derived operation optimization framework can be used as a subsystem in other supervisory-level decision support systems such as DR integrated EMSs and uncertainty management schemes.

The performance of the proposed method was evaluated for conditions prevailing in summer and winter days. Results revealed the applicability of the proposed method in minimizing the costs and emissions associated with the existing diesel-only power system. Utilization of the BESS was managed to lower its degradation while optimally deriving its set-points to operate as an energy source, energy sink, and a source providing dispatchable operating reserve. The overall methodology allowed the diesel units to achieve optimum loading levels while omitting inefficient light-loading scenarios. Also, a comparison conducted with a non-predictive hourly energy balance approach validated the ability of the predictive EMS in achieving optimized operational routines. In addition, the proposed method showed around 50% reduction in average computation times compared to a problem formulation deploying both discrete and continuous optimization variables.

Chapter 4

A Day-ahead Demand Response Integrated Energy Management Scheme

4.1 Introduction

Demand response strategies play an important role providing an extra degree of freedom for the energy management task. From the customers' point of view, DR is a profitable trade-off between their comfort and electricity bills. From the utility perspective, DR is an effective way of reshaping the consumer load profile.

In this chapter, the operation optimization framework developed in Chapter 3 will be integrated with a DR scheme for reshaping the consumer load profile in order to maximize the intended benefits of operation optimization. A novel methodology to determine the best time-of-use electricity rate structure to achieve the desired load profile with minimal bi-directional utility-consumer interactions is proposed. It minimizes communication requirements by employing a model to quantify the DR flexibility of a given population of electrical consumers. In the proposed model, both deterministic and stochastic uncertainties prevailing in the consumer decision making process is realized using Probabilistic Fuzzy Inference Systems (PFISs). The proposed method is demonstrated separately for the conditions prevailing in the winter and summer seasons, using the PV-diesel-battery remote off-grid power system developed in Chapter 2.

4.2 Background and Literature Review

The anticipated success of DR programs highly relies upon the participation and the interest of consumers to respond towards the respective motivation factors and on the availability of different appliances, loads of which can be shifted, increased, or reduced without causing discomfort to the user. DR frameworks can be implemented mainly using three popular strategies namely, peak clipping, valley filling, and load shifting [16]. Peak clipping is a direct load control technique normally initiated at the expense of customer satisfaction in order to cut down excessive peak loading levels. Valley filling on the other hand fosters the adoption of off-peak energy consumption. Load shifting is a shift of a particular load demand between two timeslots inside the control horizon. When implementing peak clipping/valley filling, the total forecasted energy usage of a customer can get reduced/increased at the end of the control period. However, under load shifting, the total predicted energy consumption remains unchanged [16], [17]. Proper identification of factors related to the specific DR integrated market/system model such as the trigger factor (i.e., cost-based, reliability-based, emission-based), targeted customers (i.e., commercial, residential), control (i.e., direct load control, passive load control), consumer motivation method (i.e., price-based, incentive-based), supporting infrastructure etc. is essential for successful implementation [16], [69], [70].

DR related energy management problems are usually formulated either as consumer comfort maximizations or as cost minimizations. The approaches used to solve them generally include game theory, dynamic programming, and convex programming [16]. Many of the existing literature discussing DR programs devise the problem from consumer perspective while using the motivations provided by the electric utilities and the consumer needs as the main inputs [71]–[74]. However, close coordination between both utility-side and consumers is required to enable an efficient utilization of the electric grid as a whole, specially in the presence of intermittent renewable sources. This further requires the supply and demand side to interact with each other, either in day-ahead or intra-day time frame in order to agree upon a win-win solution. In [75], authors have defined the objective to maximize the grid's social welfare which includes the sum of comfort functions of all users minus the cost function of energy providers constrained by the supply capacity of the grid.

The utility and consumer sides interact with each other in a distributed manner and eventually converge to a mutually beneficial solution. Authors in [17] formulate a load shifting based energy management problem as a cost minimization. The results indicate how close coordination between both parties could be beneficial in achieving cost savings. A detailed discussion on similar studies can be found in [16], [69].

However, these studies targeting DR integrated energy management applications have taken full use of the smart grid architecture expanded by the grid modernization efforts. Bidirectional communication platforms and HEMSs consisting of smart meters embedded with Energy Consumption Schedulers (ECSs) can be identified as the main technical drivers facilitating the incorporation of such DR frameworks. Different communication standards have also been used in the Home Area Network (HAN) for the exchange of control and information signals between the HEMS and the controllable devices. A communication layer is also incorporated into the grid to exchange information between the HEMS and the grid-side controller [69].

However, the existing frequent automated and/or human-in-the-loop bi-directional communication schemes thrived by the sophisticated grid infrastructure could cause concerns when trying to deploy them in remote off-grid power systems, which mostly fail to keep pace with the advancements in the communication and/or control frontiers. In such situations, instead of relying on the direct feedback from consumer-side to calibrate the price signal to achieve the utility objective, a possible alternative methodology is to use a model of the responsiveness of the consumers in the process of optimizing the price signal. With adequate amount of data archive, the utility end will have the required resources to perform the computationally complex optimization tasks. The main challenge to realize this methodology is the uncertainties prevailing in the human behavior which cannot be accurately represented in a consumer responsive model.

Estimating DR of consumers is complicated by many factors involving deterministic and stochastic uncertainty prevailing in the real-world scenarios. Several data-driven techniques can be identified in the academic literature which have used Artificial Neural Networks (ANNs) [76], price-elasticities [77], Markov chains [78], fuzzy systems [79], quantile regression [80] to estimate the responsiveness of the electrical consumers in the context of DR. Many of these statistics-based techniques have shown improved

competence for stochastic modelling but have failed to process imprecise data or the cognitive vagueness. On the other hand, techniques involving fuzzy systems adequately captured the uncertainties prevailing in the imprecise data yet failed to handle the randomness frequent in the natural world. Therefore, combining different kinds of uncertainty modelling is advocated to address the shortcomings of these individual approaches. Probabilistic fuzzy logic is one such method which incorporates a unified platform to process both fuzzy and stochastic uncertainties [81].

The survey of the literature revealed the shortcomings of the existing DR related methodologies for practical deployment in remote power systems. Although, probabilistic fuzzy logic emerged as an effective method to overcome some of the highlighted issues, an overall methodology is required to integrate DR modelling into existing EMSs while enabling a more efficient utilization of the grid resources currently available in remote power systems. Also, proper measures must be devised to enhance consumer acceptance and participation in the proposed DR programs.

4.3 Proposed DR Integrated Energy Management Scheme

When considering primarily diesel-based remote power systems, initiation of DR schemes is usually triggered by the power utility to reduce the costs and emissions of operation while ensuring reliability and energy security. Residential customers contain major portion of the electricity consumers in such communities [3], [7].Therefore, the DR schemes are usually formulated to involve them in the load shape improvement task. For most of the primarily diesel-based remote communities, the power supply to residences is limited in size as a measure to prevent using electricity for space heating/cooling. Therefore, the available load types for DR related activities mainly fall under water heating and operating household appliances. Considering the available load types, it is assumed that major load shape improvements cannot be achieved through techniques like peak clipping without causing high customer dissatisfaction. Valley filling is usually accommodated by energy storage devices like rechargeable batteries or plug-in hybrid electric vehicles, which are not currently being used at these remote households. Therefore, load shifting is identified as an ideal method to initiate a DR framework with the available

load types. As load shifting is not highly time dependent, consumers will have increased flexibility to schedule their loads resulting in relatively less user discomfort [17]. A passive load control based DR scheme is structured where electricity customers will be responsible of modifying their electricity use motivated by a price-based motivation factor. The proposed DR integrated energy management platform is depicted in Figure 4.1.

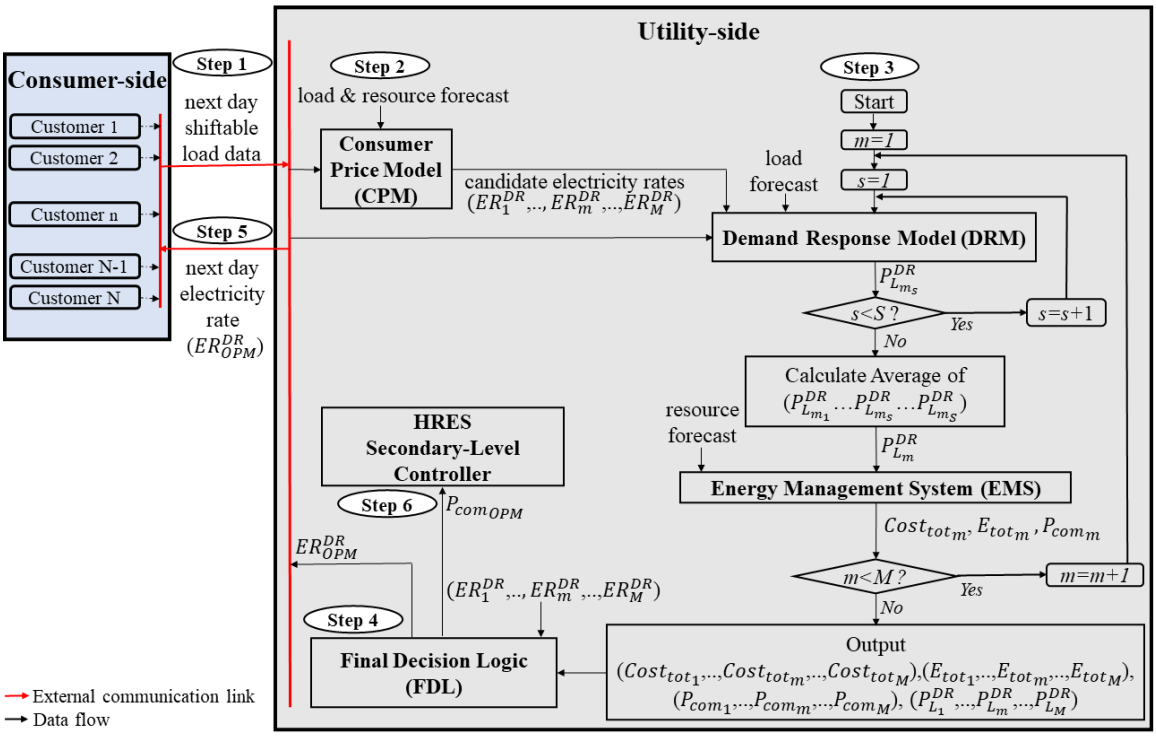

Figure 4.1 Proposed DR integrated energy management scheme

When implementing the DR platform in the day-ahead time frame, the next day shiftable load data is collected from each customer enrolled in the program as the first step and the derived best electricity rate is communicated back to the customer as the final step. Therefore, it does not rely on frequently initiated two-way interactive communication for monitoring or quantifying the DR impact. A simpler and cost-effective one-way communication method initiated twice per day is sufficient to realize its implementation. The required one-way communication is achievable using the already existing and readily available facilities of a remote community such as an online document, mobile app, or a method as simple as a phone call.

The derivation of the best electricity rate to maximize the benefits for both the parties is the joint objective of the sub-modules depicted under the "Utility-side" in Figure 4.1. In Step 2, the Consumer Price Model (CPM) generates *M* number of candidate electricity rates (ER_1^{DR},.., ER_m^{DR},..,ER_M^{DR}) where the subscript *m* is the electricity rate index. For each candidate electricity rate, the Demand Response Model (DRM) estimates the modified load curve which is given by $P_{L_{m_s}}^{DR}$ where the subscript m_s stands for the s^{th} scenario under m^{th} price signal. For each ER_m^{DR}, the operation of DRM is repeated for *S* number of scenarios to estimate an average load curve ($P_{L_m}^{DR}$) to adequately capture the randomness prevailing in the human decision-making process. Next the estimated average load curve, $P_{L_m}^{DR}$, corresponding to ER_m^{DR} is fed to the utility-side EMS which derives the next day operation plan (P_{com_m}) while minimizing the next day operating costs ($Cost_{tot_m}$) and emissions (E_{tot_m}). Once all the *M* price signals are assessed following this procedure, the output of Step 3 will be the minimized operating costs ($Cost_{tot_1}$,..,$Cost_{tot_m}$,..,$Cost_{tot_M}$), minimized emission values (E_{tot_1},..,E_{tot_m},..,E_{tot_M}), optimum operation plans (P_{com_1},..,P_{com_m},..,P_{com_M}), and the modified daily load curves ($P_{L_1}^{DR}$,..,$P_{L_m}^{DR}$,..,$P_{L_M}^{DR}$) corresponding to each ER_m^{DR}. At Step 4, the Final Decision Logic (FDL) is responsible of selecting a mutually beneficial electricity rate (denoted by the subscript "*OPM"*) based on the results obtained at Step 3. This electricity rate will be contracted as the priced-based incentive (ER_{OPM}^{DR}) in Step 5 and the respective power commands ($P_{com_{OPM}}$) will be used as set-points for the next day power system operation in Step 6. The specific functionalities of these individual modules are discussed in Section 4.4.

4.4 Overall Model Development

4.4.1 Utility-side energy management system

The utility-side EMS deploys the operation optimization framework developed in Chapter 3. The quantitative objective is set to minimize the daily operating costs and CO_2 emissions considering a remote off-grid power system energized by a PV-Diesel-Battery HRES as discussed in Section 3.4. The community load and the forecasted resource data

are used as inputs for this sub-module. Based on the inputs, EMS derives the power commands for the diesel generators along with their on/off status and the power commands for battery unit while minimizing the objective function value.

4.4.2 Consumer price model

CPM uses the forecasted load curve, solar resource profile, and the collected shiftable load data as inputs. It derives a set of price signals, each of which to be used as possible candidates to initiate the next day DR scheme. To maintain the consumer participation in the DR scheme, customers willing to shape their electricity usage must not feel penalized in case of unexpected and uneven demand patterns but should mostly feel rewarded relative to their current expenses for electricity usage [79]. To achieve this positive stimulation, the contracted rate is chosen to be either lower or equal to the current electricity rate. When billing the usage, customers enrolled in the DR program for that particular day will be charged at the contracted rate and the rest will be charged at the usual electricity rate. In the long run, more customers will tend to enrol in the DR program seeking rewards for their ideal behaviour. In addition, the derived price signals have to be less dynamic and easily manageable for the homeowners. Frequent alternations of the price signals can make tasks much complicated when managing load scheduling through personal judgement, especially in the absence of automated HEMSs.

Also, it is beneficial to identify the time periods for which these reduced rates should be given to maximize the envisioned benefits of energy management. In the proposed model, an objective load curve ($P_{L_{obj}}^{t..T}$) will be generated and compared with that of the forecasted load curve to identify time periods for which high load accumulations are desired. The reduced electricity rates will be contracted in these time periods and for the rest of the slots, the electricity rate will be kept unchanged from the existing value. $P_{L_{obj}}^{t..T}$ is derived by deploying an operation optimization framework similar to that used in the utility-side EMS. However, in contrast to the EMS optimization framework, CPM is also considering the load demand as an independent optimization variable that can be optimized in minimizing the objective function ($F_{obj_{CPM}}$) as shown in Figure 4.2. However, the solution space of $P_{L_{obj}}^{t..T}$ is limited within a range defined by time dependent constants ($P_{L_{min}}^{t..T}$ / $P_{L_{max}}^{t..T}$) based

on the forecasted load and the next-day shiftable load data received from the consumers participating in the DR program.

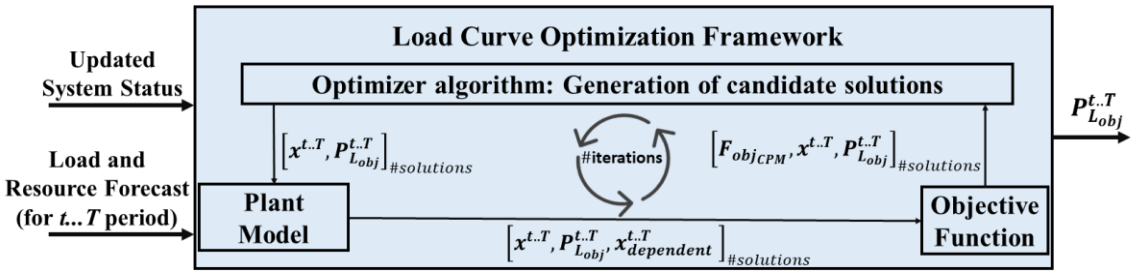

Figure 4.2 Load curve optimization framework deployed in CPM

The objective function used in CPM, $F_{obj_{CPM}}$, minimizes the same set of operating costs and emissions detailed in Section 3.4. $F_{obj_{CPM}}$ is calculated using (4.1) - (4.2):

$$F_{obj_{CPM}} = (w_C \times \frac{Cost_{tot}}{B_C} + w_E \times \frac{E_{tot}}{B_E}) \times PF_{cpm} \quad (4.1)$$

$$PF_{CPM} = PF_{PB} \times PF_{OR} \times PF_{starts} \times PF_{cpm1} \times PF_{cpm2} \quad (4.2)$$

where PF_{cpm1} and PF_{cpm2} are the additional measures used to optimize the load curve, in addition to the factors related to power balance, minimum operating reserve, and maximum generators starts as already discussed in Section 3.4. Through PF_{cpm1}, it is ensured that the total daily energy demand is the same in both forecasted and the optimized cases, assuming that the proposed price-based load shifting scheme does not result in any load curtailments but load shifts. Through PF_{cpm2}, solutions where the shifted energy amount exceeds the total energy available for shifting is penalized. With the added flexibility introduced to the optimization task, it is expected to minimize the objective function value further than that obtained when operating the HRES without DR.

4.4.3 Demand response model

For a given electricity rate and the shiftable load data for each customer willing to participate in the DR program, it is the task of DRM to estimate the updated demand profile. Estimation of the user responsiveness is complicated by various day-to-day factors that might affect the customer's decision apart from the electricity rate and the nature of the

load being considered itself. Thus, to simplify the modelling, the probable response of the customer to increase his/her load in each timeslot is first estimated using the Consumer Responsiveness Model (CRM), irrespective of the underlying characteristics of the shiftable loads. Once the customer responsiveness is determined, the Load Consumption Scheduler (LCS) is used to estimate possible changes to the forecasted load profile due to each shiftable load. The following sections present the main components that constitute the proposed DRM.

4.4.3.1. Consumer responsiveness model

CRM estimates the willingness of the customers to increase their electrical consumption through a fuzzy inference system. The contracted electricity rate (ER_m^t) and customer availability (A_n^t) for the t^{th} timeslot as well as the customer interest (I_n) will be used as the input variables to adequately estimate the response of n^{th} customer to increase his/her load in the t^{th} timeslot (R_n^t). R_n^t is characterized in the range of 0-1 for easy judgement. The linguistic interpretation of the incorporated membership functions under both input and output variables is given in Table 4.1. ER_m^t is the rate at which the customers will be charged for their load consumption for the next day. As detailed in Section 4.4.2, to maintain the user willingness to participate in the DR program, it is assumed that the utility will always retain the contracted price signal to either be equal or lower to the current electricity rate. Therefore, fuzzification of ER_m^t is done by comparing the cheapness of the offered incentive compared to the current electricity rate. The incorporated value range will have to be varied depending on the considered community. A_n^t is a time varying variable which represents the flexibility a customer has to engage in household tasks involving use of participating appliances in a given time-step. A_n^t is characterized in the range of 0-10 and can either be taken as a direct input from the customer or can be guessed based on the resident/residents type considering their occupation, age, family status, etc. For example, a customer who is working full-time during the daytime is less likely to start his/her oven during the working hours. I_n is time invariant and represents the motivation of a given customer to participate in the enrolled DR program. The value of I_n is assigned by the utility operators and ranges from 0-10. Although customers willingly enrolling in a DR program must have an interest towards participating in it afterwards, erratic behavior

patterns are central when considering human nature. Therefore, it is deemed important to integrate this factor to the fuzzy model through this variable, separately from A_n^t. Upon commencement, I_n will be set at a higher value to every enrolled customer and will be updated through continuous monitoring of their DR participation.

Table 4.1 Linguistic interpretation of fuzzy variables

	Fuzzy variable			
	Input			Output
	ER_m^t	A_n^t	I_n	R_n^t
1	Very Cheap (VC)	Low (L)	Low (L)	Very Low (VL)
2	Medium Cheap (MC)	Medium (M)	Medium (M)	Low (L)
3	Less Cheap (LC)	High (H)	High (H)	Medium (M)
4	Neutral (N)	-	-	High (H)
5	-	-	-	Very High (VH)

However, this predominantly deterministic framework is inadequate in capturing the human behavioral patterns as they will not necessarily respond the same way under the same system conditions [81], [82]. Therefore, as discussed in Section 4.2, the proposed fuzzy system will be modified to capture both deterministic and stochastic uncertainties prevailing in the consumer response using a PFIS. PFISs have made the modelling of complex real-world scenarios more realistic via integrating the randomness factor to the conventional fuzzy systems. CRM uses the simple yet effective probabilistic method involving fuzzy rule bases. In each fuzzy rule, the antecedent part remains similar to the conventional fuzzy systems whereas the consequent part is replaced with an array of probabilities, each containing the likelihood of selecting the respective Output Membership Function (OMF). A sample comparison of rule assignment for both conventional and probabilistic fuzzy logic is shown in Figure 4.3 where P_x is the probability of occurrence for a given OMF x. During each attempt, the OMFs of the rule base will be unknown until selected by a random mechanism. In CRM, the Roulette Wheel Selection (RWS) method is used to randomly select the OMF. The mechanism of RWS is given in Appendix C.1.

	Input membership functions			Output membership function
Variable	ER_m^t	A_n^t	I_n	R_n^t
Membership function	MC	H	H	H

(a) Sample assignment of a conventional fuzzy rule

	Input membership functions			Output membership function				
Variable	ER_m^t	A_n^t	I_n	R_n^t				
Membership function	MC	H	H	P_{VL}	P_L	P_M	P_H	P_{VH}
				0.5%	1%	8.5%	80%	10%

(b) Sample assignment of a probabilistic fuzzy rule

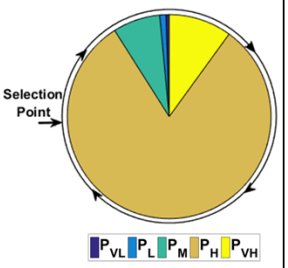

Roulette Wheel Selection

Figure 4.3 Comparion of conventional vs probabilistic fuzzy rule assignment

4.4.3.2. Load consumption scheduler

LCS is responsible of arranging the shiftable loads of all participating customers pertaining to their best interest by searching the daily control horizon for the highest responsive timeslots. The shiftable load data communicated by the customers and the customer responsiveness (R_n^t) determined by the CRM are used as its main inputs. The accuracy of load scheduling is increased by incorporating several generic characteristics of the shiftable loads influencing usual consumer decision making process. It is assumed that the customers can use the utility defined timeslots to mention strict time range preferences for their shiftable loads. Such loads will only be shifted to the preferred timeslots. For an example, consumers usually operate their coffee makers in the morning and for appliances like washer a time range preference is not customary [17]. In addition, for appliances with linked operating schedules such as washer and dryer, the operation of dryer is assumed to be postponed until the washer operation is completed [17]. An example submission of shiftable load data and their associated scheduling by LCS is shown in Figure 4.4. If the customer mentions any preferred time periods, this search will get limited only to a set of timeslots as in the case of load 3 and 4 in Figure 4.4. For each customer, the detected highest R_n^t must exceed a predefined minimum value (R_{min}^{shift}) for the LCS to schedule a

shiftable load to that time-step. This condition relates to the linguistic interpretation that, LCS would not shift loads to time-steps where the customer responsiveness to increase his/her load primarily stays within the "Very Low" or "Low" range.

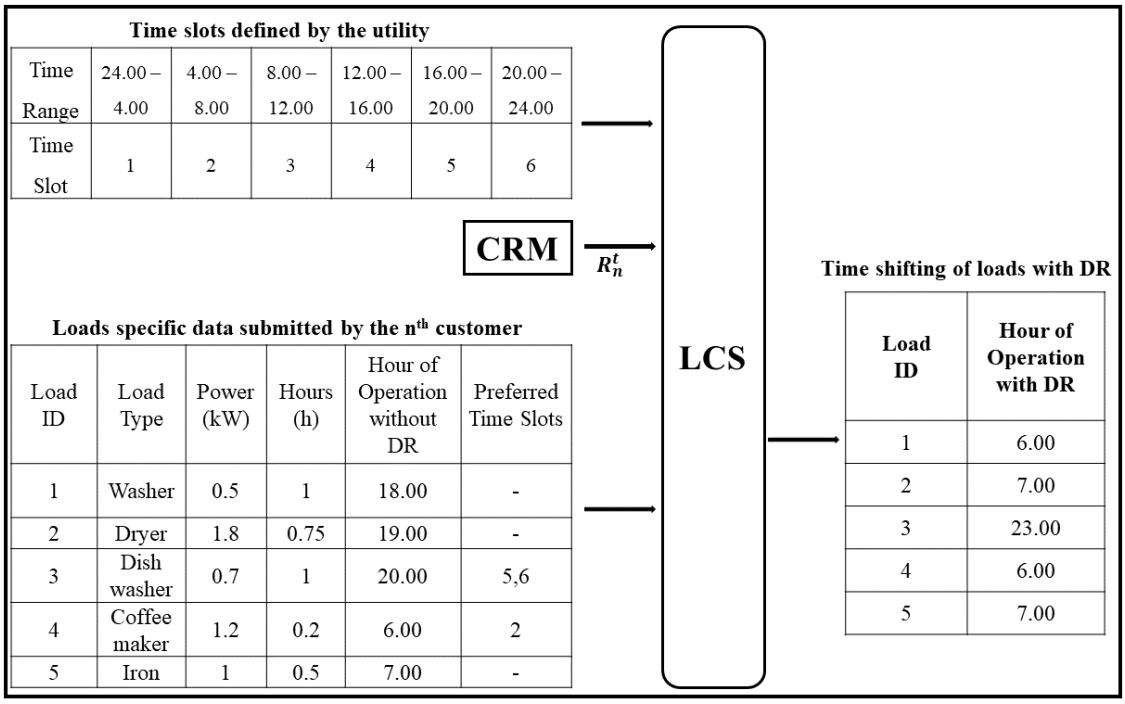

Figure 4.4 An example scheduling of household appliances by LCS

The load shifting achievable due to Electric Water Heaters (EWHs) is also considered. Unlike in the normal household appliances, the operation of EWHs is highly correlated with the diurnal hot water usage patterns which includes direct use of hot water by occupants and the hot water consumption of the household appliances. Based on the studies conducted in past, the hot water consumption has shown a strong dependency on household occupancy and composition [83]. Also, end-uses which involves direct occupant behavior patterns such as baths/showers result in more water consumption than the hot-water consuming appliances with pre-set water consumption cycles such as washers and dishwashers [83], [84]. In this study, occupancy rate and the working hours are used as the main variable characterising the hot-water consumption [83], [84]. In addition, the operation of EWHs is usually governed by an on/off controller to maintain the water

temperature in a pre-specified range [85]. Therefore, the water usage profile and the on/off controller operation must be considered when modelling EWH demand profile.

When integrated with the DR program, only the direct water uses occurring inside a pre-defined tolerance (Δ) before and after the incentive period is considered for shifting. However, the shifting is only done for consumers who show high responsiveness above R_{min}^{shift} within the incentive period. Any direct water usage occurring inside the tolerance band is shifted randomly to a slot in the highest responsive timeslot within the incentive period. Length of this tolerance band is increased depending on the detected highest R_n^t value. Example cases of direct water usage with and without DR scheme is presented in Figure 4.5 for two users falling under similar water usage patterns. In the considered sample case, R_{min}^{shift} is set at 0.5. For R_n^t values in between 0.5-0.8 only a one-hour tolerance is considered whereas for values higher than 0.8 the tolerance is extended to two hours. In Figure 4.5, WP_{Base} and WP_{DR} rows depict the time allocated for direct water usage without and with the DR program, respectively. Compared to User 1, User 2 has shown high responsiveness resulting in a higher tolerance for shifting his/her water usage into the incentive period.

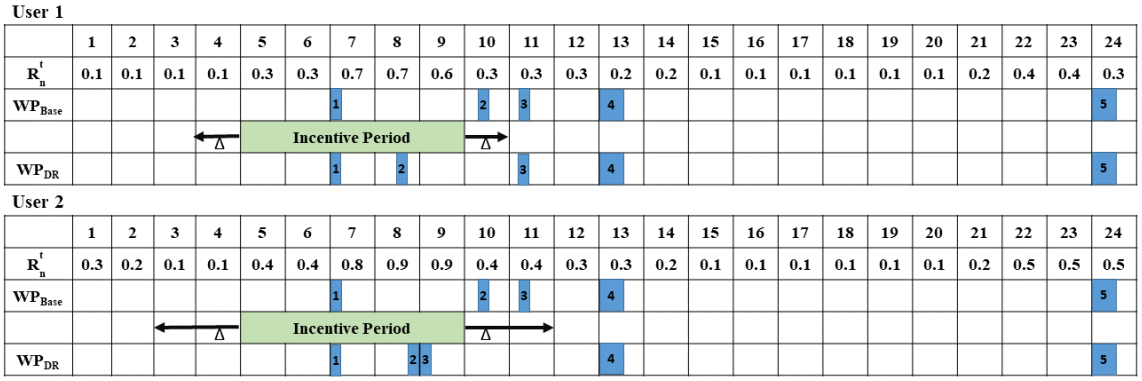

Figure 4.5 An example comparison of time allocation for direct water usage

Finally, WP_{DR} and WP_{Base} along with the associated water flow rates are used to mathematically model the power consumption of the EWHs (EWH^t) governed under an on/off controller for both with and without DR cases as discussed in [85]. EWH^t is calculated as given in (4.3):

$$EWH^t = w_{WH}^t \times \eta_{WH} \times P_{WH}^R \tag{4.3}$$

where w_{WH}^{t} is the status of the on/off controller, P_{WH}^{R} is the rated power of the EWH, and η_{WH} is the efficiency of the EWH.

According to the obtained EWH demand profiles, the load curve is modified to account for the EWH load shifts of individual customers participating in the DR scheme. A more detailed representation of the scheduling process implemented in LCS can be found in Appendix C.2.

4.4.4 Final decision logic

In FDL, the objective function for selecting the best electricity rate is defined using the weighted sum method as in (4.4):

$$F_m^{FDL} = (w_C^{FDL} \times \frac{Cost_{tot_m}}{B_C} + w_E^{FDL} \times \frac{E_{tot_m}}{B_E} + w_{Con}^{FDL} \times \frac{Cost_{Con_m}}{B_{Con}}) \quad (4.4)$$

where $Cost_{tot_m}$ is the daily utility operation costs, E_{tot_m} is the daily emissions, $Cost_{Con_m}$ is the daily consumer costs obtained for a given electricity rate *m* whereas w_C^{FDL}, w_E^{FDL}, and w_{Con}^{FDL} are the incorporated weighting factors. Also, in (4.4), B_{Con} is the average value used in normalizing the consumer costs. $Cost_{Con_m}$ defines the electricity bill of the participating consumers. The candidate electricity rate with the lowest F_m^{FDL} will be selected as the optimum solution (ER_{OPM}^{DR}). Therefore, the adopted decision criterion includes the environmental benefits as well as the cost reductions obtained by utility and consumers to achieve a mutually beneficial result. Finally, ER_{OPM}^{DR} will be contracted to the consumers in the DR program as the next day rate and the respective power commands will be used for the upper-level control tasks of the power system.

4.5 Study System Description and Data Inputs

To demonstrate the applicability of the proposed DR integrated EMS, it was simulated on the same remote off-grid system as modelled and detailed in previous chapters. The community load demand is met by the PV-Diesel-Battery system as derived in Chapter 2. From the utility perspective, the DR scheme would give an extra degree of freedom to

further improve on daily operating costs and emission reductions that is not achievable through an operation optimization scheme as discussed in Chapter 3. Therefore, in the study that follows, the optimized operation routines derived for the considered first day of the summer and winter seasons in Section 3.6.1.3 as depicted in Figure 3.10 and Figure 3.11, respectively, will be used as the reference cases in exhibiting the applicability of the DR integrated EMS proposed in this chapter.

Among the electricity consumers in this territory, 80% falls into the residential category [3], [7]. For most of the diesel-based remote communities in Northern Canada, the power supply to residences is limited in size as a measure to prevent using electricity for space heating [7]. Therefore, houses are heated using either oil or wood furnaces. Also, given the sub-arctic temperatures, there are negligible usage of air-conditioners. Thus, electricity is mainly used for the purpose of water heating and operating household appliances [7]. The data corresponding to the shiftable load components used in this study are given in Table 4.2 [17], [65], [76], [86].

Table 4.2 Shiftable devices data for residential consumers

Load type	Power rating (kW)	Hours of operation (h)
Washer	0.5-1	0.5-1
Dryer	1.2-2.4	0.5-1
Dish washer	0.7-2.4	0.9-1
Oven	1.2-2	0.1-1
Vacuum cleaner	0.4-1.5	0.25-1
Rice cooker	0.85-1.2	0.3-0.5
Iron	1-1.8	0.25-0.75
Coffee maker	0.8-1.4	0.1-0.25
Electric water heater	4.5-6.5	-

When developing the CPM and the utility-side EMS, the input parameters similar to those given in Table 3.1 and Table 3.2 were used. The characterization of the input and output membership functions used in the DRM and the associated fuzzy rule base are given in Appendix C.3 and Appendix C.4, respectively. In LCS, the utility defined timeslots were

assumed to be similar to that shown in Figure 4.4. Also, the definition of tolerance bands used in shifting the direct hot water usage was set similar to the example discussed in Figure 4.5. Rest of the input parameters are given in Table 4.3.

Table 4.3 Input data used in modelling DR-integrated EMS

Participating households	Summer: 80, Winter: 100
Current electricity rate [cents/kWh]	8
Range of price reduction [cents/kWh]	5-8
M	6
S	50
R_{min}^{shift}	0.5
B_{Con} [$]	Summer: 340, Winter: 450
w_C^{FDL} [%]	60
w_E^{FDL} [%]	20
w_{Con}^{FDL}[%]	20

The proposed framework can accommodate the selection of the best-suited electricity rate from a pool of price signals. For ease of comparison, the proposed method is demonstrated using only six price signals. Also, it should be noted that the existing rate itself represents a subsidized value. Therefore, it is assumed that the power utility can only provide price-based incentives in a limited range as given in Table 4.3. Also, it is assumed that the residents in these diesel-based communities are willing to cooperate in order to further optimize their power supply and to achieve increased social welfare.

All the simulated results were computed using the software package MATLAB R2021a considering an hourly time-step and a daily control horizon.

4.6 Results and Discussions

4.6.1 Winter study cases

When analysing the operation plan derived for the first day of winter season without any influence of a DR program, it was identified that the over-sized generator (DG_2) has to operate during the peak load period to meet the demand with sufficient reliability. As

the load ranges in the vicinity of the 400-kW generator (DG_1) capacity, even small reductions in peak load can be useful to operate the power system with either reduced or zero operating hours for the over-sized generator.

As discussed in Section 4.3, first the CPM (Step 2 in Figure 4.1) was deployed to determine the objective load curve and the candidate electricity rates. The derived objective load curve, as shown in Figure 4.6, suggested a scheduling of shiftable loads to the morning and late-night periods reducing the peak load. This resulted in a reduction of the contracted electricity rates for the morning and late-night hours as given in Table 4.4.

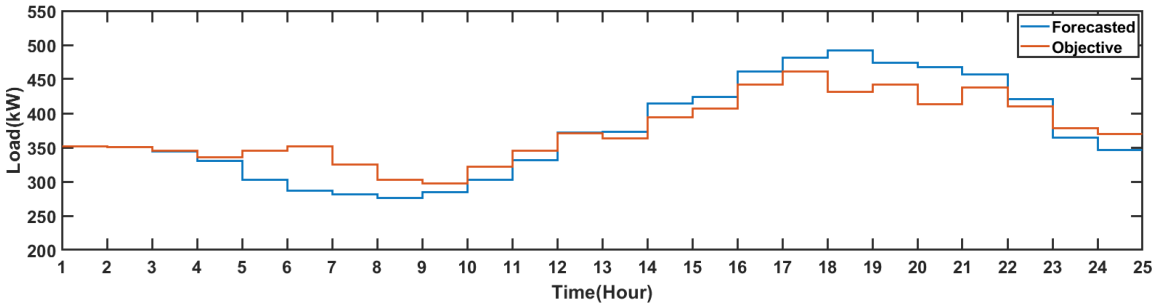

Figure 4.6 Objective load curve for winter day

Table 4.4 Electricity rates in cents/kWh for winter day

	1	2	3	4	5	6	7	8	9	10	11	12	13	14	15	16	17	18	19	20	21	22	23	24
ER_1	8	8	8	5	5	5	5	6	6	6	6	8	8	8	8	8	8	8	8	8	8	8	7	7
ER_2	8	8	8	5	5	5	5	7	7	7	7	8	8	8	8	8	8	8	8	8	8	8	6	6
ER_3	8	8	8	6	6	6	6	5	5	5	5	8	8	8	8	8	8	8	8	8	8	8	7	7
ER_4	8	8	8	6	6	6	6	7	7	7	7	8	8	8	8	8	8	8	8	8	8	8	5	5
ER_5	8	8	8	7	7	7	7	5	5	5	5	8	8	8	8	8	8	8	8	8	8	8	6	6
ER_6	8	8	8	7	7	7	7	6	6	6	6	8	8	8	8	8	8	8	8	8	8	8	5	5

The generated electricity rates were then subjected to the process presented from Step 3 to Step 4 in Figure 4.1. As discussed in Section 4.3, during this process, operation of the DRM constituting both CRM and LCS was repeated a number of times to simulate the random responses of the customers. For better understanding, the proposed method is first demonstrated on an individual consumer. As shown in Figure 4.7(b), this individual show high interest in participating in the DR program. Also, high availability of participation towards household activities is predicted out of the usual working hours and sleeping times.

Figure 4.7(d) shows responsiveness values estimated by the CRM when contracted with ER_1 signal under three attempts with the same input conditions as given in Figure 4.7(a-c). For all attempts, the recorded high response values are visible during the morning hours where the consumer can actively participate in the household activities while claiming the reduced rates. Also, the variations showed for the estimated R_n^t values recorded under different attempts relate to the probabilistic and uncertain nature of the human decision-making process which was captured using the PFIS. This process was repeated for all participating customers and in each attempt, the recorded R_n^t values were used in the LCS to estimate the updated load curve.

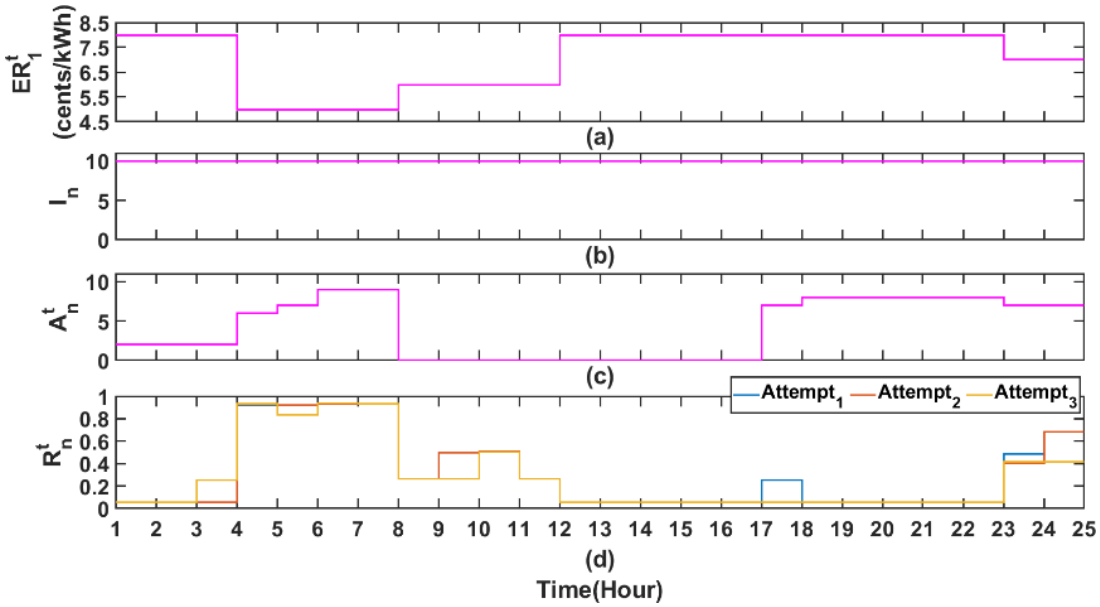

Figure 4.7 Operation of the CRM: (a) Input - electricty rate, (b) Input - customer Intersest, (c) Input - customer availability, and (d) Output - customer responsiveness

Figure 4.8 demonstrates the modified load curves estimated by the DRM under three attempts considering all the participating customers. The observed differences in the obtained DR curves pertain to the stochastic nature of the human behaviour as depicted in Figure 4.7. Also, the estimated demand responses have followed the variations suggested by the objective load curve in relation to the forecasted one. The magnitudes of those changes have varied according to the contracted rates, availability, and interest of the consumers as well as the respective characteristics of their shiftable loads. The average demand curve estimated for each electricity rate is given in Figure 4.9. Table 4.5 presents

a comparison of objective function values calculated by the FDL for each electricity rate. Based on the results, ER_1 with the lowest weighted sum corresponding to utility costs, emissions, and consumer costs was selected as the optimum electricity rate.

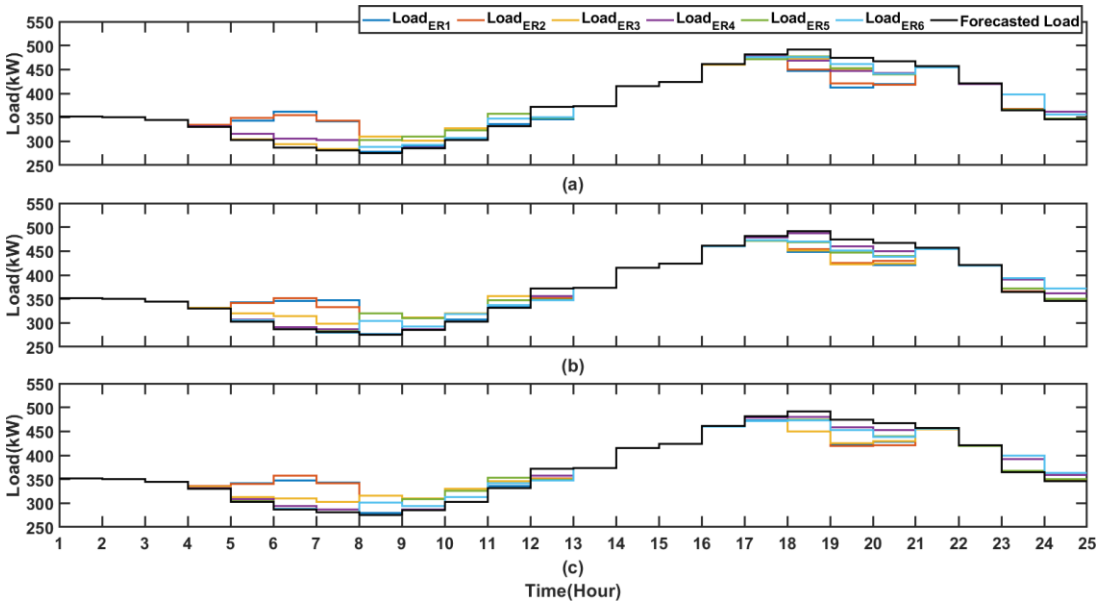

Figure 4.8 Winter day: updated load curves obtained for each contracted electricty rate: (a) Atttempt 1, (b) Attempt 2, and (c) Attempt 3

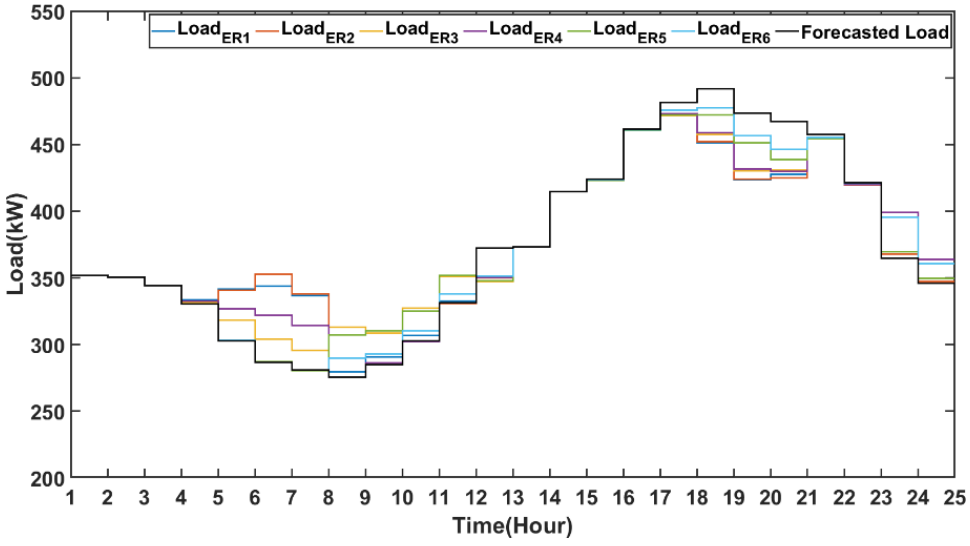

Figure 4.9 Winter day: Average load curves obtained for each contracted electricty rate

Table 4.5 Objective function value under each candidate electricity rate *m* for winter day

m	1	2	3	4	5	6
F_m^{FDL}	0.9680	0.9694	0.9691	0.9734	0.9731	0.9829

The power commands for the next day operation after modifying the load demand with the modifications predicted under ER_1 is given in Figure 4.10. Also, a comparison of results with respect to the without DR case (as discussed in Section 3.6.1.3) is given in Table 4.6. With the anticipated changes in the load profile, the 400 kW generator (DG_1) will be able to energize the power system avoiding the start of 800 kW generator (DG_2). Thus, the observed costs and emission reductions were mainly influenced by the reduced use of DG_2 facilitated by the peak load reduction. Also, compared to the without DR case, the BESS utilization has been increased to support DG_1 in both providing the required operating reserve and supplying the load as reflected in the increased battery degradation costs.

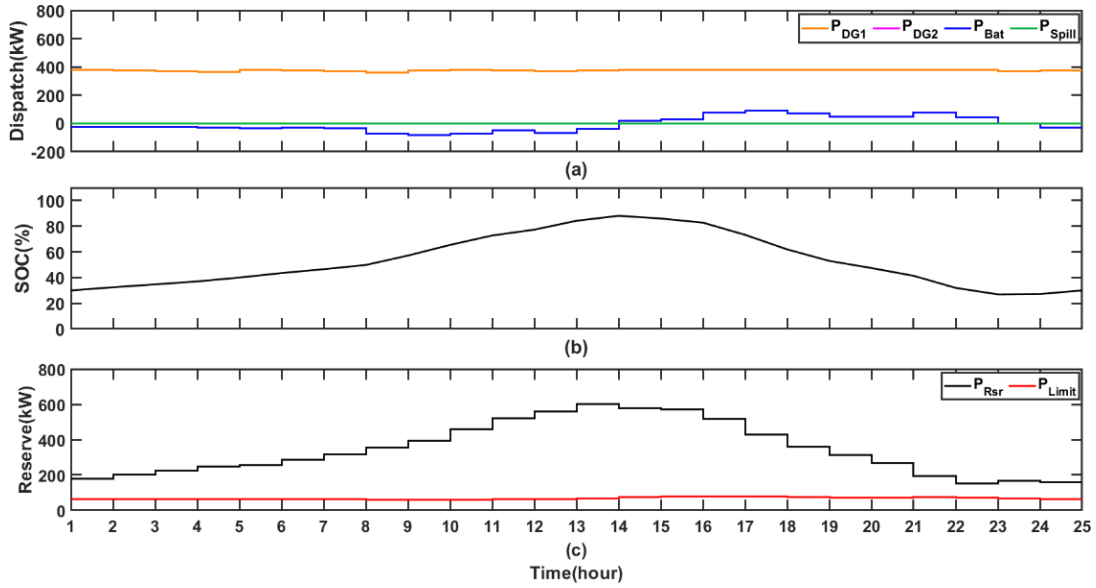

Figure 4.10 Winter - Optimum operational routine of the HRES with DR: (a) Operational routine, (b) SOC, and (c) Available operational reserve and minimum requirement

Table 4.6 Results comparison for the optimized HRES operation with and without DR

	Without DR	With DR
Total utility costs [$]	4066	3868
Total CO_2 emissions [kg]	6335	6294
Consumer costs [$]	480	430
Diesel costs [$]	3977	3738
Battery degradation costs [$]	89	130
Energy spillage penalty costs [$]	0	0
System penalties	-	-

4.6.2 Summer study cases

As revealed through the analysis of the first day summer case depicted in Figure 3.10, part of the available solar energy had to be spilled following an energy surplus period. Thus, for summer with low loading conditions, the main challenge is to reduce the wastage due to the spilling of low-cost and environmentally friendly solar power.

The objective load curve generated using the CPM, is shown in Figure 4.11. The objective load curve suggested a load increase for the afternoon and early evening hours indicating the advantage of increased load and resource correlation. This resulted in reduced electricity rates for the suggested time period as given in Table 4.7.

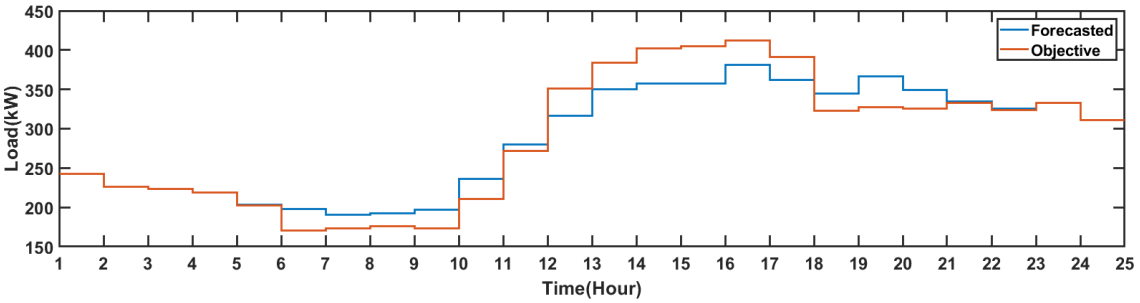

Figure 4.11 Objective load curve for summer day

Table 4.7 Electricity rates in cents/kWh for summer day

	1	2	3	4	5	6	7	8	9	10	11	12	13	14	15	16	17	18	19	20	21	22	23	24
ER_1	8	8	8	8	8	8	8	8	8	8	8	5	5	5	6	6	6	8	8	8	8	8	8	8
ER_2	8	8	8	8	8	8	8	8	8	8	8	5	5	5	7	7	7	8	8	8	8	8	8	8
ER_3	8	8	8	8	8	8	8	8	8	8	8	6	6	6	5	5	5	8	8	8	8	8	8	8
ER_4	8	8	8	8	8	8	8	8	8	8	8	6	6	6	7	7	7	8	8	8	8	8	8	8
ER_5	8	8	8	8	8	8	8	8	8	8	8	7	7	7	5	5	5	8	8	8	8	8	8	8
ER_6	8	8	8	8	8	8	8	8	8	8	8	7	7	7	6	6	6	8	8	8	8	8	8	8

Then, the derived electricity rates were subjected to Step 3- Step 4 in Figure 4.1. The DRM operation was repeated under several attempts similar to winter study cases and the estimated average demand curves for each electricity rate are given in Figure 4.12. A comparison of the FDL objective function values calculated for each rate is given in Table 4.8. Among the candidate priced-based incentives, ER_3 achieved the lowest objective function value and will be selected as the best rate. The next-day power system set-points after modifying the load demand with the modifications predicted under ER_3 is given in Figure 4.13. A comparison of its performance with the reference case is given in Table 4.9. The load conditions influenced under ER_3 allowed the EMS to optimize the system operation while reducing the spilled solar energy by an amount of 73 kWh, aiding to the slight reduction in operating costs and emissions observed in the DR integrated case.

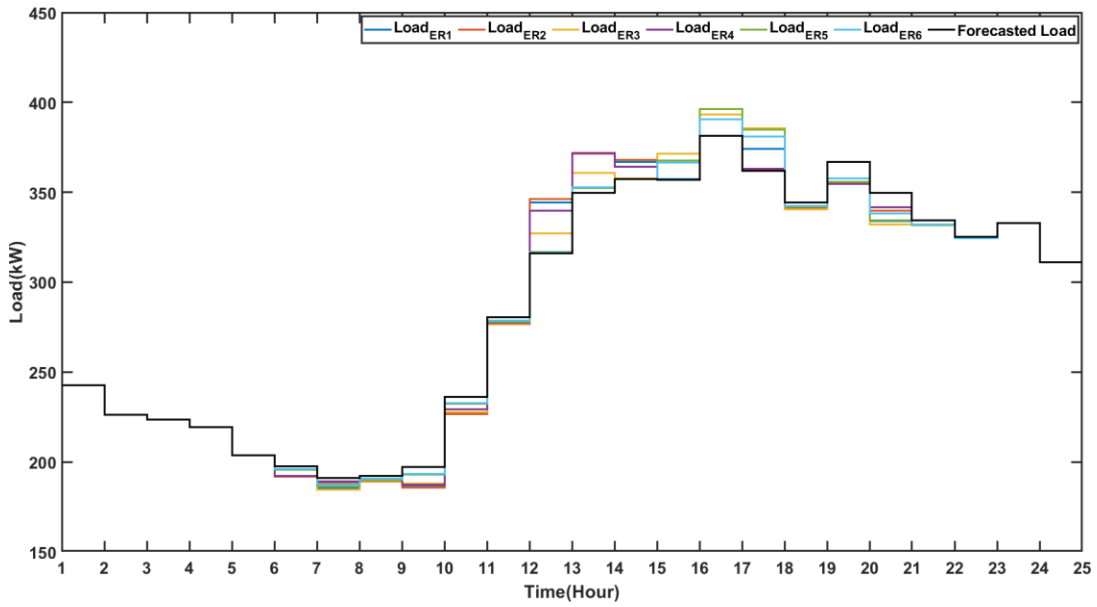

Figure 4.12 Average demand responses for summer day

Table 4.8 Objective function value under each candidate electricity rate *m* for summer

m	1	2	3	4	5	6
F_m^{FDL}	0.9225	0.9326	0.9222	0.9400	0.9428	0.9505

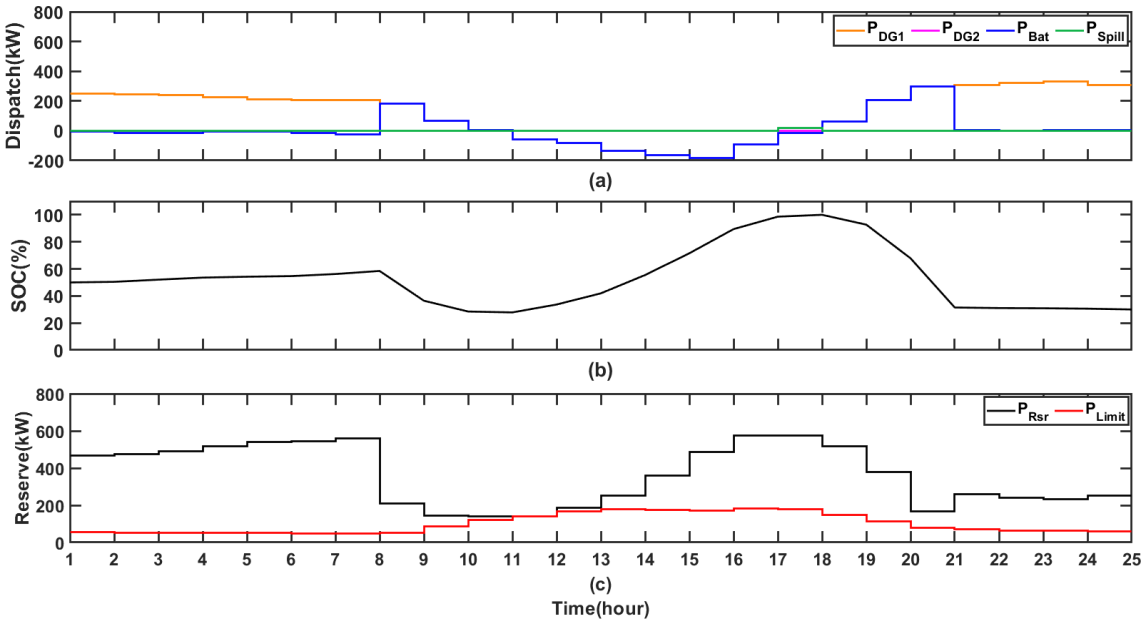

Figure 4.13 Summer - Optimum operational routine of the HRES with DR: (a) Operational routine, (b) SOC, and (c) Available operational reserve and minimum requirement

Table 4.9 Results comparison for the optimized HRES operation with and without DR

	Without DR	With DR
Total costs [$]	1680	1611
Total CO_2 emissions [kg]	2146	2095
Consumer costs [$]	368	331
Diesel costs [$]	1427	1405
Battery degradation costs [$]	220	199
Energy spillage penalty costs [$]	33	7
System penalties	-	-

4.6.3 Overall discussion

When the existing diesel-only system is retrofitted with PV and energy storage and optimized with the proposed DR integrated energy management scheme, 31% costs and 11% emission reductions can be achieved for the considered winter day compared to the diesel-only operation. Also, over 60% cost and emission reductions were achieved for the considered summer day operation. When compared to the optimized PV-Diesel-Battery operation as discussed in Chapter 3, the integration of DR as proposed in this chapter achieved 4.9% costs and 0.6% emission reductions for the winter day. Also, furthering of cost and emission reductions through DR integration was estimated to be around 4.1% and 2.4%, respectively, for the summer day operation.

Although, the overall result confirmed the applicability of the proposed DR integrated energy management framework to further maximize the benefits of operation optimization, the extent of these benefits was limited due to several site-specific externalities minimizing the overall load shifting achieved. Due to the prevailing restrictions, the loads available for shifting is lower than a usual community reference, in both variety and magnitude. Specially, the absence of big power consumption items, such as space heating/cooling loads have affected the performance of the DR framework adversely.

For winter season, operation of both regular-sized and over-sized diesel units are a usual occurrence in the considered power system as shown in Section 3.6.1. Thus, inclusion of a DR scheme can be helpful in further optimizing their commitment in a daily basis. Also, peak load reductions as demonstrated in Section 4.6.1, could pave the way for reduced operating hours and even eventual replacement for the over-sized diesel generators. In contrast to winter season, inclusion of DR did not prove to be much effective for summer season. During summer days, with high solar power availability, the operation cost as well as the spillage of solar energy can be reduced if the system operation can be continued for longer durations without the use of diesel generators in Isolated mode. However, during the Isolated mode, which usually coincides with the energy excess period, the required operating reserve is supplied only by the battery unit. Therefore, the battery SOC at the start of the Isolated mode must be optimized to satisfy both power balance and operating reserve requirements as well as to minimize the spilling of the solar energy,

depending on the forecasted load and resources. However, with the inclusion of DR, the overall load shifting allows the battery unit to initiate the Isolate mode with relatively less energy reserve which results in a slightly higher capacity to absorb the excess solar energy relative to the without DR case. For example, for the with DR and without DR cases, the SOC at the start of Isolated mode was observed to be 58% and 61%, respectively. However, the loads available for shifting were not sufficient to achieve considerable reductions in the spilled solar energy or to further increase the length of the Isolated mode as shown in the example case in Section 4.6.2. Also, these energy excess periods are of low occurrence. Therefore, inclusion of DR would not maximize the benefits of operation optimization on a daily basis compared to winter season.

In addition, it must be noted that the proposed DR modelling framework relies upon the utility-side's knowledge of the underlying power system and its electricity consumers. However, the behavioural characteristics of the participants will not remain static over time. Therefore, to account for the changing user characteristics, the consumer-related inputs and the structured PFIS model parameters must be subjected to regular modifications. Once the DR model is in operation, the utility can constantly update the consumer data archives either manually or using a learning technique to accurately keep up with the changing user characteristics.

4.7 Concluding Remarks

This chapter presented a DR integrated day-ahead energy management framework to maximize the benefits of operation optimization in remote communities. The proposed DR strategy was structured for a price-based program utilizing a simplified communication platform with minimal interactions and rewarding electricity rates. These measures enhance the practicality of the proposed DR framework while influencing an increased customer participation in the long run. Special attention was given to estimate the responsiveness of the consumers to reshape their load profiles using a PFIS. This approach aided the utility-side to realize the best-suited electricity rate while avoiding the communication intensive two-way iterative process found in the conventional DR approaches.

While providing an opportunity for the consumers to lower their electricity bill, the proposed DR model also facilitated the utility-side to minimize the daily operating costs and emissions. The optimized commitment of the diesel units and the increased penetration of solar energy mainly contributed to the observed benefits in the DR integrated case compared to the reference case results. Also, for the considered power system, winter season showed higher benefits associated with DR integration compared to summer. The observed benefits of the proposed method can be further maximized if applied to other remote sites with less restrictions on the available load types.

Chapter 5

Uncertainty Management in Operation Optimization

5.1 Introduction

The operation optimization task can be complicated by the sources of uncertainties mainly rooting through deviations of actual load and resource profiles from the respective forecasts. Deviations of load profile can arise from different sources like weather conditions, community events, and programs pursued by the utility/government. When considering intermittent renewable energy, variations occurring in their primary energy sources (i.e., solar irradiance) and weather patterns can affect the total production. Remote power systems often count on past generation log data and historical meteorological data collected through distant weather stations in generating the load and resource forecasts further increasing the associated uncertainty. In addition, the absence of a strong grid to manage the load balancing task pose several challenges to the optimum energy management of these isolated power systems compared to its grid-connected counterpart. Depending on the required load demand and the freely available renewable energy, isolated networks undergo transitions between the diesel-in (Gensup), and diesel-out (Isolated) modes as discussed in previous chapters. Therefore, optimum scheduling of resources must be achieved while allocating enough reserves for demand-supply balance during both operating modes while coping with the associated uncertainties. In this context, operation

optimization employed with uncertainty management strategies is imperative to ensure a reliable, cost-effective, and secure energy supply for the remote off-grid power systems.

In this chapter, the energy management control layer developed in Chapter 3 and Chapter 4 is reinforced with the uncertainty management capability. A novel hybrid uncertainty management method is proposed utilizing deterministic and stochastic techniques. The proposed method maintains the simplicity of the deterministic techniques and incorporates the effective representation of uncertainties provided by the stochastic frameworks to derive an optimum operation plan in a computationally efficient manner with reduced dependence on frequent updates. The proposed method is demonstrated through numerical experiments for an isolated remote power system for both summer and winter seasons. Quality of the obtained results and the computation efficiency of the overall framework have been verified compared to the existing energy management techniques.

5.2 Background and Literature Review

Different techniques have been proposed in the literature to address the uncertainty issues in optimal multi-resource scheduling. They can be mainly categorized under robust optimization [21], closely-tracked deterministic optimization [22], stochastic optimization [23], [24], chance-constrained optimization [25], and hybridization of these approaches [28], [30]. Their implementation has been carried out in either a single-layered or a multi-layered framework. Many studies [23], [24] have also proposed the inclusion of a pre-defined operating reserve margin to address possible intra-time-step deviations in forecasts in combination with aforementioned uncertainty management techniques.

In robust optimization, a sub-optimal dispatch strategy is formulated by subjecting a single worst-case scenario over an uncertainty set. However, complications associated with the formulation of the uncertainty set may lead to a computationally intractable solution [26]. Also, the prioritization of a worst-case scenario usually leads to a conservative resource-handling solution degrading the achievable benefits [27].

In closely-tracked deterministic optimization, the conventional deterministic framework is unified with a feedback mechanism to adjust the initial dispatch solution to compensate for the deviations occurring in uncertain decision variables. Among the

available feedback mechanisms, Model Predictive Control (MPC) has emerged as a proven technique to handle large set of uncertain variables [12], [29]. In MPC, the decision variables are iteratively adjusted over a finite future time horizon based on the optimization model and most up-to-date forecasts. However, as discussed above, most studies solve the underlying operation optimization problem under deterministic conditions considering predictions averaged over a given time-step. Therefore, even when embedded with MPC, if the intra-time-step variations of the uncertain variables show higher fluctuations, the pre-determined deterministic solution might become infeasible. Therefore, precise implementation of closely-tracked deterministic optimization depends on the frequency of the variable updates which could be quite cumbersome and data-intensive when increased.

As a solution, one can find a single optimum dispatch solution for a finite set of scenarios, which lays the foundation for stochastic optimization [87]. In studies deploying stochastic approaches [87]–[91], uncertainties are contained within the problem formulation as a finite set of possible realizations and the optimization minimizes the expected cost of the formulated objective function. The conventional multi-scenario stochastic approach used in multi-resource scheduling does not consider any recourse actions making the dispatch solutions vulnerable in case of inaccurate representation of uncertainty variables [26]. Also, as the forecast horizon extends, the operation uncertainty increases significantly while degrading the accuracy of the predicted scenarios, which limits attaining realistic conclusions [28]. Studies proposing stochastic MPC strategies can be found in [92]–[94]. However, due to the deployment of multi-scenarios, stochastic approaches often result in a computationally demanding optimization problem [28]. Chance-constrained optimization is another technique to handle uncertainties in multi-resource scheduling [25]. This method also deploys a probabilistic description of uncertainties to the problem formulation and guarantees the probability of satisfying a given constraint above a certain level [30]. However, when deployed with high confidence levels, an accurate representation of uncertainty distributions is required to deliver meaningful results [26].

In this context, multi-layered and/or hybrid uncertainty management methods have emerged as effective alternatives to address the shortcomings of these individual approaches. Authors in [27] have included a two-stage optimization layer to the

conventional MPC approach considering a PV-Diesel-Battery isolated network. The first layer consists of an optimal control problem for the calculation of the power dispatch. The second layer adjusts the diesel generator start/stop time solving a boundary value problem over a shorter control horizon to improve the control robustness towards forecast uncertainties. However, when subjected to varying load and solar predictions, adjusting the diesel generator routine in near-real-time could cause frequent starts/stops which can adversely affect its lifetime. In [26], a stochastic-predictive EMS is proposed for an isolated microgrid. Uncertainty is addressed using a two-stage decision making process. The first stage deploys a stochastic mixed integer linear programming approach to find the commitment whereas a shrinking horizon optimal power flow performs the final dispatch in the second stage. Due to the complexity associated with stochastic programming approaches, the underlying problem is solved using the branch and bound method which can be exponential in terms of time complexity. Also, the proposed approach could undergo potential convergence issues during actual implementation pertaining to different time resolutions and details included in the two-stages. Moreover, this study has not included a minimum deterministic operating reserve requirement in formulating the problem, which is imperative when considering isolated power systems that can undergo scenarios with high renewable penetration and grid-forming modes with no synchronous generation.

A near-real-time stochastic look-ahead dispatch strategy is formulated in [28] where operation uncertainty is mapped to economic risks in order to devise a control horizon division technique. The subjected look-ahead dispatch horizon is decomposed into a deterministic portion and a stochastic portion to minimize the data-intensiveness of a fully stochastic approach. However, due to higher emphasis given for capturing the uncertainties in near-real-time operation, special problem decomposition methods are required to meet the tight time constraints during actual deployment. In [30], authors manage uncertainty concerns of a day-ahead optimal energy trading management problem using a combination of stochastic and robust optimization. A two-stage, stochastic, and p-robust approach is proposed where the benefits of the two techniques are integrated together to find a robust solution with a minimum increase of expected operating cost. A chance-constrained two-stage stochastic method is proposed in [95] to solve the unit commitment problem while maximizing the wind penetration. Sample average approximation method is used to handle

the probabilistic constraints under three different wind power utilization policies. The probabilistic constraints are reformulated as mixed integer constraints. The demonstrated numerical results verify the effectiveness of the proposed approach in maximizing the wind power penetration. However, the complexity of the problem is greatly impacted by the incorporated number of scenarios.

The reviewed studies employing multi-layered and/or hybrid techniques have showed several advantages in the respective contexts when handling optimum multi-resource scheduling under uncertainties. However, developing a cost-efficient, secure, and reliable energy management technique with integrated uncertainty management is a non-trivial task and majorly depends on the system layout, operational constraints, geographic location, weather patterns, capabilities of the lower-level controllers, computational power, as well as the projected objectives of the system operators. To this end, more focus is needed on addressing the issues faced by primarily fossil-fuel based remote off-grid power systems when achieving optimum multi-resource scheduling under uncertainties.

As discussed in Chapter 3 and Chapter 4, in addition to the main objectives such as costs and emissions reduction, the operation optimization frameworks adopt several measures to maximize the envisioned benefits such as allowing safe navigation between diesel in and out operating modes, minimizing inefficient loading events for the diesel generators, minimizing the spilling of available energy, prolonging the lifetime of system components, ensuring energy security etc. However, achieving of these objectives must be ensured while effectively addressing the uncertainty issues faced by remote power systems as discussed in Section 5.1. Also, high reliance on forecasts generated through historical records and data collected from distant weather stations further increases the associated uncertainty. In the presence of quantitatively optimized dispatch solutions generated through such forecasts, confirmation of the logical operation and making corrective adjustments if required is important as further discussed in Chapter 6. Moreover, as this process may be time consuming, adequate amount of time must be leveraged for this purpose. Therefore, the multi-layered and/or hybrid arrangements can be further improved while considering the aforementioned operational requirements pertaining to remote off-grid power systems. Reduced dependency on frequently updated forecasts, feasibility to

implement corrective control actions during actual deployment, simplicity, and computational efficiency can be highlighted as the identified areas for improvement.

5.3 Proposed Two-stage Framework for Operation Optimization under Uncertainties

The proposed operation optimization platform considering uncertainties features a two-stage decision making process as depicted in Figure 5.1.

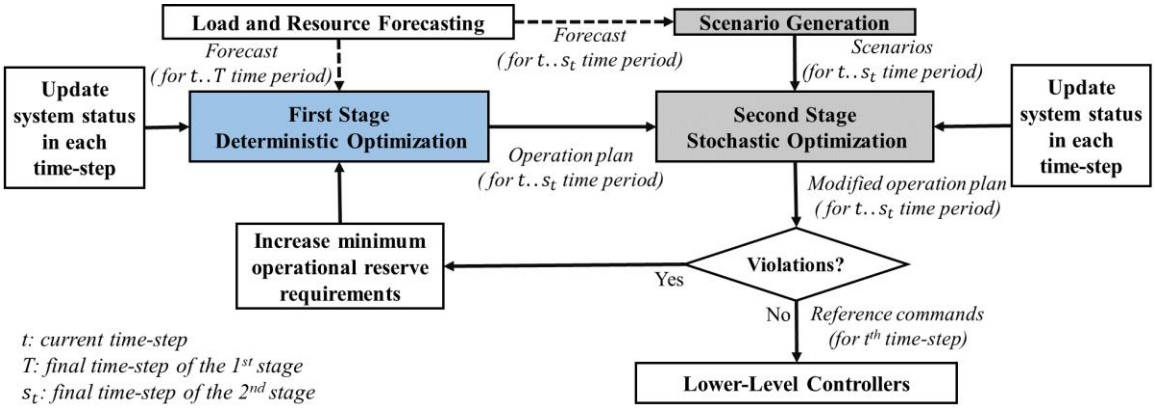

Figure 5.1 Proposed two-stage decision making process

At the start of each time-step t, the first stage solves a deterministic optimization problem to obtain a set of quantitatively optimized unit commitment and dispatch commands based on the current system status and updated forecasts for the considered look-ahead window. The second stage deploys a stochastic optimization layer and adjusts the derived operation plan considering a set of candidate scenarios. The objective of the scenario-based stochastic layer lies on ensuring the reliability and security of system operation. The stochastic problem is solved by optimally adjusting the references of the dispatchable grid-following sources with minimum changes to the unit commitment commands generated by the first stage. For violations that cannot be fixed by the stochastic layer (i.e., depletion of available operating reserves), corrective actions are requested from

the first stage as shown in Figure 5.1. Such corrective measures will initiate a new run of the deterministic optimization layer with increased minimum reserve requirements.

The proposed method deploys two look-ahead windows and is formulated in a MPC framework where only the references for the first time-step *t* is communicated to the lower-level controls of the actual power system and subsequently the control horizons of both stages are shifted by one time-step. There are two main approaches to MPC based on how the control horizon is being shifted namely; the Rolling Horizon method [96] and the Receding Horizon method [12]. The current study focuses on the operation optimization of a daily control horizon and the Receding Horizon MPC technique is deployed in the first stage where the look-ahead window length at the start of a given time-step *x* (L_x) is reduced in each successive control action as shown in Figure 5.2.

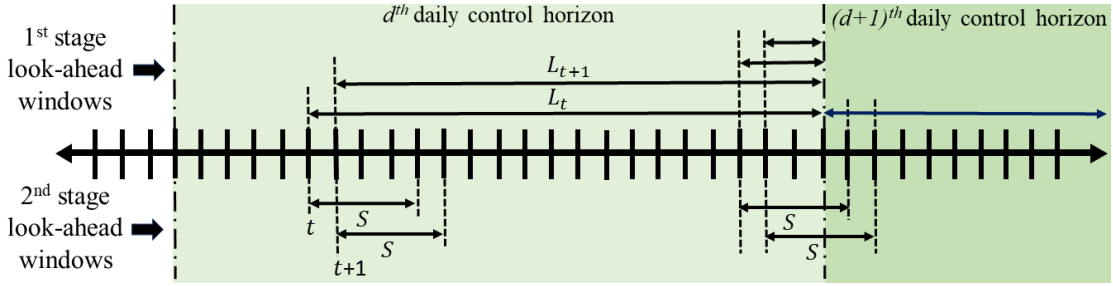

Figure 5.2 Look-ahead windows of the two stages

The second stage uses the Rolling Horizon MPC strategy with a fixed look-ahead window length S, which remains constant in contrast to the first stage. When the length of the first stage horizon gets shorter than S as the day progresses, the next day day-ahead deterministic control commands will also be used to provide reference unit commitment and dispatch information for the second stage as shown in Figure 5.2. Length S can be adjusted to find a better trade-off between quality of results and sub-problem size for the underlying stochastic optimization.

The following sub-sections detail the specific functionalities of each layer considering a PV-Diesel-Battery power system.

5.3.1 Deterministic optimization layer (first stage)

The operation optimization framework proposed in Chapter 3 is embedded into a Receding Horizon model predictive controller to update the unit commitment and dispatch commands in regular intervals as the system progresses and more reliable forecasts are received during the actual system operation.

5.3.2 Stochastic optimization layer (second stage)

Section 5.3.2.1 briefly explains the methods adopted from existing literature to generate the load and solar power scenarios for the stochastic layer. The proposed problem formulation in the stochastic optimization problem is discussed in 5.3.2.2.

5.3.2.1. Scenario generation

The actual Probability Distribution Function (PDF) of the forecasting error of each uncertain variable is approximated as a discrete distribution with a tractable number of finite states with a certain probability. The discretized sets of the respective continuous PDFs can be represented as in (5.1) [23]:

$$\delta_x = \left\{(e_x^1, \mathfrak{p}_x^1), \ldots, \left(e_x^i, \mathfrak{p}_x^i\right), .., (e_x^M, \mathfrak{p}_x^M)\right\} \text{ where } \sum_{i=1}^{M} \mathfrak{p}_x^i = 1 \tag{5.1}$$

where e_x^i and $\mathfrak{p}_x^i$ are the forecasting error and the associated normalized probability of each state, respectively. M is the total number of discrete states.

For each time interval, the developed discrete sets are used to create a set of possible realizations of the uncertain variables along with their associated probabilities using the RWS method as described in [88]. The generic functionality of RWS is given in Appendix C.1. The normalized probability of the n^{th} scenario is derived using (5.2):

$$\rho_n = \frac{\prod_{t=t}^{s_t} \rho_{PV}^t{}_n \rho_{L}^t{}_n}{\sum_{n=1}^{K} \prod_{t=t}^{s_t} \rho_{PV}^t{}_n \rho_{L}^t{}_n} \tag{5.2}$$

where K is the total number of generated scenarios, $\rho_{PV}^t{}_n$ and $\rho_{L}^t{}_n$ are the probability of solar and load forecasting errors for t^{th} time-step of n^{th} scenario, respectively.

After generating the scenarios, it is necessary to remove scenarios with either low probability of occurrence or the ones with many similarities to the rest of the scenarios [87]. Scenario reduction also aids to increase the tractability of the underlying optimization problem. The scenario reduction process proposed in [87] is applied to obtain a total number of $N(<K)$ scenarios to be used in the stochastic optimization layer. The functionality of the deployed scenario reduction process is given in Appendix D.

As the focus of this study lies within the operation optimization, effectiveness of the generated scenarios will not be assessed through their statistical properties, but through the improvement in the overall operation plan. A different scenario generation mechanism can be easily adopted to the proposed stochastic layer.

5.3.2.2. Stochastic optimization

The objective of the stochastic layer is to ensure a probabilistic guarantee of feasibility for the final operation plan by considering a finite set of candidate scenarios with high probability of occurrence. Inputs to this stage include the generated N candidate scenarios (which represent probable load and solar power profiles for the current stochastic look-ahead window) and the updated system status. The diesel unit commitment and battery power commands derived by the deterministic layer for the considered stochastic look-ahead window is also taken as an input by this stage as shown in Figure 5.3.

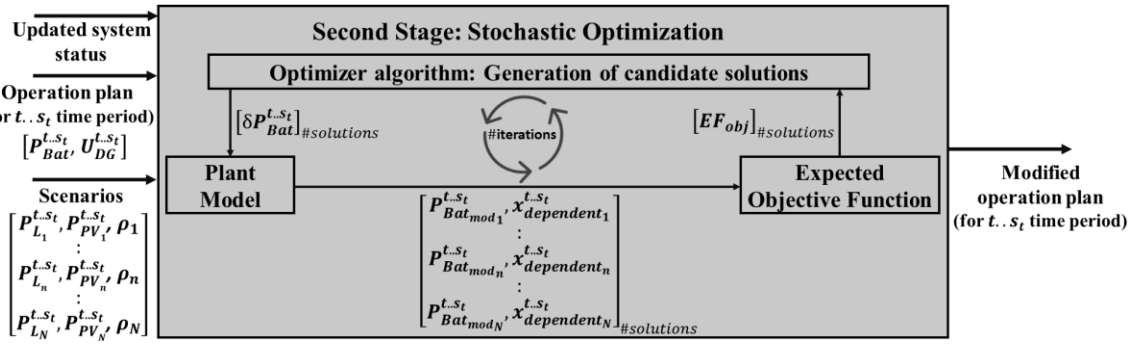

Figure 5.3 Second stage stochastic optimization layout

The stochastic optimization problem is formulated having a similar layout to the operation optimization framework developed in Section 3.4. However, the change in battery power command ($\delta P_{Bat}^{t..s_t}$) when operating as a grid-following source is defined as

the independent optimization variable within the range of $\pm\delta_B$. The plant model only constitutes the component models developed in Section 3.3.2. Also, in contrast to deterministic optimization, the developed stochastic optimization layer optimizes the expected value of the objective function denoted by EF_{obj}.

In each iteration, the plant model follows the unit commitment and dispatch commands generated by the deterministic layer as the reference for the considered stochastic look-ahead window and derives the modified battery power commands as in (5.3):

$$P^t_{Bat_{mod_n}} = \begin{cases} P^t_{Bat_{mod}} = P^t_{Bat} + \delta P^t_{Bat}, & U^t_{Gensup} = 1, U^t_{Isolated} = 0 \\ P^t_{Bat_n}, & U^t_{Isolated} = 1, U^t_{Gensup} = 0 \end{cases} \quad (5.3)$$

where subscript *n* denotes conditions in each considered scenario, and U^t_{Gensup} and $U^t_{Isolated}$ denotes the Gensup mode and Isolated mode of operation, respectively.

During time-steps operating under Gensup mode, plant model uses $P^t_{Bat_{mod_n}}$ and the suggested commitment of the diesel units to derive the dependent variables to achieve steady state power balance for each considered scenario. Similar to that discussed in Section 3.3.2.3, the derived diesel loadings were maintained within their limits. For time-steps operating under Isolated mode, plant model derives $P^t_{Bat_{mod_n}}$ mimicking the load-balancing task of the battery unit ($P^t_{Bat_n}$). Under both modes, $P^t_{spill_n}$ is used to curtail the excess energy under each scenario and the SOC update is conducted based on (5.4):

$$SOC^{t+1}_n = SOC^t_n + \frac{\left(1-U^t_{d_n}\right)\times\left(\left|P^t_{Bat_{mod_n}}\right|\times dt\times 100\times\eta_c\right)}{Bat_{cap}} - \frac{U^t_{d_n}\times(P^t_{Bat_{mod_n}}\times dt\times 100)}{Bat_{cap}\times\eta_d} \quad (5.4)$$

To maintain the SOC within permitted limits, $P^t_{Bat_{mod_n}}$ derived under each scenario was adjusted similar to (3.3) - (3.5) for the Isolated mode. However, for Gensup mode, rule-based conditions can not be applied for $P^t_{Bat_{mod}}$ as its value has to be the same under all scenarios. Therefore, for time-steps operating under Gensup mode, the SOC limits were maintained by relying on a cost-based penalty as discussed later in this sub-section.

The objective function value for each scenario is formulated to ensure reliability and security of operation with minimum required modifications to the initial operation plan determined by the first stage deterministic process as given in (5.5):

$$F_{obj}^{sto}{}_n = (Cost_{spill_n}^{mod} + Cost_{bat_n}^{mod}) \times PF_n^{sto} \tag{5.5}$$

where PF_n^{sto} is the penalty factor of n^{th} scenario, $Cost_{spill_n}^{mod}$ and $Cost_{bat_n}^{mod}$ account for the penalty costs incurred due to the modified energy spillage requirement and change in battery reference, respectively. For each scenario, $Cost_{spill_n}^{mod}$ and $Cost_{bat_n}^{mod}$ are calculated as in (5.6) and (5.7), respectively:

$$Cost_{spill_n}^{mod} = \sum_{t=t}^{s_t} (P_{spill_n}^t \times dt) \times c_{spill} \tag{5.6}$$

$$Cost_{bat_n}^{mod} = \sum_{t=t}^{s_t} U_{Gensup}^t \times (\left| P_{Bat}^t - P_{Bat_{mod_n}}^t \right| \times c_{Bat_{change}}) \tag{5.7}$$

where $c_{Bat_{change}}$ is the penalty factor for battery reference changes.

$Cost_{spill_n}^{mod}$ and $Cost_{bat_n}^{mod}$ are incorporated to minimize the deviation from the optimum operation trajectory suggested by the first stage deterministic layer.

The magnitude of PF_n^{sto} is calculated using (5.8)-(5.11):

$$PF_n^{sto} = PF_{PB_n} \times PF_{OR_n} \times PF_{Limit_n}^{Bat} \tag{5.8}$$

$$PF_{PB_n} = \prod_{t=t}^{s_t} (1 + c_{PB} \times \left| \frac{P_{L_n}^t - P_{G_n}^t}{P_{L_n}^t} \right|) \tag{5.9}$$

$$PF_{OR_n} = \prod_{t=t}^{s_t} (1 + c_{OR} \times \frac{P_{Limit_n}^t - P_{Rsr_n}^t}{P_{Limit_n}^t}) \tag{5.10}$$

$$PF_{Limit_n}^{Bat} = \prod_{t=t}^{s_t} (1 + c_{Limit}^{Bat} \times U_{Gensup}^t \times Violation_{Limit_n}^t) \tag{5.11}$$

where PF_{PB_n}, PF_{OR_n}, and $PF_{Limit_n}^{Bat}$ denote the detected violations in power balance, minimum operating reserve, and the battery maximum charge/discharge power limits under each scenario, respectively. The associated penalty rates are denoted by c_{PB}, c_{OR}, and c_{Limit}^{Bat}. In (5.9) and (5.10), $P_{G_n}^t$, $P_{L_n}^t$, $P_{Limit_n}^t$, and $P_{Rsr_n}^t$ are calculated similar to Section

3.4. $Violation^{t}_{Limit_n}$ is the violation detected in maximum charging/discharging battery references derived during Gensup mode for each scenario n.

Finally, the expected objective function value is derived to minimize the expected costs of all the N scenarios as given in (5.12):

$$EF_{obj} = \sum_{n=1}^{N} [\, \rho_n \times F^{sto}_{obj\,n}] \tag{5.12}$$

where ρ_n is the probability of each scenario as calculated in Section 5.3.2.1.

5.4 Study System and Data Inputs

The proposed method will be demonstrated for distinctive days in both summer and winter seasons, considering the PV-Diesel-Battery HRES and system conditions used in previous chapters. Most of the input parameters were incorporated similar to that given in Table 3.1-Table 3.2 and the rest can be found in Table 5.1. The discretized PDFs of percentage error associated with the hourly-averaged forecasts are given in Table 5.2.

Table 5.1 Input data used in the two-stage operation optimization framework

K	800
N	25
S [hours]	6
δ_B [kW]	±50
$c_{Bat_{change}}$ [$]	0.5
c^{Bat}_{Limit} [$]	100

Table 5.2 Discrete probability distribution of forecasting errors

Load (Summer)		Load (Winter)		Solar	
Error (%)	Probability	Error (%)	Probability	Error (%)	Probability
-4	0.075	-3	0.075	-3	0.05
-2	0.15	-1.5	0.15	-1.5	0.15
0	0.55	0	0.55	0	0.6
+2	0.15	+1.5	0.15	+1.5	0.15
+4	0.075	+3	0.075	+3	0.05

The data given in Table 5.2, were constructed considering the trends given in [23], [87] and the sources of uncertainties inherent to the considered test system such as load variability introduced by the DR program as devised in Chapter 4, seasonal variations in load demand as well as the increased uncertainties associated with past generation data and historical meteorological data used in producing the forecasts. All the simulated results were computed using the software package MATLAB R2021a.

5.5 Comparison Cases

For both seasons, a numerical analysis is also conducted to approximate the actual power system status over the 24-h control horizon. As discussed in Section 1.3, the power system control was realised in a hierarchical architecture, where the proposed two-stage operation optimization framework occupies the top-most layer. During actual deployment, the generated optimum operation plan will be integrated to the primary controls employed at each system component through the incorporation of secondary-level power management strategies. Also, in order to maintain a stable operation within the component limits, the adopted lower-level control layers can result in certain modifications to the optimum operation plan depending on the system conditions encountered during the actual operation. In the demonstrated study cases, such lower-level control actions were represented using simplified mathematical formulations to obtain the modified hourly-averaged steady state behaviour of the components based on the actual load and resources. A detailed discussion on the lower-level control actions will be given in Chapter 6.

The proposed method is also compared with two other energy management approaches namely, the closely-tracked deterministic method realised using the conventional MPC approach (MPC case) and the day-ahead energy management with perfect information (Perf case). In MPC case, the EMS uses the deterministic optimization layer detailed in Section 5.3.1 embedded in MPC to provide the reference commands for the lower-level controllers in each time-step as the control horizon progresses. No further adjustment is made to the reference commands as in the case of the proposed two-stage decision making process. The Perf case is a theoretical exercise where the operation plan generated considering a perfect 24-h forecast is used to provide the reference commands for the

lower-level controllers [26]. In this case, the actual realizations of the hourly-averaged solar and load profiles are used as the generated forecast. Therefore, the operation plan generated at the start of the 24-h control horizon by the deterministic optimization layer detailed in Section 5.3.1 is used to govern the system operation without the inclusion of MPC. As the Perf case generates its results with the best possible forecast, it can be considered as a benchmark to assess the actual system performance under the operation trajectories suggested by other energy management approaches.

5.6 Results and Discussion

5.6.1 Summer study cases

Figure 5.4 presents the load forecasts generated for the first three successive MPC processes along with the actual load variation for the first two hours. The generated forecasts for the first three MPC trials have showed considerable variability for time-steps at the end of the control horizon. This shows the increase of uncertainty as the control horizon extends and further heightens the need of deploying proper recourse actions.

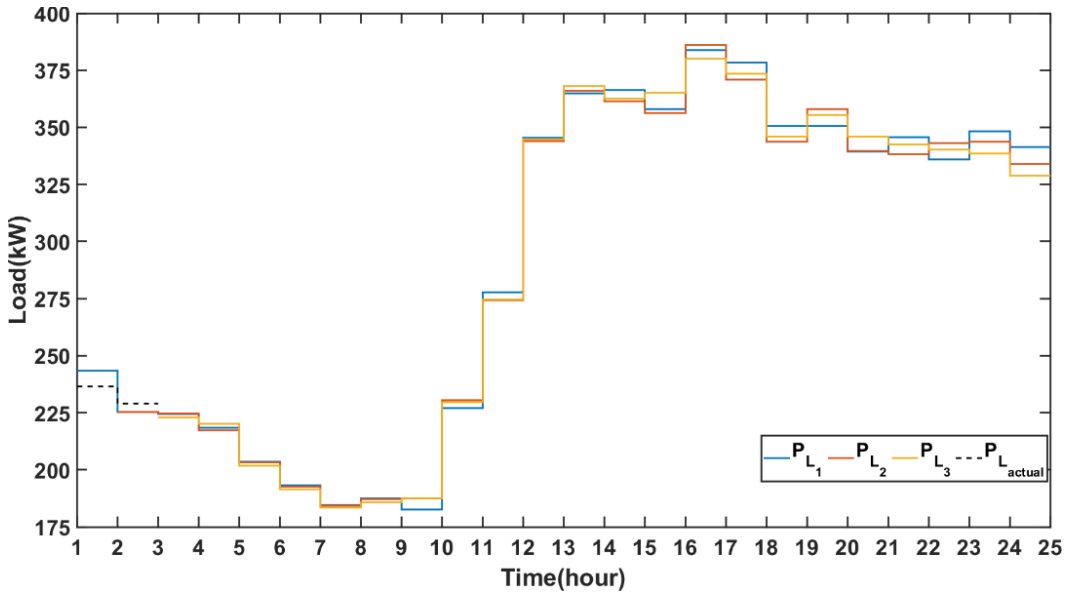

Figure 5.4 Generated load forecasts and actual load demand variation up to the start of 3rd hour MPC process

In Figure 5.5, a sample set of the generated load scenarios used in the second stage stochastic layer are showed for the first three MPC processes of the considered summer day. Following a similar procedure, updated forecasts and scenarios were generated for rest of the MPC windows covering the entire 24-h horizon for both load and solar variables.

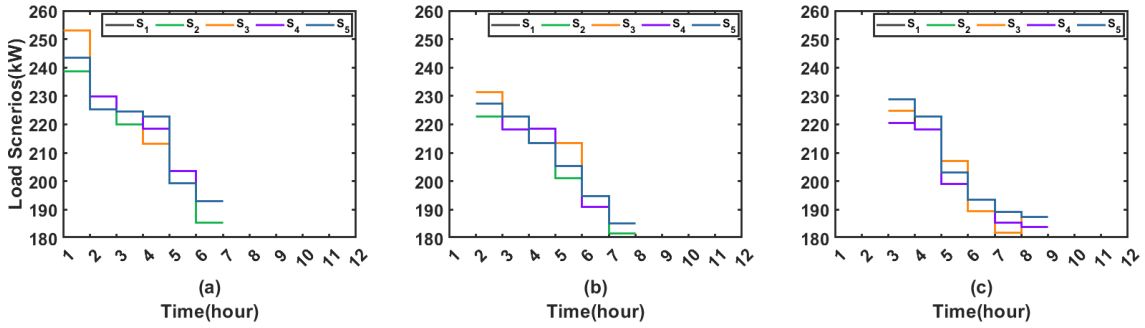

Figure 5.5 Set of load scenarios used for: (a) 1st hour, (b) 2nd hour, and (c) 3rd hour

Figure 5.6 presents the forecasts and dispatch commands generated by both proposed method and the MPC method for the first hour of each look-ahead window for the entire 24-h horizon.

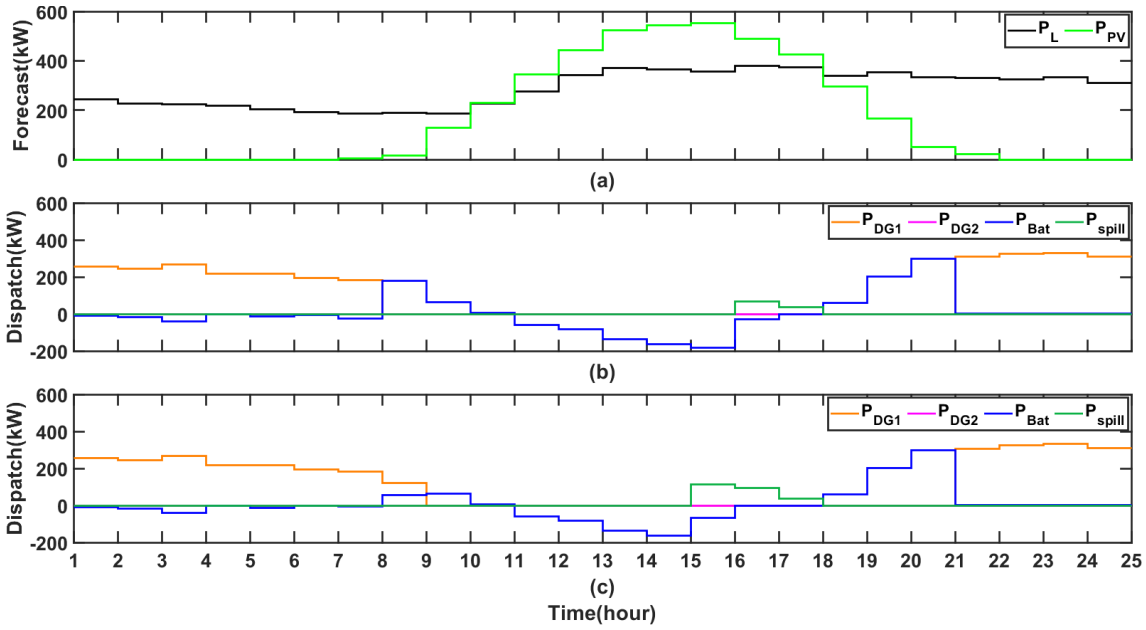

Figure 5.6 Summer: (a) Forecasts, (b) Dispatch solution of proposed method, and (c) Dispatch solution of MPC method

The proposed approach (Figure 5.6 (b)), has suggested the Gensup mode for the early morning and late-night hours whereas the Isolated mode is suggested for the mid-day time frame to harness the available solar power as much as possible. For the 6th and 7th hours, the charging battery power commands suggested by the first stage has been further increased in the second stage stochastic layer as shown in Figure 5.7 to be able to reliably navigate all the candidate scenarios considered within the stochastic look-ahead window. Figure 5.7 also emphasize that the second stage has suggested the required minimal adjustments to maintain the optimum trajectory recommended by the first stage deterministic optimization layer.

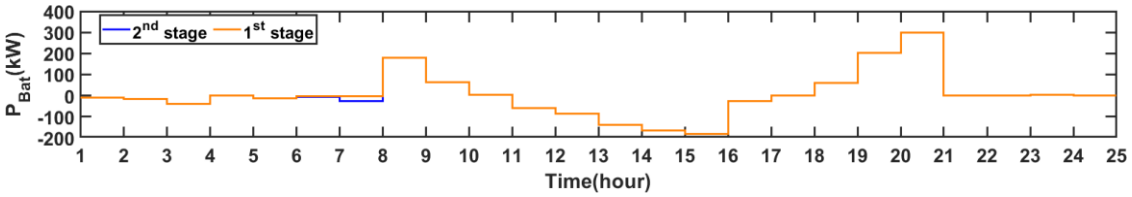

Figure 5.7 Proposed method: Adjustment of battery power commands

When comparing the proposed dispatch solution with that suggested by the conventional MPC approach (Figure 5.6 (c)), a similar trend of operation modes can be seen. However, due to the lack of future operating reserves maintained by the dispatch solutions suggested prior to the 8th hour, the initiation of the Isolated mode has been delayed by one hour to save the available battery energy to maintain the feasibility and continuation of operation during the Isolated mode. The battery power command for the 8th hour is optimized to maintain the diesel power output at its minimum loading level.

Table 5.3 and Figure 5.8-Figure 5.11 represent an approximation of the actual power system status over the 24-h control horizon under actual load and solar power variations. In terms of total costs, emissions, and the curtailed energy, the proposed method outperforms the MPC method and have delivered results closer to a scenario where perfect forecast information is available in the day-ahead time frame (Perf case).

Table 5.3 Summer: Actual power system operation status

	Proposed method	MPC method	Perfect information (Perf case)
Total costs [$]	1644	1745	1600
Total CO_2 emissions [kg]	2113	2203	2067
Diesel costs [$]	1412	1493	1392
Battey degradation costs [$]	188	162	188
Energy spillage penalty costs [$]	44	90	20
DG_1 min loading violation hours [h]	0	1	0
DG_1 max loading violation hours[h]	0	0	0
System penalties	-	-	-

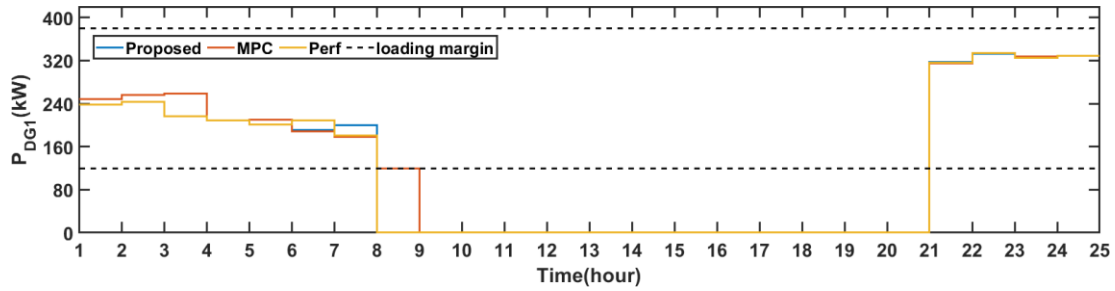

Figure 5.8 Summer: DG1 loading during actual operation

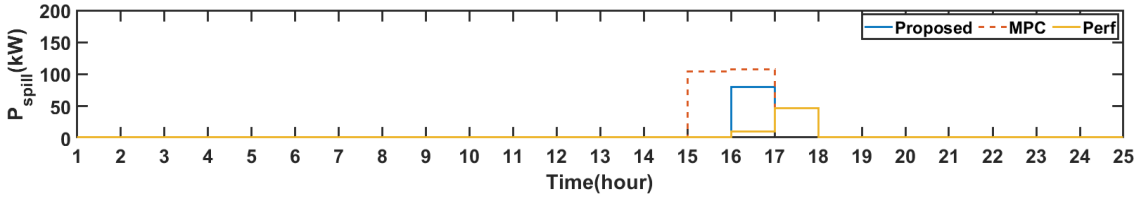

Figure 5.9 Summer: Curtailed energy during actual operation

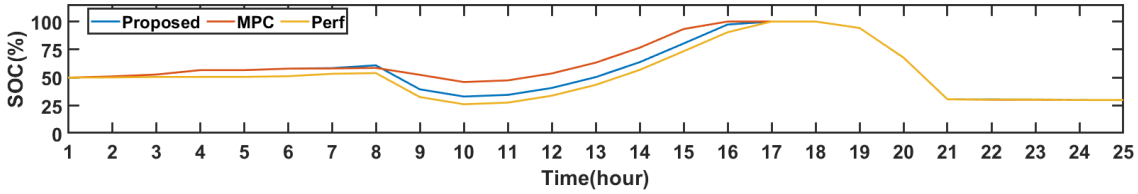

Figure 5.10 Summer: Variation of SOC during actual operation

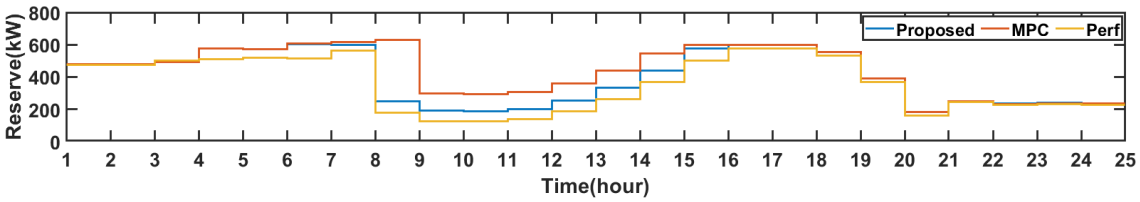

Figure 5.11 Summer: Availability of operating reserves during actual operation

During actual operation, DG_1 has formed the grid during Gensup mode while operating within its loading margins for all the considered cases as shown in Figure 5.8. However, in the MPC case, DG_1 is operating marginally at its minimum loading margin for the 8^{th} hour. Figure 5.9 and Figure 5.10 show the average energy curtailment and battery SOC during the actual performance, respectively. Due to the high SOC maintained at the end of 8^{th} hour, the MPC approach has failed to harness most of the available solar energy compared to the proposed case. This is further highlighted by Figure 5.11 which depicts actual operating reserve levels maintained by each case during the 24-h control horizon. The proposed dispatch solution has maintained the operating reserve levels closer to that of the perfect information case while navigating the power system operation in an optimum and reliable manner.

During summer days, with high solar power availability, the operation cost as well as the spillage of energy can be reduced if the system operation was to continue for longer durations without the use of diesel generators in Isolated mode as observed during Chapter 3 and Chapter 4. In contrast to MPC case, the proposed method functions with higher awareness of possible future operating conditions and optimally adjusts the battery power commands to satisfy operation constraints of all possible scenarios. This allows it to achieve longer durations of Isolated mode with lower spilled energy amounts, resulting in reduced costs and emissions compared to the MPC case.

5.6.2 Winter study cases

Generation of forecasts and the determination of load and solar scenarios was conducted similar to that discussed in Section 5.6.1. Figure 5.12 depicts the forecasts and the dispatch solutions generated by the proposed method and the MPC method for the first hour of each look-ahead window for the 24-h control horizon. Both operation plans have

not suggested the Isolated mode considering the low availability of solar power with high load demand. In both cases, the battery operation has been optimized to energize the power system using DG_1 while ensuring power balance, operating reserve, and maximum generator starts requirements. Also, both approaches have produced similar trends in committing the diesel generators as well as considering the battery charging/discharging operation. Compared to the MPC approach, in the proposed method, the discharging battery references suggested by the first stage have been further increased by the stochastic layer during the peak demand period as shown in Figure 5.13 to ensure the maximum loading margin for DG_1 considering the candidate scenarios generated in each hour.

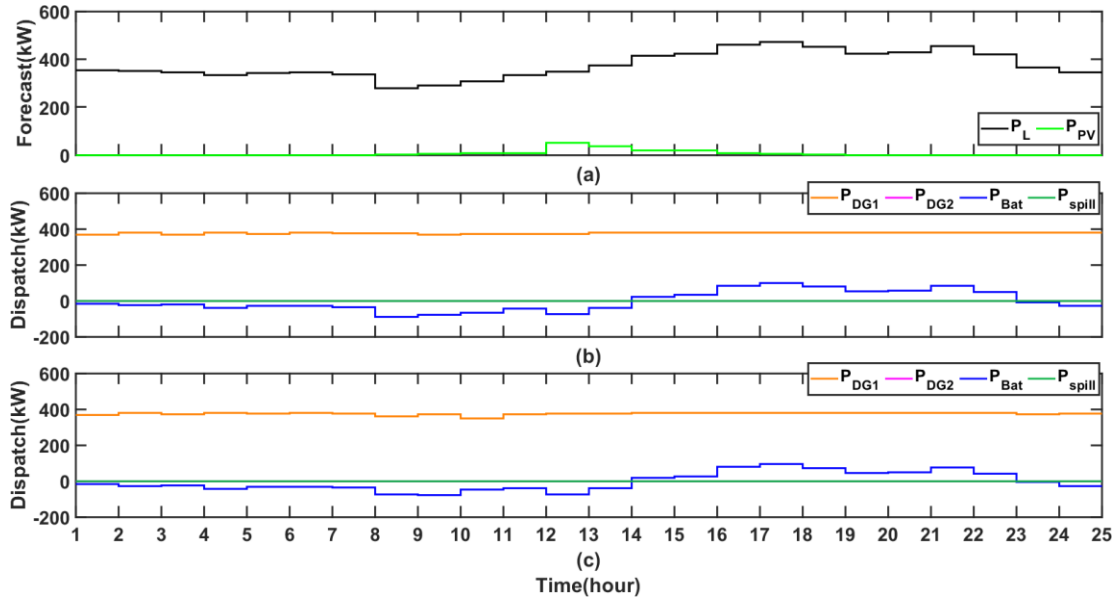

Figure 5.12 Winter: (a) Forecasts, (b) Dispatch solution of proposed method, and (c) Dispatch solution of MPC method

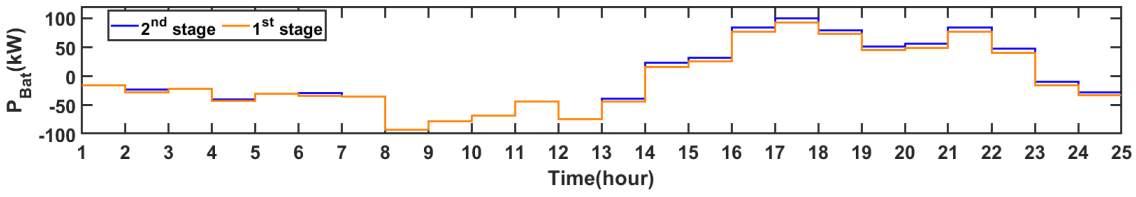

Figure 5.13 Proposed method: Adjustment of battery power commands

Table 5.4 and Figure 5.14-Figure 5.16 depict the approximation of actual power system status over the 24-h control horizon. In terms of total costs and emissions, the

proposed method and the MPC method operated similarly with slightly reduced values compared to the Perf case. However, in terms of maximum loading hours for DG_1, Perf case depicted the best performance followed by the proposed method. Compared to the MPC case, the proposed method and the Perf case incurred slightly higher battery degradation costs due to its increased utilization to ensure the DG_1 maximum loading margin during the peak load period.

Table 5.4 Winter: Actual power system operation status

	Proposed method	MPC method	Perfect information (Perf case)
Total costs [$]	3873	3876	3890
Total CO_2 emissions [kg]	6285	6313	6325
Diesel costs [$]	3734	3747	3752
Battey degradation costs [$]	139.2	129.3	138.48
Energy spillage penalty costs [$]	0	0	0
DG_1 min loading violation hours [h]	0	0	0
DG_1 max loading violation hours [h]	2	9	0
System penalties	-	-	-

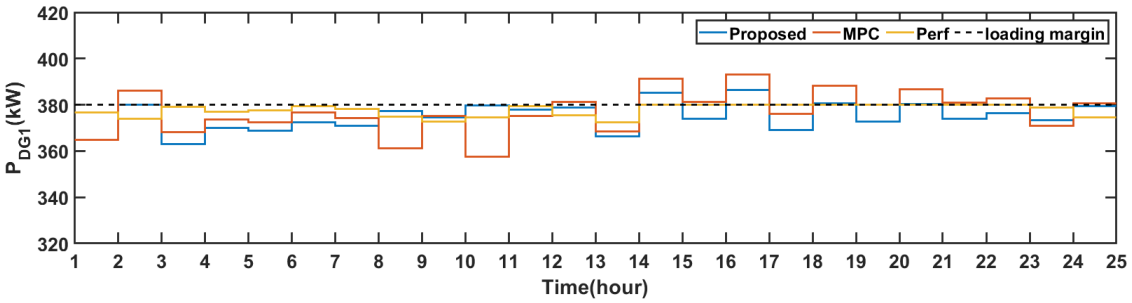

Figure 5.14 Winter: DG_1 loading during actual operation

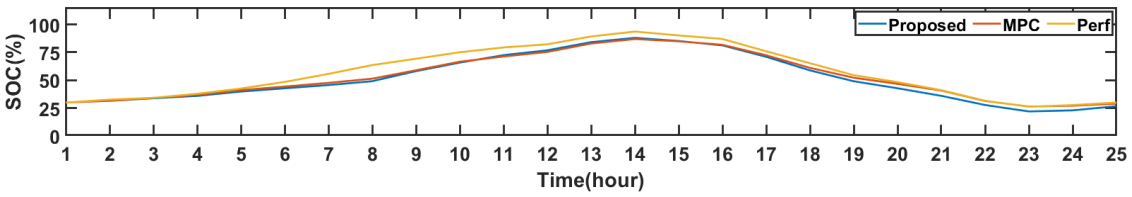

Figure 5.15 Winter: Variation of SOC during actual operation

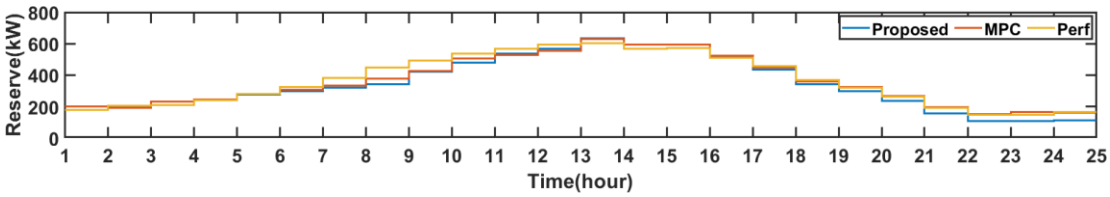

Figure 5.16 Winter: Availability of operating reserves during actual operation

In the MPC case, a total of 9 hours were detected where DG_1 operated above its maximum loading level during actual system operation as depicted in Figure 5.14. Such conditions pose an operational risk to the grid-forming task of DG_1 due to its own capacity limits and possible depletion of available operating reserves. Therefore, such loading conditions degrade the quality of the MPC solution in terms of both reliability and security of operation. Under the proposed method, DG_1 showed only 2 maximum loading hours, with only slight increase above the loading margin. This observation shows its competence in handling the operational constraints under forecast uncertainties. The three cases showed similar variations in battery SOC and available operating reserves during actual operation as shown in Figure 5.15 and Figure 5.16, respectively.

5.6.3 Computational performance

This section presents an analysis conducted on the computational performance of the proposed method. All the results were computed in a PC with AMD Ryzen 3600 CPU @ 3.6 GHz base (4.2 GHz boost) and 32GB DDR4 RAM @ 3600 MHz. The average computational time taken for the first hour MPC process of a given day with a deterministic look-ahead window of 24 hours and a stochastic look-ahead window of 6 hours while considering 25 scenarios was estimated to be around 21.81 s for the proposed method. When considering the same 24-hour window, an entirely deterministic approach would take an average computational time of 12.8 s to generate the results whereas for an entirely stochastic approach with 25 scenarios, the computational time showed an exponential growth averaging around 755.53 s. Therefore, the proposed method shows a good improvement over the entirely stochastic approaches in terms of computational performance and results in a slight increase in computational times with respect to an entirely deterministic framework, however with improved operational feasibility as

showed in Section 5.6.1 and Section 5.6.2. Table 5.5 presents the average computational times taken by the proposed method for different look-ahead window lengths and different number of scenarios considered in the second stage. In all cases, a 24-h look-ahead window was considered for the first stage deterministic layer. According to Table 5.5, only the number of considered scenarios showed some impact on the computation times. However, the observed computation times, even for higher scenario numbers and longer look-ahead windows, were considerably lower compared to the entirely stochastic framework.

Table 5.5 Average computational time taken for the first hour MPC process in seconds.

		No of Scenarios			
		5	25	75	100
Stochastic look-ahead window length	4	17.86	21.58	34.33	42.25
	6	17.92	21.81	34.70	42.49
	12	18.29	22.42	36.37	44.26

The observed computational performance of the proposed method is mainly influenced by the problem formulation techniques used in devising the second stage stochastic layer. The second stage optimization layer receives the diesel unit commitment and battery power commands derived by the first stage for the considered stochastic look-ahead window as an input. Use of this input as a reference trajectory greatly reduces the burden of the underlying optimization problem. Also, the second layer optimizes the required change in battery power command within a pre-defined range to ensure a probabilistic guarantee of feasibility for all the considered scenarios. Therefore, the search space is also reduced compared to a fully stochastic problem and allows fast convergence. The observed computational performance is advantageous when deploying this method in actual system operations even with higher time resolutions and also when using this method for operation analysis purposes prior to actual deployment.

5.6.4 Impact of the stochastic optimization layer parameters on the quality of results

For the second stage stochastic decision-making process, selection of both the look-ahead window length (S) and the scenario number (N) is a compromise between the associated optimization problem size and the delivered quality of results. To study this effect, operation of the proposed method under the summer day conditions were analyzed for different look-ahead window lengths and scenarios numbers. The change in results is given in Table 5.6 while keeping the summer study case with a 6-h stochastic look-ahead window and 25 scenarios as the reference.

Table 5.6 Effect of stochastic layer parameters on the quality of results.

		Deviations [%]		
		Costs	Emissions	Energy curtailment
Stochastic look-ahead window length	4	+6.2	+4.35	+106
	12	-0.005	-0.087	-11.9
Number of scenarios	5	-0.4	-0.33	-6
	75	0	0	0

The battery output power is governed by the grid conditions (grid-forming source) once the system moves into the Isolated mode leveraging less flexibility for the stochastic layer. Therefore, when encountered with possible longer periods of operation under Isolated mode, longer S values increase the ability of the stochastic layer to appropriately adapt to futuristic scenarios while the system still operates in the Gensup mode where the grid-following battery command is available for adjustment.

The analysis considering the effect of scenario number on the quality of the results revealed some interesting points. When the scenario number was decreased to 5 from 25, a very small reduction in cost, emissions, and energy curtailment was detected. Excluding some of the forecast realizations has allowed the stochastic layer to adapt to the futuristic scenarios with fewer committed reserves compared to the reference case. When the actual realization also stays within the lower and upper boundary of the considered scenarios, the

overall result has appeared as an improvement over the reference case. However, it must be noted that if the actual load and solar variations were to deviate more form the suggested scenarios, the adjustments provided by the stochastic layer with 5 scenarios would not have provided a high assurance on a feasible system operation. When the scenario number was increased to 75, the change in results were negligible related to the reference case. This is expected as the newly accounted scenarios either has a very low probability of occurrence or are similar to that already accounted within the 25 scenarios considered in the reference case. Thus, for the studied power system conditions and the associated discrete probability distributions, the considered 25 scenarios have captured most of the uncertainty spectrum allowing the stochastic layer to adequately strengthen the operational feasibility of the derived unit commitment and dispatch commands.

5.7 Concluding Remarks

A two-stage operation optimization framework that accounts for both economical and environmental considerations as well as the underlying forecast uncertainties of a remote off-grid HRES is presented. Both deterministic and scenario-based stochastic problem formulation techniques are integrated while considering several operational requirements inherent to remote off-grid power systems. The proposed energy management platform is robust towards uncertainties, computationally inexpensive, and results in minimum daily costs and emissions while satisfying several system constraints.

The proposed method is tested for system conditions prevailing in both summer and winter seasons. Also, the obtained results are compared with both the MPC approach and the day-ahead operation optimization scenario with perfect information. In addition, a detailed analysis is presented to evaluate the computational performance of the proposed method and to evaluate the effects of the stochastic layer parameters on the quality of results. The results revealed the improved performance of the proposed method in maintaining an optimum operation trajectory while addressing the uncertainties associated with the forecasts for both summer and winter seasons. The proposed method showed significant improvement over the entirely stochastic framework in terms of computational burden and resulted in average computational times slightly above that caused by an

entirely deterministic framework. For the considered system conditions, look-ahead window lengths above or equal to six hours proved to be beneficial in enhancing the quality of results whereas about 25 scenarios provided an adequate approximation of the forecast uncertainties.

Chapter 6

Power Management and Operation Evaluation

6.1 Introduction

In Chapter 3 to Chapter 5, focus was on the EMS that derives the unit commitment and dispatch solutions to achieve a quantitatively optimized operation trajectory. The devised energy management algorithms considered the steady state system behaviour while prioritizing parameters such as operational costs and emissions. However, when deploying such reference commands to the actual system operation, maintaining a logical operation is imperative. The logical operation constitutes maintaining a stable and secure operation under dynamic conditions accommodating the capability of lower-level control functions that act on a shorter time frame managing both continuous and discrete events. At certain instances, the set-points advocated by the supervisory-level may need adjustments to ensure stability and security of the power system, but such changes must be minimized to avoid deviations from the optimum operation trajectory determined by the EMS. Also, these dynamic control functions must be tested for their robustness in handling unexpected system disturbances that may encounter while following the operation trajectory suggested by the EMS.

This chapter proposes a set of power management strategies to effectively deploy the EMS set points to the unit-level controls in a maximally permissive manner while adapting to limitations of diesel, battery, and PV system during actual operation. Also, an operation evaluation routine is proposed to provide a set of guidelines to assess and modify the EMS

set-points considering system dynamics, lower-level control capabilities, and equipment limitations based on EMT simulations. Results are demonstrated for several operational scenarios in the PSCAD/EMTDC^{TM} simulation environment for a remote off-grid power system with PV, diesel, and battery energy sources.

6.2 Background and Literature Review

Although microgrid energy management as well as microgrid control are highly researched topics, relatively few studies have addressed the close coordination and performance verification of energy management and power management control layers.

In [97], authors have presented a master and slave control framework for a stand-alone hybrid energy system. A master controller generates dispatch commands considering economic aspects and component limits whereas a slave controller modifies those reference commands to ensure power system dynamic limitations adapting to real-time conditions. Both master and slave controllers highly depend on pre-defined operational modes and the current net power requirement without considering a predictive look-ahead window. However, sole dependence on current information to derive the dispatch strategy can degrade the overall controller competence in the presence of non-dispatchable sources.

Coordinated control frameworks subjecting both predictive and real-time data can be found in [11], [98]–[103]. Authors in [98] propose to achieve the quantitatively optimized logical operation through close coordination of a schedule layer and a dispatch layer. The schedule layer obtains an economic operational scheme based on a look-ahead multi-step optimization. The dispatch layer navigates the derived operational plan while considering stability and security of operation. However, the logical criteria are incorporated to the dispatch layer only by means of power flow and voltage limit considerations. Authors in [103] have proposed a hierarchical control technique in which both the energy management layer and the primary control layers utilize a Economic Model Predictive Controller (EMPC). Two separate optimization problems are solved in real-time with the use of reduced order models developed for the two control layers. Performance of the controller is experimentally validated over different time horizons considering both economic and logical criteria. However, given the high dependence on model-based controls, the

practicality of incorporating EMPC to primary control layers is limited to power systems with relatively few resources.

A real-time EMS for a hybrid energy system is proposed in [99] from both cost and stability points of view. The energy commitment problem is majorly formulated based on case-specific rules. For instances with power deficiency to cover the net-load, a fuzzy controller is designed to control the power sharing between the grid and a battery system. However, when deriving the dispatch commands, predictive information of future scenarios is only considered for the peak hours within the fuzzy controller. In [100], a fuzzy logic controlled two-stage EMS is deployed to achieve a quantitative control objective subjecting a multiport multioperation mode residential microgrid. The EMS incorporates both real-time microgrid parameters and long-term predicted data to select the appropriate operation mode and works in close coordination with a mode selection and transition unit to achieve seamless operation. Results are thoroughly analysed considering both quantitative and logical criteria. A rule-based real-time controller closely coupled with a predictive dynamic programming-based optimization technique can be found in [101]. The competence of the proposed control framework to optimally manage the power flow according to the derived energy plan has been experimentally verified. However, dynamic programming-based energy management can result in extensive computational efforts in the presence of large number of system variables and operating modes. A distributed intelligent EMS coupled with a real-time control module is presented in [102]. The operation optimization module developed using linear programming and heuristics integrates the hourly forecasts predicted using a fuzzy ARTMAP neural network. However, the real-time controller only investigates power balance to ensure the logical operation. Also, a proper explanation has not been provided on how the pre-defined optimum set-points are updated to compensate for forecast deviations.

Authors in [11] present a supervisory controller deploying hybrid automation and discrete decision-making to generate economic dispatch commands for the lower-level controllers that ensure the stability criteria. However, this study does not provide a clear representation of the impact of lower-level controllers, and the adopted controls are only evaluated considering frequency stability.

In contrast to the conventional simplified system representations used in EMSs, a detailed three-phase system model is featured in [104], which allows the EMS to account for the effects of power flow constraints and system unbalances on the optimal operation of standalone microgrids. However, due to the extent of details integrated into the operation optimization framework, extra problem decomposition approaches are required to make the problem tractable in a reasonable time. Although the EMS formulation has revealed insightful conclusions on its competence to facilitate a logical operation, authors of [104] further emphasize the importance of capturing the dynamic effects of primary controllers to assess the quality of solutions in real-time operation.

A study mainly investigating the logicality of a quantitatively optimized operation plan through a detailed dynamic simulation model can be found in [20], considering a Wind-Diesel-Battery power system. Power management is only discussed considering a post-processing unit which modifies the derived optimum diesel set-points to increase its own operational efficiency as well as to operate the battery within its SOC limits. The dynamic analysis has been performed covering the entire daily control horizon, which in the respective system set-up has taken approximately four days in actual clock-time to complete. Several operational scenarios and sensitivity analysis are performed to analyse the robustness of the optimized operation plan. However, dynamic simulation of the entire operation trajectory is impractical when considering daily operation evaluation. It requires a larger computation effort and much longer simulation time. Also, it would not leverage the system operators with enough flexibility in terms of implementing corrective control actions during actual intra-day operation.

The reviewed studies [11], [20], [97]–[104] considering both logical and quantitative objectives have showed results verifying the achieving of long-term operational objectives while maintaining logicality in the short-term operation using different evaluation criteria. However, only [11], [20], [97], [100]–[103] have provided a rigorous transient type of validation to their respective control frameworks while capturing enough system dynamics.

Many remote power systems with limited or seasonal access due to geography, harsh weather, etc. rely on past generation log data for demand predictions and the meteorological data is often collected from distant weather stations as discussed in Chapter 5. When adopting a steady state dispatch solution generated through such long-term data

with higher uncertainty, verification of the logical optimality and making corrective adjustments if required is crucial. Also, sufficient time must be leveraged for this purpose as this process may be time consuming. Thus, the power management strategies practical for such remote power systems must be less dependent on high-resolution forecast updates, simple in the problem formulation, and should be subjected to a proper transient-type performance evaluation process.

6.3 System Set-up and Control Requirements

The supervisory level control layers as devised in previous chapters usually do not consider the transient behaviour corresponding to fast system dynamics. Therefore, in Chapter 3 to Chapter 5, the system components and the involved control functionalities were modelled using simplified mathematical equations. However, when considering lower-level control tasks, a detailed representation of the overall system is required to properly design and assess the system operation. An example schematic of such a representation considering a PV-Diesel-Battery power system is given in Figure 6.1 in contrast to the simplified representation used in Chapter 3 to Chapter 5.

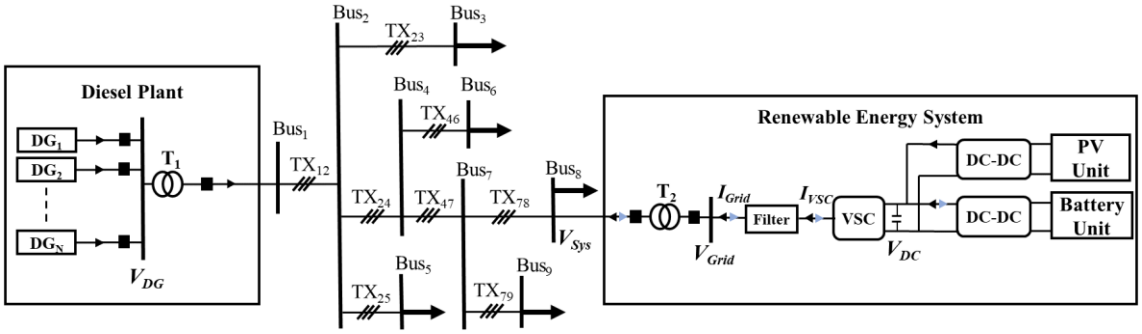

Figure 6.1 Representation of a PV-Diesel-Battery power system

The PV array and the battery unit, which jointly form the renewable component of the hybrid configuration is connected to a common DC-link capacitor through two DC-DC converters. Energy transfer from the renewable system to the AC side and vice versa is achieved using a two-level Voltage Source Converter (VSC). The system demand usually consists of many different types of loads. Thus, the usual practice for modelling of the

system load is to use an aggregate load by breaking it down to different classes such as commercial, industrial, residential etc.

When navigating the system operation as suggested by a quantitatively optimized operation plan, special care must be given to several discrete and continuous-state events to accommodate a stable and secure operation while minimally obstructing the suggested operational routine. Based on the analysis conducted in Chapter 3 to Chapter 5, operation routines derived by EMSs subjecting HRESs often operate in two distinct continuous states. When at least one diesel-based synchronous generator is operating, it generates the voltage and frequency references for the stable power system operation (Gensup mode). For periods with low loading and/or high renewable penetration, operation planning often recommends schedules where the diesel generator goes out of operation and the load is supplied by the available renewable sources and storage units (Isolated mode). Isolated mode of operation is suggested under the assumption that at least one inverter-interfaced DER can facilitate the grid-forming task. Although it is theoretically sound, forming the grid and continuing the system operation under almost zero synchronous inertia with high penetration of intermittent energy can be a challenging task [105]. Also, rigorous validation is needed to confirm whether the power system can achieve seamless transition between the two modes without any interruption to the energy sources and the load.

The derived operation routines might also suggest schedules where the adopted operating reserves are maintained only by a very short margin. These scenarios have a high probability of violating the system limits and thus require further verification. The complications imposed by reactive power regulation is another aspect that needs to be tested before deploying the operational plan in an actual system. Also, the applicability of control commands/parameters deployed in the adopted dynamic control functions must be tested under several scenarios to avoid oscillations in their respective control loops.

In addition to these, employing measures to handle unanticipated events, initiation of restoration controls, providing necessary feedback to the supervisory control layers in the presence of possible violations, etc. can be identified as some other control functionalities required from the lower-level control layers.

6.4 Integration of Energy and Power Management Functions with Unit-level Controls

Integration of energy and power management functions to the unit-level controls is realized in a hierarchical control architecture as shown in Figure 6.2.

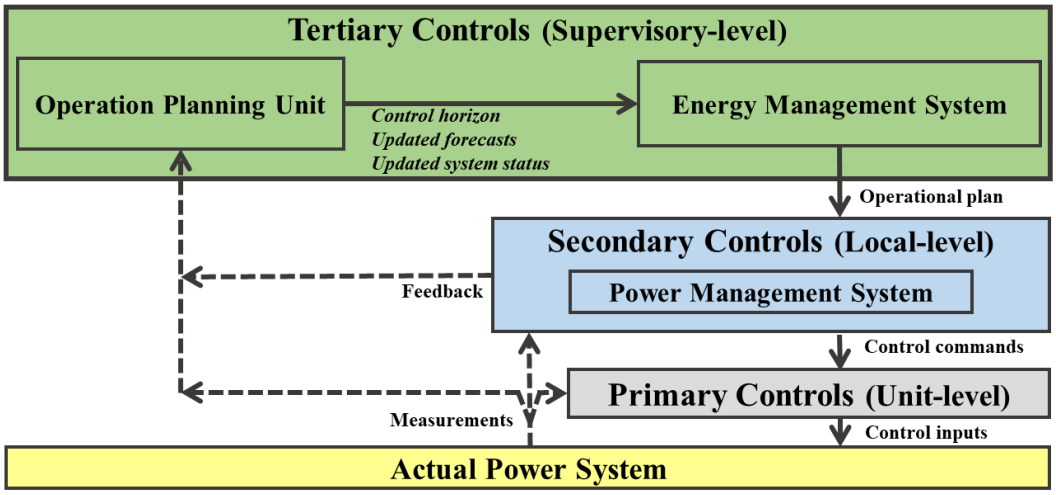

Figure 6.2 Integration of energy and power management controls in a hierarchical architecture

The tertiary controls operate in the supervisory-level and deploy the slowest responses (hours to one-day) accommodating control tasks in management and planning. Integration of energy management function into the tertiary layer will be discussed in Section 6.4.1.

In contrast to the tertiary control layer, secondary controls act in a shorter time frame (seconds to minutes) and manipulate the unit-level controls to manage interactions between all components within the power system. In this study, the secondary controller obtains the set-points from the tertiary layer under expected/forecasted operating conditions. The development of conventional secondary-level controls such as voltage and frequency restoration and transition controls, which are based on existing literature, are discussed in Section 6.4.2. In addition to these, a coordinated set of power management functions are proposed to modify the EMS set-points considering the limitations of diesel, battery, and PV modules during actual operation in Section 6.4.2.3, Section 6.4.2.4, and Section 6.4.2.5, respectively.

Also, each system component is assigned with a dedicated unit-level controller to govern their operation based on current system conditions and the reference commands provided by the secondary layer. These control functions, usually referred to as the primary controls, deploy the fastest responses (sub-seconds to seconds). To demonstrate the applicability of the overall control framework, the unit-level controls are also developed based on existing methods as briefly discussed in Section 6.4.3.

6.4.1 Tertiary controls

In this study, an EMS, and an Operation Planning Unit (OPU) form the base of the adopted tertiary control layer as shown in Figure 6.2. The OPU assigns the control horizon and provides the required data to the EMS including network data, component data, system status, forecasts etc. Also, it is assumed that the system operator acts as a unique entity in charge of overseeing the OPU functionality, aimed at enhancing the envisioned objectives for both the utility-side and the consumers. In the intra-day time frame, the two-stage operation optimization framework as devised in Chapter 5 occupies the EMS.

6.4.2 Secondary controls

6.4.2.1. Normal operation and grid-forming controls

Under normal operation, the secondary controller must facilitate two continuous-state operation modes as discussed in Section 6.3.

When at-least one diesel-based synchronous generator is included in the unit commitment schedule for the next time period, the system operates under Gensup mode. During the Gensup mode, the grid-forming control is assigned to the diesel plant and the VSC-interfaced renewable system is governed under the grid-following control mode. The commitment of the diesel generators and the battery reference are obtained from the derived optimum operation plan. The PV array output is controlled independent of the other units using the power reference provided by the unit-level MPPT strategy. The active power reference command of the VSC is defined as in (6.1):

$$P_{VSC}^{Ref} = (P_{Bat}^{Ref} + P_{PV}) \times \eta_{con} \tag{6.1}$$

where P_{Bat}^{Ref} is the battery reference, P_{PV} is the locally measured PV output, and η_{con} is a factor accounting for the converter losses depending on the inverter/rectifier operation of the bi-directional VSC. The derivation of P_{Bat}^{Ref} is discussed in Section 6.4.2.4.

The reactive power reference of the VSC is derived using (6.2) [106]:

$$Q_{VSC}^{Ref} = -Q_{VSC}^{Set} + Q_{filter} \tag{6.2}$$

where Q_{VSC}^{Set} is the reactive power set point of the renewable system and Q_{filter} is the reactive power contribution of the AC side filter.

If the dispatch schedule suggests the system load to be supplied only by the available renewable sources and storage units, Isolated mode is activated. During the Isolated mode, the diesel plant is taken out of operation and the VSC controls are configured to operate as a voltage source to form the grid as detailed in Section 6.4.3.2. Among the DERs, PV unit is considered unreliable for load-balancing due to the intermittency associated with its primary energy source and complexities involving power reserve estimation. Therefore, the output power regulation of PV unit is done similarly to the Gensup mode. Battery storage unit, being a dispatchable energy source, is used to aid the VSC grid-forming task by providing the required power slack to balance the grid conditions [36].

6.4.2.2. Transitioning controls

When the tertiary controller suggests the Isolated mode of operation for a given time period, the Gensup to Isolated transitioning mode will be activated first. During this mode, the secondary controller gradually increases both active and reactive power references of the grid-following VSC to allow the diesel generator to supply the balance of the grid power at lowered active and reactive power values. Once the system reaches steady-state, the interface breaker of the diesel unit is opened activating the Isolated mode of operation. Simultaneously, the VSC control is switched from grid-following to grid-forming mode. When transitioning from Isolated to Gensup mode, proper synchronization of the incoming diesel generator to the AC grid formed by the VSC must be facilitated. Therefore, during this transition mode, the secondary controller first activates the synchronization mode ($Mode_{Sync_n} = 1$) for the respective generator where an active synchronization scheme will

be initiated to make corrective adjustments in the detected differences in the voltage magnitude, phase angle, and frequency across the interfacing breaker. Once the diesel breaker gets closed, its synchronization mode will be disabled. Simultaneously, the connected diesel unit will take over the grid-forming task and the VSC control mode will be switched from grid-forming to grid-following at the reference active and reactive power values defined by the tertiary controller.

6.4.2.3. Diesel power management

The EMS usually imposes a minimum loading limit as a percentage of the DG rating when deriving power commands of diesel generators as discussed in the previous chapters. However, during actual deployment, when a diesel unit balances the grid, changes in system conditions could violate such limits irrespective of what had been suggested in the operation plan. Therefore, when diesel generators operate close to their minimum loading limit, $Mode_{MinLoad}^{Diesel}$ is activated and the battery power command is modified to a value $P_{Minload}^{Limit}$ within its operational limits. $P_{Minload}^{Limit}$ is derived based on the operating conditions detected in the rest of the power system as given in (6.3) - (6.4):

$$P_{MinLoad}^{Limit} = [e^{-sT_d}(P_{Gen}^{Total} - P_{Diesel}^{Min})]\frac{1}{\eta_{con}} - P_{PV} \tag{6.3}$$

$$P_{Diesel}^{Min} = \sum_{n=1}^{N}(DG_{min_n}^{PMS} \times DG_n^{Rated} \times U_{DG_n}^{t}) \tag{6.4}$$

where P_{Diesel}^{Min} is the minimum loading level of diesel plant, P_{Gen}^{Tot} is the measured total generation, e^{-sT_d} is the communication delay, and $DG_{min_n}^{PMS}$ is the minimum loading margin set by the secondary-level power management strategies for DG_n. However, if battery had already reached its overcharge limit, the available PV power will have to be spilled by reducing its maximum power limit.

Also, the EMS always prioritises in committing the lowest rated generator that could satisfy the operational requirements. Therefore, the maximum loading limit is always kept below the rated active power of the diesel generators during the operation optimization leveraging more flexibility to facilitate the gird-forming task irrespective of the forecast deviations encountered in the actual system operation. However, in scenarios where such

low-rated diesel generators operate close to their maximum loading limits, $Mode_{MaxLoad}^{Diesel}$ is first activated and precautions are taken to use the other grid-following dispatchable sources to aid the grid-forming task, unless restricted by their component limits. Since PV is considered as non-dispatchable, the battery reference will be adjusted in such scenarios to a value of $P_{Maxload}^{Limit}$ derived as given in (6.5) - (6.6):

$$P_{MaxLoad}^{Limit} = [e^{-sT_d}(P_{Gen}^{Total} - P_{Diesel}^{Max})]\frac{1}{\eta_{con}} - P_{PV} \tag{6.5}$$

$$P_{Diesel}^{Max} = \sum_{n=1}^{N}(DG_{max_n}^{PMS} \times DG_n^{Rated} \times U_{DG_n}^{t}) \tag{6.6}$$

where P_{Diesel}^{Max} is the maximum allowed power contribution from the diesel plant and $DG_{max_n}^{PMS}$ is the allowable maximum loading margin set by the power management strategies for DG_n.

6.4.2.4. Battery power management

The battery unit receives its original reference command from the EMS in the Gensup mode. This reference will be first adjusted to ensure the diesel loading limits as in (6.7):

$$\begin{aligned} P_{Bat}^{Dispatch} = {} & Mode_{MaxLoad}^{Diesel}\left[\min\left(P_{Bat}^{Rated\_max}, \max\left(P_{Bat}^{EMS}, P_{Maxload}^{Limit}\right)\right)\right] \\ & + Mode_{MinLoad}^{Diesel}\left[\max\left(-P_{Bat}^{Rated\_max}, \min\left(P_{Bat}^{EMS}, P_{Minload}^{Limit}\right)\right)\right] \end{aligned} \tag{6.7}$$

where P_{Bat}^{EMS} is the set-point generated by the tertiary-level EMS and $P_{Bat}^{Rated\_max}$ is the battery rated operating capacity.

In the approximate representation used in the EMS, the battery operation is regulated at an idle mode when the SOC reaches either its maximum or the minimum limit as depicted in Chapter 3. However, in actual operation, the suggested idle mode is realized at a relatively small non-zero power level to allow the battery DC-DC converter to continue the DC-link voltage regulation undisturbed. Also, stepwise preventive measures are taken to stall possible violations in the battery SOC limits. Three SOC regions are defined for both overcharge and overdischarge scenarios namely, “Warning”, “Boundary”, and “Critical” as shown in Figure 6.3.

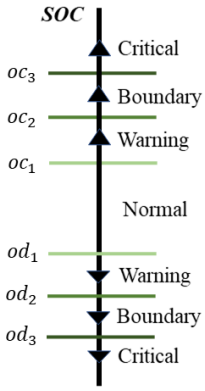

Mode	Gensup mode	
	Overcharge conditions	Overdischarge conditions
Normal	$P_{Bat}^{Ref} = P_{Bat}^{Dispatch}$	
Warning	$Mode_{SOC}^{Warning}=1$ → Warning	
Boundary	$Mode_{SOC}^{Boundary}=1$ → $P_{Bat}^{Ref} = -P_{Bat}^{Boundary}$	$Mode_{SOC}^{Boundary}=1$ → $P_{Bat}^{Ref} = P_{Bat}^{Boundary}$
Critical	$Mode_{SOC}^{Critical}=1$ → $P_{Bat}^{Ref} = P_{Bat}^{Critical}$	$Mode_{SOC}^{Critical}=1$ → $P_{Bat}^{Ref} = -P_{Bat}^{Critical}$

	Isolated mode	
	Overcharge conditions	Overdischarge conditions
Normal	Normal operation	
Warning	$Mode_{SOC}^{Warning}=1$ → Warning	
Boundary	$Mode_{SOC}^{Boundary}=1$ → $P_{Bat}^{Limit_{SOC}} = -P_{Bat}^{Boundary}$	$Mode_{SOC}^{Backup}=1$ (until changed by Tertiary Control)
Critical	$Mode_{SOC}^{Critical}=1$ → $P_{Bat}^{Limit_{SOC}} = P_{Bat}^{Critical}$ (until SOC reduces to 90%)	

Figure 6.3 Overcharge and overdischarge preventive measures

In the Gensup mode, the battery reference (P_{Bat}^{Ref}) given to the primary controls is defined based on the SOC operating regions as shown in Figure 6.3. Within the normal SOC limits, P_{Bat}^{Ref} was defined similar to $P_{Bat}^{Dispatch}$. In the overcharge region, if the SOC surpasses oc_1 while charging, as in Figure 6.3, a "overcharge warning" signal will be issued to the OPU while continuing the battery operation at the suggested $P_{Bat}^{Dispatch}$. If battery SOC reaches the boundary region ($Mode_{SOC}^{Boundary}$=1) and continues its charging operation, the secondary controls overwrite $P_{Bat}^{Dispatch}$ and change P_{Bat}^{Ref} to $-P_{Bat}^{Boundary}$ decreasing the charging rate to a lower value. After reaching the critical SOC stage ($Mode_{SOC}^{Critical}$=1), P_{Bat}^{Ref} will be set to $P_{Bat}^{Critical}$ such that it slowly discharges until P_{Bat}^{EMS} is adjusted by the tertiary controller in the next time-step. Similar set of steps will be initiated for the overdischarge region as shown in Figure 6.3.

In contrast to the Gensup mode of operation, battery overcharge preventive measures have to be taken without interfering the VSC grid-forming controls in the Isolated mode. Therefore, once the battery SOC satisfies conditions for either overcharge boundary ($Mode_{SOC}^{Boundry}$) or critical ($Mode_{SOC}^{Critical}$) regions as shown in Figure 6.3, the secondary controls activate $Mode_{SOC}^{Limit}$. Under this mode, the power available through the rest of grid-following sources is limited to allow the battery operation at a minimum reserved power

level ($P_{Bat}^{Limit_{SOC}}$) defined under each overcharge region. As shown in Figure 6.3, a minimum charging power level of $-P_{Bat}^{Boundary}$ is allowed for the overcharge boundary region. Once the battery SOC exceeds the overcharge critical conditions, the power reserve margin is set to a discharging power level of $P_{Bat}^{Critical}$. Once activated, the overcharge critical mode is forced until the SOC reduces to a pre-defined SOC level (oc_{min}) to curb frequent cycling of the battery unit. During possible overdischarge events ($Mode_{SOC}^{Backup}$ = 1), the secondary controller warns the OPU, and a diesel generator will be reconnected to the grid to ensure reliability and supply security.

In addition, the generated duty factor for the battery DC-DC converter is appropriately limited to mitigate battery maximum power violations due to sudden transients in the unit-level [107]. However, if the duty factor gets restricted in its upper limit for prolonged periods, the regulation of the DC-link voltage gets interrupted. Therefore, precautionary measures must be utilized in both tertiary and secondary layers to avoid such scenarios. Violation of this condition in the Gensup mode is restricted by limiting the battery reference within its rated value. For the Isolated mode, when the battery power reaches close to its maximum limit, secondary controller activates $Mode_{Power}^{Limit}$. If this mode gets activated during a charging operation, the power available through the grid-following sources is limited to allow the battery operation at a power level ($P_{Bat}^{Limit_{Power}}$) close to its limit. If $Mode_{Power}^{Limit}$ is activated during a discharging mode, the secondary controller issues a warning signal to the OPU, suggesting the re-connection of a diesel generator.

6.4.2.5. PV power management

In Chapter 3 to Chapter 5, it was identified that remote power systems can undergo scenarios with low loading and high solar penetrating conditions. Although such events are of low probability, a dynamic control strategy is needed to manage the available solar resource without causing violations in the individual system components and stability of the overall operation. The maximum allowable PV power (P_{PV}^{Max}) is usually set at a value, P_{PV}^{Limit}. By default, P_{PV}^{Limit} is set equivalent to the PV array rated power unless changed by the tertiary controls. Three possible scenarios that require adjustments to P_{PV}^{Max} from the secondary controls are identified.

During the Gensup mode, if the diesel generator undergoes a minimum loading scenario and battery unit is unable to recover this, the secondary controls will derive P_{PV}^{Max} based on the required adjustment level to maintain the minimum diesel loading. In the Isolated mode, however, P_{PV}^{Max} is switched from P_{PV}^{Limit} only when the secondary controller initiates either the battery overcharge power reserve mode ($Mode_{SOC}^{Limit}$=1) and/or the battery charging power limit mode ($Mode_{Power}^{Limit}$=1) as shown in Figure 6.4.

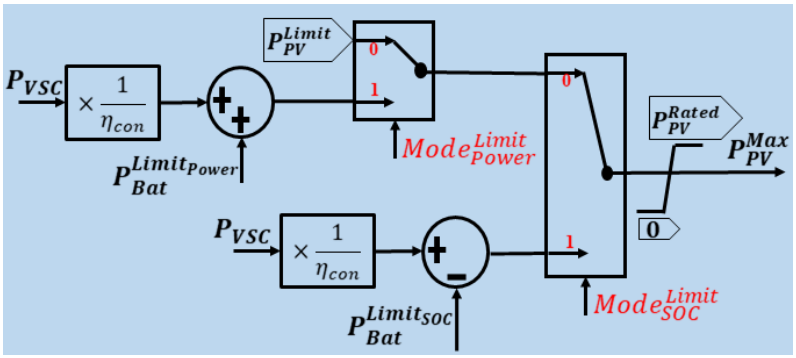

Figure 6.4 Formulation of the maximum PV power limit in Isolated mode

If both modes get initiated together, $Mode_{SOC}^{Limit}$ get priority over $Mode_{Power}^{Limit}$. During $Mode_{SOC}^{Limit}$, P_{PV}^{Max} is derived depending on the battery power reserve margin ($P_{Bat}^{Limit_{SOC}}$) as given in Figure 6.3 and the locally measured VSC active power output (P_{VSC}) as shown in Figure 6.4. During the overcharge boundary region ($P_{Bat}^{Limit_{SOC}} = -P_{Bat}^{Boundary}$), P_{PV}^{Max} is kept higher than the required power system demand by an amount of $P_{Bat}^{Boundary}$. This will allow the battery to remain in the charging mode at the required power reserve margin. If the energy surplus period persists and the battery moves into the overcharge critical region ($P_{Bat}^{Limit_{SOC}} = P_{Bat}^{Critical}$), P_{PV}^{Max} is reduced further to a value lower than the current system demand by an amount of $P_{Bat}^{Critical}$ to move the battery operation into the discharging mode. If $Mode_{Power}^{Limit}$ gets activated during battery charging operation, P_{PV}^{Max} is derived by adding the absolute value of the maximum allowable battery power ($P_{Bat}^{Limit_{Power}}$) to P_{VSC} as shown in Figure 6.4. This allows the battery unit to store the excess energy at a power level just below its maximum charging power.

6.4.2.6. Voltage and frequency restoration

During scenarios which require more than one diesel generator, the droop mode is activated ($Mode_{Droop} = 1$). Under droop mode, a restoration process with a slower control compared to the respective primary control loop is also activated to restore the nominal operating conditions [33]. Both frequency and voltage adjustments (ω^{Sec}, V^{Sec}) are derived to modify the frequency and voltage references used in the primary controls of each diesel unit. To derive ω^{Sec}, the system frequency is regulated at its nominal value using a PI compensator. Similarly, to derive V^{Sec}, the AC voltage at the diesel plant is regulated at its nominal value.

6.4.2.7. Unplanned initiation of isolated mode

Under normal conditions, the secondary controller evokes the Isolate mode as a planned event proposed by the tertiary controller. This ensures that adequate operating reserves are in order for the VSC grid-forming controls as predicted by the load and meteorological forecasts. Even if the grid-forming controls get interrupted due to an unexpected energy/power shortage, it is assumed that the diesel generators can be brought back online when deemed necessary. However, if the Isolated mode is enabled due to an unplanned event (Ex: in the event of a diesel plant failure) precautionary measures must be taken to maintain system stability and the operational limits. Therefore, whenever the system moves into an unplanned Isolated mode of operation with inadequate operating reserves, a load shedding scheme is needed to be integrated to supply power only to the critical loads and to avoid complete collapse of the system [108]. However, in this chapter, the focus is on the planned initiation of the Isolated mode as suggested by the tertiary layer.

6.4.3 Primary controls

6.4.3.1. Diesel plant

In the Gensup mode, diesel plant is responsible of controlling system frequency and voltage at their nominal values via proper adjustment of its active and reactive power output, respectively. The deployed voltage and frequency references ($\omega_{DG_n}^{Ref}, V_{DG_n}^{Ref}$) are generated using (6.8) and (6.9), respectively:

$$\text{ᘐ}_{DG_n}^{Ref} = \text{ᘐ}^{Nom} - Mode_{Droop}\left[Droop_{DG_n} \times P_{DG_n} - \text{ᘐ}^{Sec}\right] + Mode_{Sync_n}\left[\text{ᘐ}_{DG_n}^{Syn}\right] \quad (6.8)$$

$$V_{DG_n}^{Ref} = V_{DG}^{Nom} - Mode_{Droop}\left[Droop_{DG_n} \times Q_{DG_n} - V^{Sec}\right] + Mode_{Sync_n}\left[V_{DG_n}^{Syn}\right] \quad (6.9)$$

where ᘐ^{Nom} is the nominal frequency, V_{DG}^{Nom} is the nominal voltage, and $Droop_{DG_n}$ is the droop value of the considered diesel generator. $\text{ᘐ}_{DG_n}^{Syn}$ and $V_{DG_n}^{Syn}$ derived using a unit-level active synchronization scheme are used to adjust the references when $Mode_{Sync_n}$ is activated by the secondary power management strategies [109].

6.4.3.2. Renewable energy system

The PV power reference (P_{PV}^{Ref}) is obtained by controlling the PV output voltage at the extracted MPPT voltage using a PI compensator. The upper limit (P_{PV}^{Max}) of P_{PV}^{Ref} is determined as discussed in Section 6.4.2.5. The derived P_{PV}^{Ref} will be deployed in the PV Boost DC-DC converter controls to regulate the PV output power using a PI controller.

During all operating modes, the battery DC-DC converter is used to maintain the DC-link voltage at its reference value using a PI controller. The direction of the battery current is used to identify its mode of operation (charging/discharging). Based on the identified mode, the DC-link control loop is adjusted to facilitate the Buck mode for charging and Boost mode for discharging operation.

The VSC control is formulated in the dq rotational framework. A Phase Locked Loop (PLL) unit as in Figure 6.5 is integrated to identify the angle (θ_{Grid}) and the frequency (ᘐ_{Grid}) of the VSC output voltage (V_{Grid}) [110]. The PLL adjusts the rotational speed of the dq frame (ᘐ) with respect to a reference frequency such that in steady state the q-axis component of the VSC output voltage (V_{Grid_q}) is forced to zero and its d-axis component (V_{Grid_d}) get effectively aligned with the voltage vector. In the Gensup mode, as V_{Grid} is determined by the AC grid formed by the diesel units, the angle between d-axis and the stationary α-axis and ᘐ represent θ_{Grid} and ᘐ_{Grid}, respectively. Thus, in steady-state, ᘐ equals ᘐ^{Nom} while V_{Grid_q} settles at zero. However, in the Isolated mode, it is the task of VSC controls to form and regulate the amplitude and frequency of the VSC output voltage.

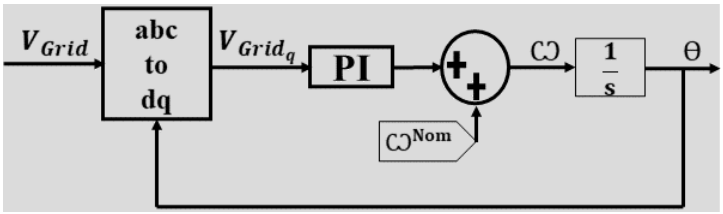

Figure 6.5 Schematic of the PLL [110]

The derived d-q components of the converter output current I_{vsc} (I_{vsc_d}, I_{vsc_q}) are independently regulated at their respective references (I_d^{Ref}, I_q^{Ref}) to derive the VSC switching signals through the Pulse Width Modulation (PWM) scheme as in Figure 6.6. [106]. Also, to decouple the control of I_{vsc_d} and I_{vsc_q}, the feedforward terms $I_{vsc_q} L_f \omega$ and $I_{vsc_d} L_f \omega$ are included where L_f is the filter inductance.

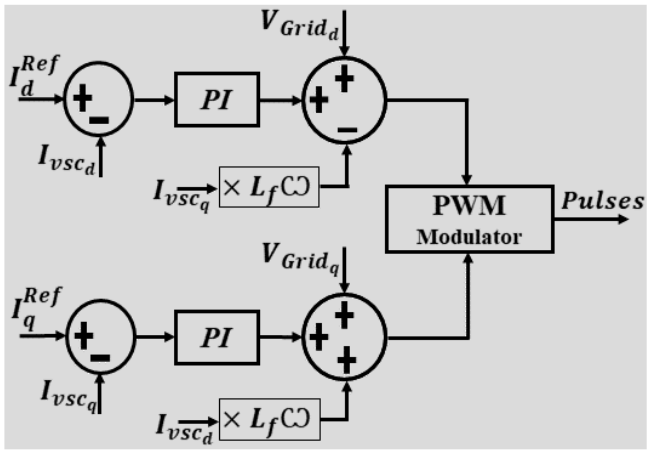

Figure 6.6 VSC current control [35], [106]

During the Gensup mode, the VSC active power reference (P_{VSC}^{Ref}) and the reactive power reference (Q_{VSC}^{Ref}) provided by the secondary controls are used to calculate I_d^{Ref} and I_q^{Ref}, respectively, as shown in Figure 6.7, where $V_{Grid_{L-N}}^{peak}$ is the nominal peak value of the line-to-neutral voltage at the VSC output [106].

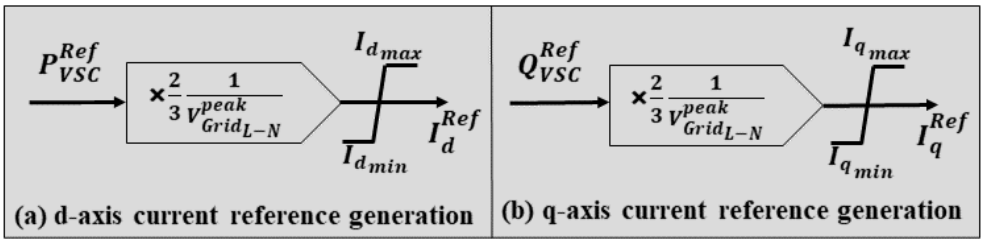

Figure 6.7 VSC grid-following mode: current reference generation [106]

In the Isolated mode, the diesel plant goes out of operation and the VSC is operated as a grid-forming unit to establish and regulate the grid voltage and frequency. As depicted in Figure 6.8, two outer-voltage control loops are deployed to generate the d-q axis current references.

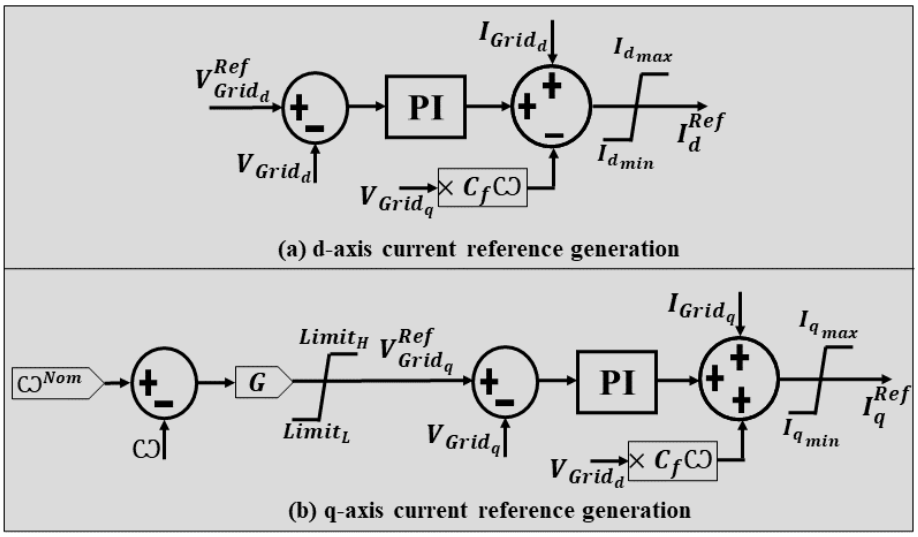

Figure 6.8 VSC grid-forming mode: current reference generation [106], [110]

As V_{Grid_q} settles at zero in steady-state, regulation of V_{Grid_d} at the specified reference value ($V_{Grid_d}^{Ref}$) is deemed adequate to control the grid voltage [106]. Therefore, the voltage control loop as given in Figure 6.8(a) is used to generate I_d^{Ref} where C_f is the filter capacitance and $V_{Grid_d}^{Ref}$ is defined as $V_{Grid_{L-N}}^{peak}$. The frequency control is achieved by generating I_q^{Ref} by controlling V_{Grid_q} at the q-axis voltage reference value ($V_{Grid_q}^{Ref}$), which is derived through regulating ω at the nominal grid frequency ω^{Nom} as depicted in Figure

6.8(b) where G is a pure control gain [106]. In Figure 6.8, I_{Grid_d} and I_{Grid_q} are the d-q components of the VSC grid side current.

6.5 Proposed Operation Evaluation Procedure

Operation evaluation serves three main purposes, 1) Identification of possible scenarios suggested by the EMS that could impede the logical progression of the system operation in a dynamic environment subjected to frequent disturbances such as random changes in load, PV output, etc., 2) Verification of the competence of lower-level controllers to stably and securely navigate such scenarios considering a sufficiently accurate representation of the subjected power system, and 3) Applying proper modifications to the derived operation routines when required. Such analysis increases the system security and reduces any apparent risks when encountered unanticipated situations. By making necessary adjustments to the unit commitment and dispatch schedules, any dynamic instabilities, and undesired operating conditions such as temporary overloading of equipment, limit violations, etc., can be minimized. The proposed operation evaluation routine is shown in Figure 6.9.

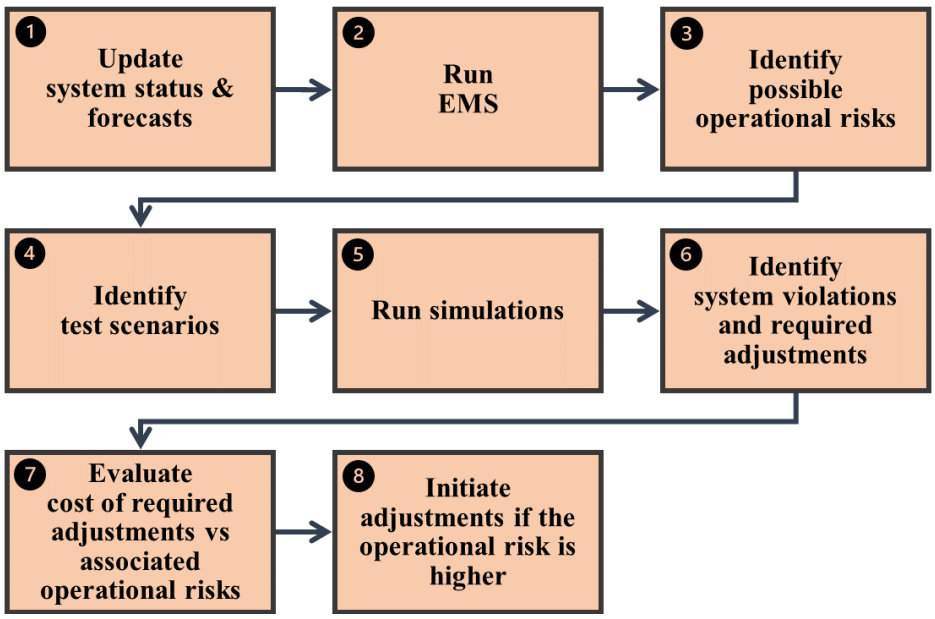

Figure 6.9 Proposed operation evaluation routine

Once the updated forecasts are received, the updated operation plan is analysed to identify possible operational risks and required test scenarios. In general, the scope of the required analysis in Step 3-4 in Figure 6.9 depends on the assumptions made during the EMS formulation and the extent of uncertainty related to the actual operation. In Table 6.1, the general requirements for operation evaluation of remote off-grid power systems are identified by comparing the traits of actual power systems with that of their representation used in the EMS. In Step 5, an EMT simulation model is used to further analyse the identified scenarios through dynamic simulations of selected test cases. The simulations will be used to detect scenarios that would deteriorate the stable progression of the system variables and violate their nominal values in Step 6. In Step 7-8, the original set-points will be adjusted based on engineering judgment if the operational risk associated with the detected violations is deemed significant compared to the losses incurred in the quantitative objectives (i.e., increase of costs and emissions) due to required remedial adjustments in the initial operational routine to prevent the identified risk.

The operation evaluation process can be performed either once prior to the start of each day or can be repeated with updated system conditions and forecasts as the control horizon progresses. However, given the highly priced technical manpower in these remote communities, deploying a system operator throughout the day to conduct this EMT simulation-based operation evaluation process will be both impractical and cost-prohibitive. Therefore, in the current study, it is assumed that this evaluation process is only conducted once prior to each daily control horizon based on engineering judgement.

Table 6.1 Identification of test cases for operation evaluation

	Actual system	EMS representation	Operation evaluation
Active power regulation	- Performed by the grid-forming controller. - Depends on system inertia, component limits, operational reserve etc.	- Steady state power balance is always maintained through rules and/or cost-based penalties.	Grid-forming controller performance must be tested for scenarios where, - Grid-forming unit is operating close to its rated capacity. - Grid-forming unit is operating under limited availability of reserves. - The adopted test cases must consider conditions under varying loads/resources, possible load unbalance, motor starting transients etc.
Reactive power regulation		- Not considered	
Mode transitions	- Controlled by the adopted transition controls. - Depend on pre- and post-transition system status.	- Seamless	- The transition controls must be validated for critical transitions suggested in the operation routine with varying system conditions.
Component limits	- Ensured by lower-level controls. - Subjected to violations	- Always maintained through rules and/or cost-based penalties.	- Violation-prone scenarios identified in the operation routine must be tested to validate lower-level controller performance under varying system conditions.
Component failures and faults	- Can cause due to unanticipated system conditions.	- Not considered	- Capability of the power system to navigate through component failures, faults, and any other plausible extreme conditions must be tested.
Forecast uncertainties	- The actual load and resources are subjected to variations from the forecasted values.	- Assumes the uncertainty spectrum can be captured using finite set of scenarios.	- Scenarios operating closer to the minimum operating reserve must be tested under worst-cases.

.

6.6 Study System Description and Data Inputs

To demonstrate the applicability of the proposed power management strategies and the operation evaluation framework, simulations were performed considering the same remote off-grid system used in previous chapters. When developing the tertiary level EMS, the input parameters were incorporated similar to that presented in Chapter 3 to Chapter 5.

The main input data used in the lower-level control functions in producing the discussed results is given in Table 6.2. To obtain the simulated results, a detailed EMT model of the system as shown in Figure 6.1 was developed in PSCAD/EMTDC™ software environment to capture the electrical transients and other dynamic effects with adequate accuracy. For PV and battery, the specifications similar to Appendix A were used. Rest of the main data used in modelling the system components in the simulated cases is given in Appendix E.

Table 6.2 Input data used in the lower-level control layers

Parameter	Value
$DG_{min_n}^{PMS}$ [%]	30
$DG_{max_n}^{PMS}$ [%]	97
T_d [s]	0.1
oc_1, oc_2, oc_3 [%]	95, 97, 99
od_1, od_2, od_3 [%]	15, 13, 11
oc_{min} [%]	90
$P_{Bat}^{Boundary}$ [MW]	0.05
$P_{Bat}^{Critical}$ [MW]	0.025
$P_{Bat}^{Limit_{Power}}$ [MW]	± 0.55
ω^{Nom} [rads^{-1}]	376.9911
V_{DG}^{Nom}(L-L rms) [kV]	0.6
V_{DC} [kV]	1
V_{Grid} (L-L rms) [kV]	0.48
V_{sys} (L-L rms) [kV]	25

The system loads were represented using five major load centers as shown in Figure 6.1 with residential sector consuming bulk of the produced electricity (approximately 80%) compared to the share of industrial/commercial loads [3]. Residential loads were represented using 80% of constant impedance loads and 20% of constant power loads with power factor in the range of 0.97-1. Under normal operating conditions, the industrial/commercial load were consisted of 50% of constant impedance loads and 50% of constant power loads with power factor in the range of 0.95-0.97 [104]. Under specific test cases, induction motor loads were also added to the test network. Compared to winter, the remote off-grid power systems operate under relatively high load unbalance during summer. Therefore, to replicate realistic conditions for summer season, loads were unevenly distributed among the three phases (phase-a 30.2%, phase-b 35.6%, and phase-c 34.2% [104]), in contrast to the balanced representation used in the EMS.

Although the developed power system model is assumed accurate for the purpose of demonstrating the proof-of-concept of the derived methodologies, when deploying in an actual real-world system, the simulation model must be validated with actual system data during the commissioning stage to verify its competence in capturing the important properties of the respective real-world power system.

6.7 Results and Discussion

6.7.1 Operation evaluation

This section demonstrates the operation evaluation process considering the day-ahead optimum operation plan derived for a summer day similar to that shown in Figure 6.10.

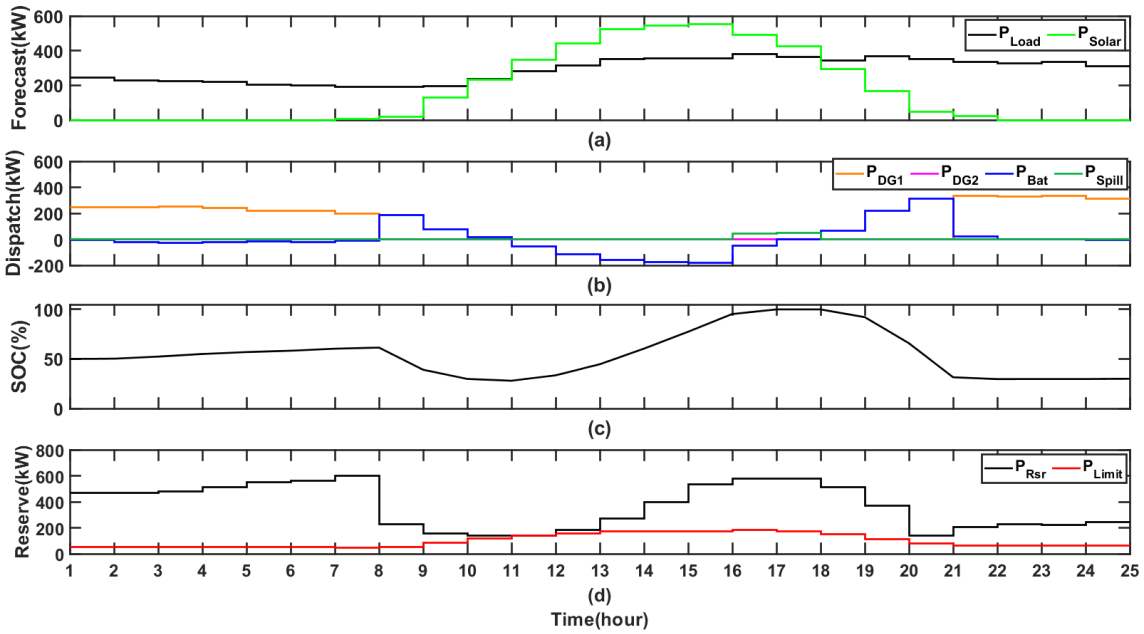

Figure 6.10 Day-ahead optimum operational routine: (a) Hourly forecast, (b) Operational routine, (c) SOC, and (d) Available operational reserve and minimum requirement

6.7.1.1. Step 1-4 of operation evaluation process

In Figure 6.10, EMS suggests the Gensup mode for morning and late-night hours whereas the Isolated mode is suggested for the mid-day time frame to extract the maximum possible solar energy within the system limits. The EMS initiates the Isolated mode for the 8th hour, just before the predicted increase of available solar power. The battery discharges during 8-10 am and gradually moves into the charging mode as the solar power increases during mid-day. As the battery reaches its overcharge limit, the available solar power has been curtailed to ensure operational safety of the battery unit. Also, as the solar power decrease in the evening hours, battery moves back to the discharging mode from 18-20th hour. The Gensup mode is re-initiated from the 21st hour.

Given the high penetration of intermittent PV energy and the initiation of VSC grid-forming mode, several testing scenarios can be identified for the considered summer day operation. The transitions occurring from Gensup to Isolated mode in 8th hour and Isolated to Gensup in 21st hour must be verified under varying system conditions to ensure the competence of lower-level controls to facilitate seamless transfer of power. In 10th to 12th hour, the required minimum operating reserve has met only marginally. The battery unit

hits its overcharging limit in the 17th hour and this scenario is also prone to violations if the lower-level controls are unable to curtail the excess PV power.

6.7.1.2. Step 5-6 of operation evaluation process

The scenario depicted in Figure 6.11-Figure 6.12 shows the Gensup to Isolated mode transition occurring in 8th hour. The load and solar irradiance have been changed slightly from the forecasted average values to capture the intra-hour variations. The Gensup to Isolated transitioning mode is activated around 4 s and the diesel active and reactive power output is gradually decreased by increasing the VSC active and reactive power output, respectively, as discussed in Section 6.4.2.2. Once the diesel power reaches a value close to zero and the system becomes stable, the secondary controller enables the Isolated mode at 16 s by opening the diesel breaker while transferring the grid-forming controls to the VSC. The transition occurs smoothly and the VSC grid-forming controls stabilize the system rather quickly as depicted in Figure 6.11 and Figure 6.12.

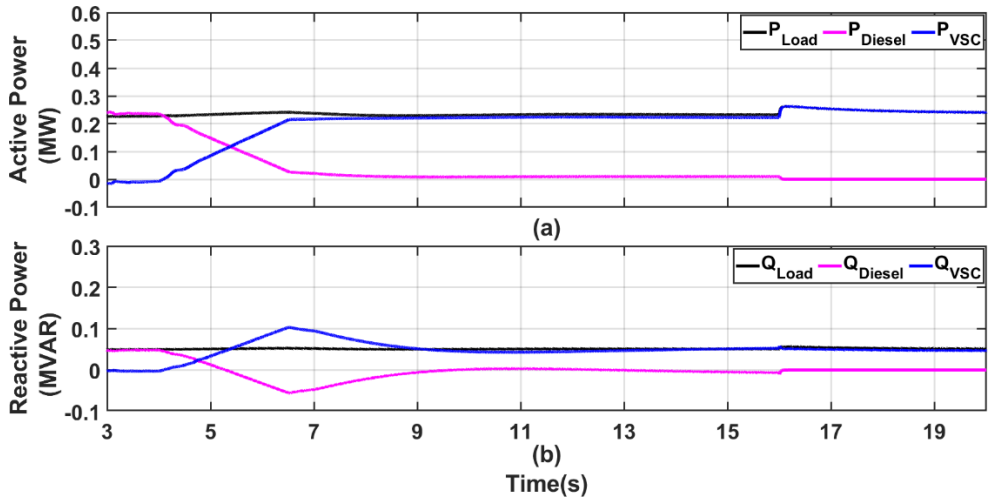

Figure 6.11 Transition from Gensup to Isolated mode: (a) Active power and (b) Reactive power

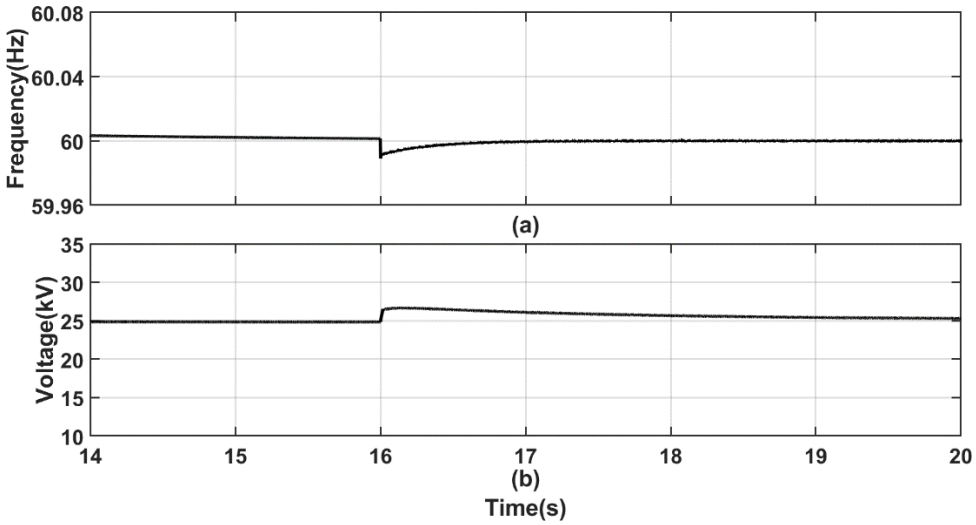

Figure 6.12 Transition from Gensup to Isolated mode: (a) Frequency and (b) Voltage

The system operation was also tested for conditions prevailing in the 10th hour under low availability of operating reserves and high variability of loads and resources. Prior to the considered disturbances, the power system is in a stable operating condition supplying a load of 0.25 MW/0.05 MVAR as shown in Figure 6.13. At 11s, the system undergoes a small transient period due to a start of an induction motor and quickly recovers to the stable system condition. During the period from 14-27s the system undergoes variations in both solar irradiation and load demand.

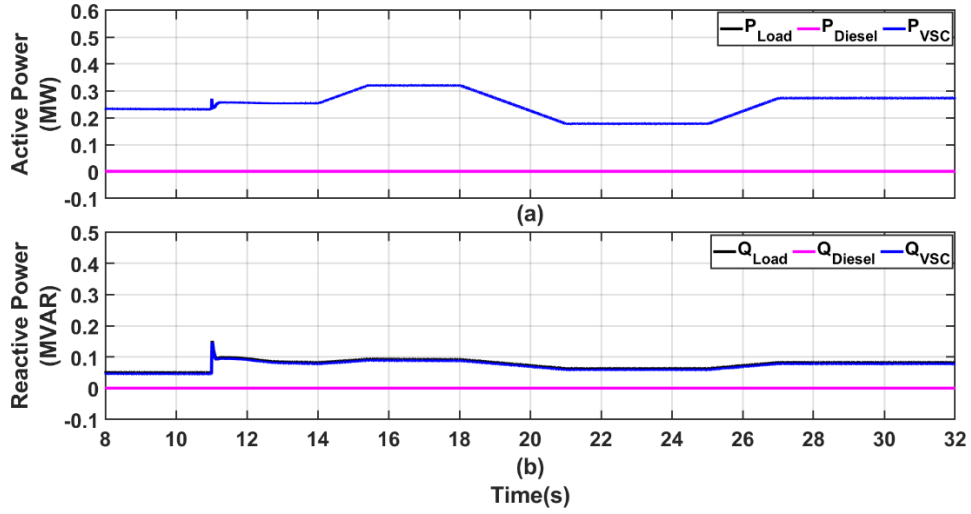

Figure 6.13 Summer day (10th hour): (a) Active power and (b) Reactive power

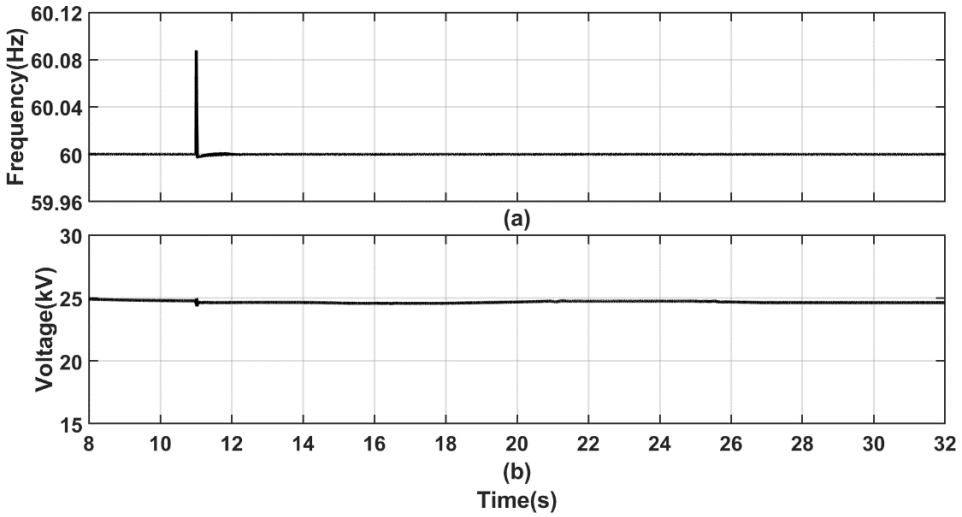

Figure 6.14 Summer day (10th hour): (a) Frequency and (b) Voltage

Throughout this period, the VSC gird-forming controls effectively adjust the battery power output and balance the grid power stably as in Figure 6.15. It is evident that the VSC grid-forming controls has enough power reserves even if the system undergoes high load demands with less availability of solar power compared to the forecasted values. If this period continues, the operation mode will have to be changed back to Gensup mode considering the low availability of energy reserves. However, the probability of occurrence for an unstable transition under such conditions is extremely low.

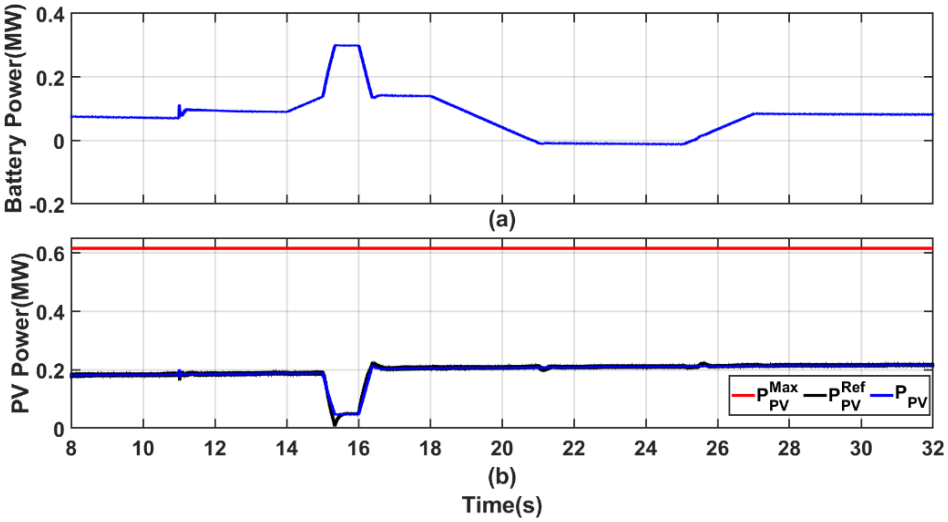

Figure 6.15 Summer day (10th hour): (a) Battery power and (b) PV power

Figure 6.16-Figure 6.18 depict the simulation results for a system condition prevailing around the 17th hour. According to Figure 6.16, initially the battery is in a discharging mode with the SOC just above 97%. Although the battery has passed both SOC limits corresponding to the overcharge "Warning" and "Boundary" regions, those modes are not activated due to the detected discharging mode of operation. A gradual increase of irradiance moves the battery into the charging mode around 10 s and the overcharge boundary is triggered around 13.5 s. During this mode, the maximum limit of PV output power (P_{PV}^{Max}) gets reduced to curtail the excess PV power while allowing the battery to operate in the charging mode at a lowered power level as defined by $P_{Bat}^{Boundary}$. The VSC grid-forming controls effectively facilitates the start of an induction motor around 18 s. The required active power slack is taken through the PV unit and the battery continue its operation in the overcharge boundary region. At 30 s, the upper limit of the PV reference gets increased due to a reduction in the available solar irradiance and the battery shifts back into the discharging mode to provide the required active power slack. This again allows the PV MPPT operation to get enabled. Under all scenarios, the frequency and voltage variations demonstrate a stable response as shown in Figure 6.18.

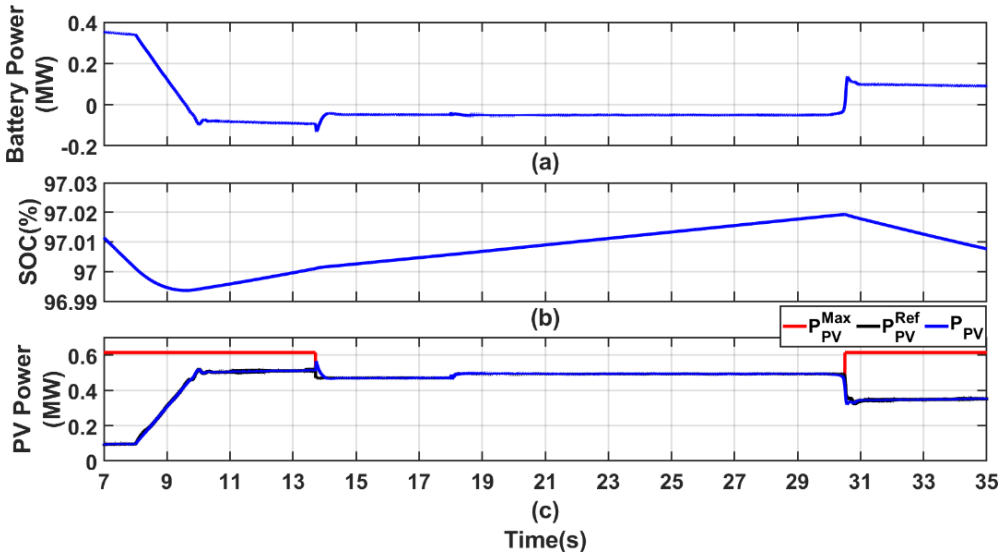

Figure 6.16 Summer day (17th hour) case 1: (a) Battery power, (b) SOC, and (c) PV power

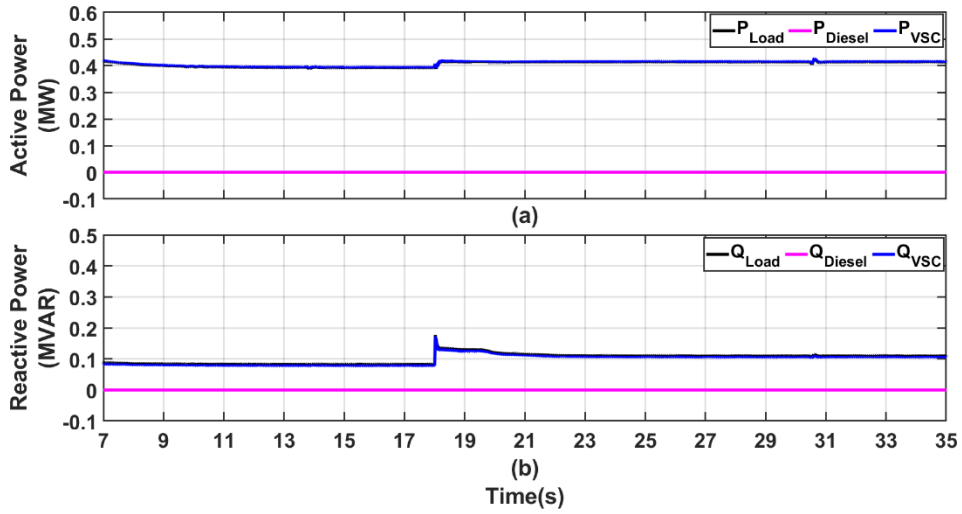

Figure 6.17 Summer day (17th hour) case 1: (a) Active power and (b) Reactive power

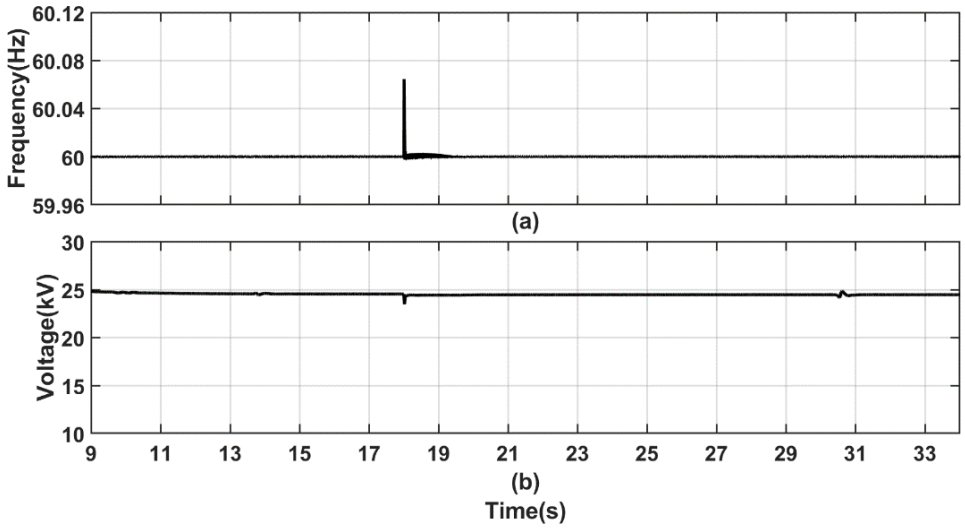

Figure 6.18 Summer day (17th hour) case 1: (a) Frequency and (b) Voltage

The capability of the power system to navigate through fault conditions during the energy excess period was also assessed. In Figure 6.19, the induction motor starting event previously simulated in the 17th hour scenario is replaced with a three-phase to ground fault applied at Bus_3 in Figure 6.1. The applied fault was cleared after 0.15 s by breaking the faulty section at Bus_2. The system undergoes a transient period and quickly recovers to the normal operating conditions in about 3 s following the fault clearing. As shown in Figure 6.19, the events initiated after 30 s take place similar to that discussed under 17th hour case 1 scenario.

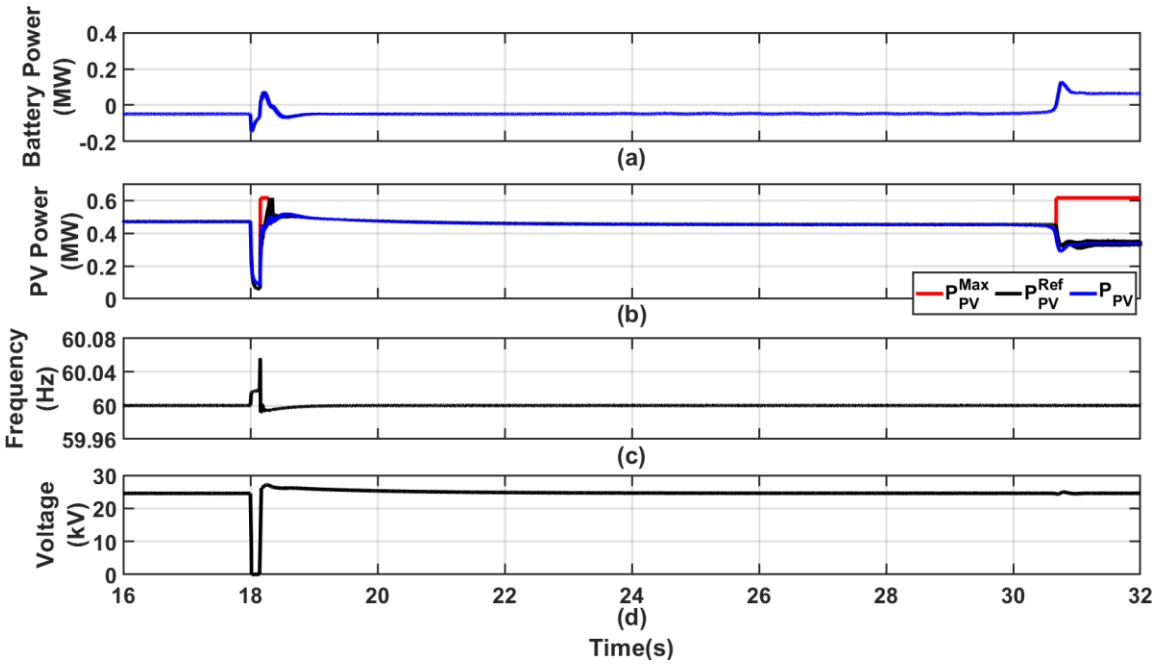

Figure 6.19 Summer day (17th hour) case 2: (a) Battery power, (b) PV power, (c) Frequency, and (d) Voltage at Bus_8

The scenario depicted in Figure 6.20-Figure 6.21 simulates the Isolated to Gensup mode transition occurring in 21st hour. Around 10 s, the transitioning mode gets activated by closing the main breaker of the diesel plant while initiating the synchronization controls for the scheduled incoming diesel generator (DG_1). Under the simulated system conditions, it takes about 1 s for the detected differences in voltage magnitude, frequency, and phase angle across the interfacing breaker of DG_1 to satisfy the pre-defined requirements. At about 11 s, the DG_1 interfacing breaker is closed while switching the VSC control mode from grid-forming to grid-following. Then the secondary controller gradually moves the active and reactive power references of the grid-following VSC to the values defined for the 21st hour as shown in Figure 6.20. The transition occurs smoothly, and the initial transients seen in the frequency and voltage variations remain within the acceptable values as shown in Figure 6.21.

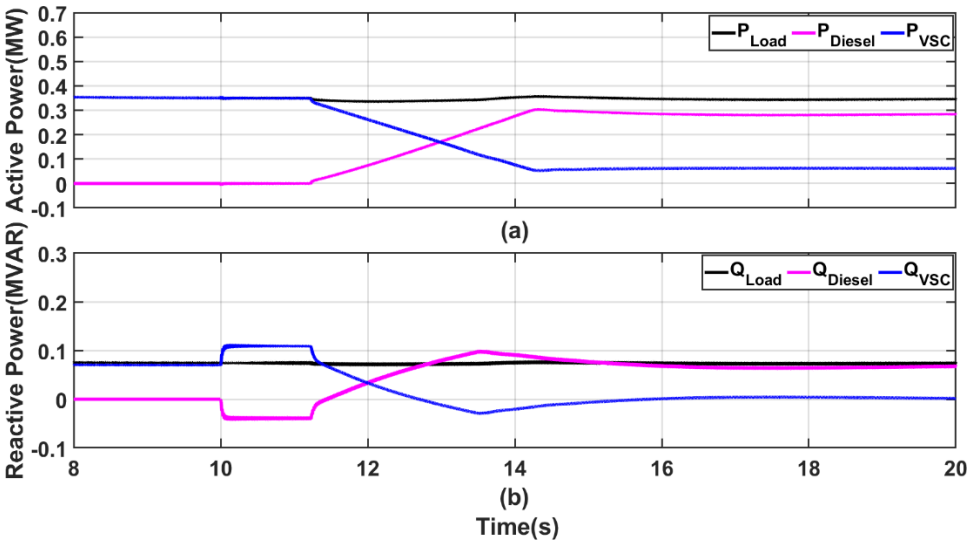

Figure 6.20 Transition from Isolated to Gensup mode: (a) Active power and (b) Reactive power

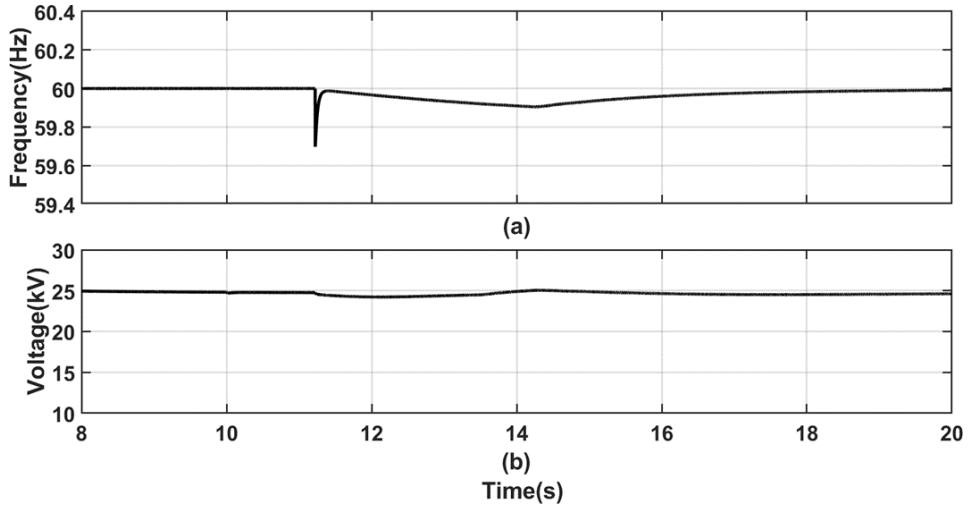

Figure 6.21 Transition from Isolated to Gensup mode: (a) Frequency and (b) Voltage

6.7.1.3. Step 7-8 of operation evaluation process

The operational evaluation revealed the competence of the lower-level power management strategies to navigate the suggested operation trajectory. High operational risks requiring modifications to the derived optimum operational trajectory were not discovered. Although only a short operational reserve margin is available in 10^{th} -12^{th} hour, the operation risk only exists in terms of the available energy as the required demand lies well within the power capability of both the battery unit and the VSC. Also, as the EMS

operates with an integrated uncertainty management scheme as discussed in Chapter 5, the hierarchical controller has the flexibility to appropriately change the operation trajectory when more reliable forecasts are available during the intra-day time frame. Therefore, the unit commitment and dispatch commands will be kept unchanged from what was proposed in the original operational plan as suggested in Figure 6.10.

6.7.2 Operation evaluation for other possible scenarios

This section demonstrates the applicability of the proposed power management strategies and operation evaluation considering possible critical operating scenarios detected in other optimum operation routines derived by the EMS.

6.7.2.1. Diesel maximum loading scenario

In Chapter 4 and Chapter 5, it was noted that the developed operation optimization framework under the influence of DR can deploy the battery unit and DG_1 to meet the demand for the considered winter cases as discussed in Figure 4.10 and Figure 5.12(b) for the day-ahead time frame and intra-day time frame, respectively. Under such scenarios, during the peak load period, DG_1 operates close to its maximum loading limit allowed during the EMS formulation. During this period, the deployed power management strategies should be able to appropriately adjust the battery power command in order to maintain the DG_1 maximum loading while ensuring system stability.

In Figure 6.22 - Figure 6.24, the system operation has been simulated for the conditions prevailing during a winter day peak load period under such conditions. Initially, VSC is operating under the grid-following mode with the battery command (P_{Bat}^{Ref}) set at the reference (P_{Bat}^{EMS}) given by the EMS while DG_1 is forming the grid close to its operating capacity. A 25 kVA induction motor starts around 13 s and DG_1 manages to recover the system operation from the initial transient. As the active power demand increases, the secondary power management controls gradually increase P_{Bat}^{Ref} from P_{Bat}^{EMS} to mitigate possible violations in DG_1 loading limits and the stable operation prevails.

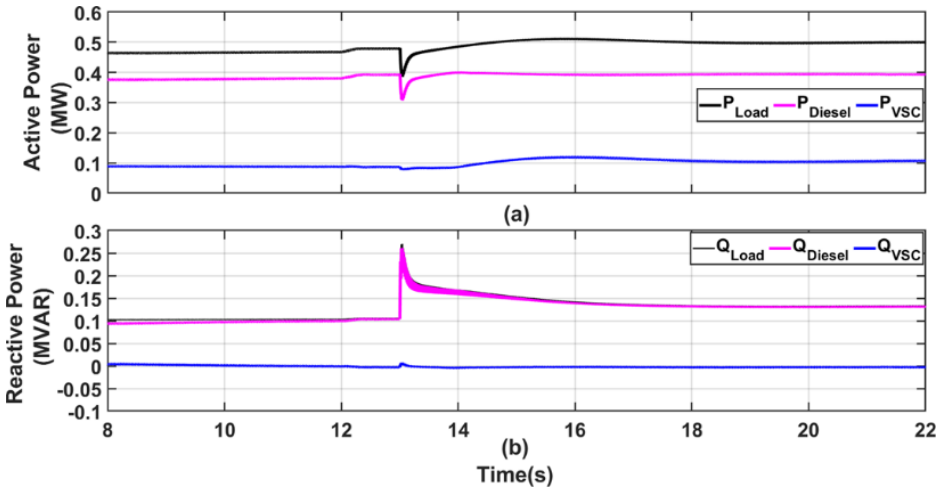

Figure 6.22 Maximum loading case 1: (a) Active power and (b) Reactive power

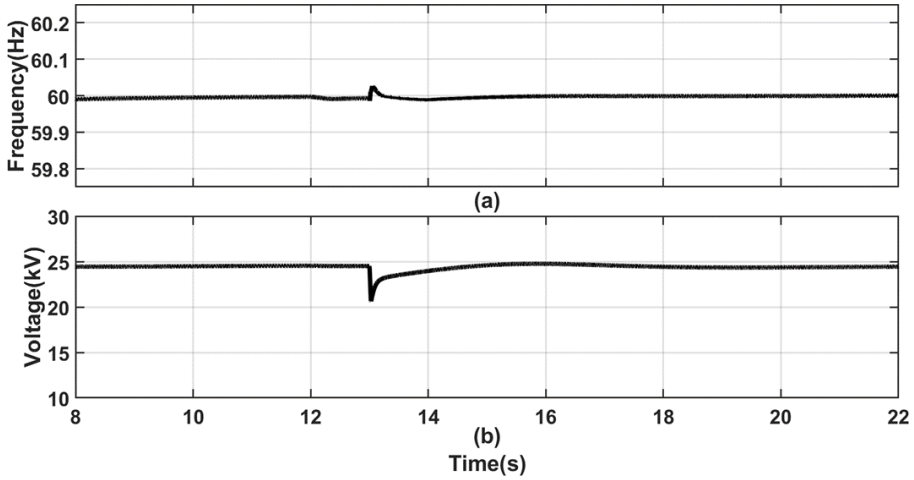

Figure 6.23 Maximum loading case 1: (a) Frequency and (b) Voltage

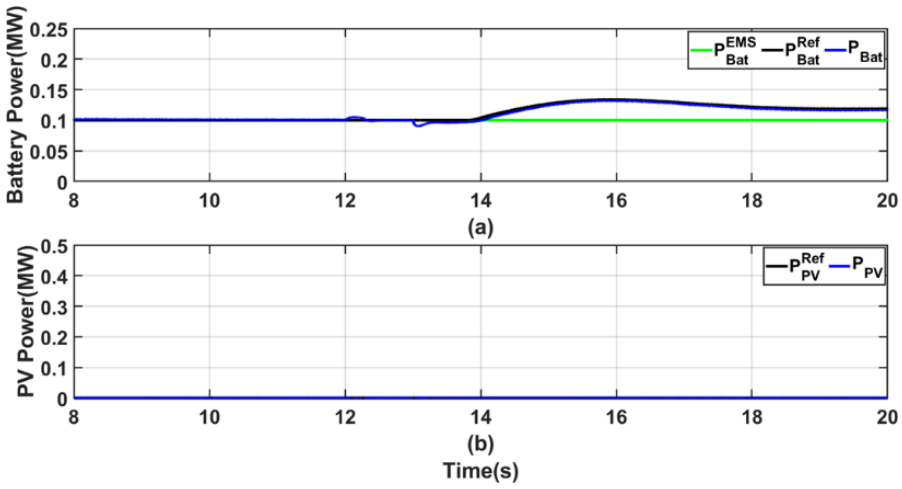

Figure 6.24 Maximum loading case 1: (a) Battery power and (b) PV power

However, if the battery reserves deplete earlier than anticipated, the grid-forming task of DG_1 can be obstructed in both power and energy considerations, if the start of DG_2 had not been scheduled. Figure 6.25 - Figure 6.27 demonstrate the system response under such conditions. Battery reaches its overdischarge boundary around 8.2 s and the battery power management restricts P_{Bat}^{Ref} to a value of 0.05 MW discharging. As the load increases with a start of an induction motor, DG_1 passes its maximum limit which obstructs its grid-forming capability, and the system goes unstable afterwards. Although the scenario depicted in Figure 6.25 - Figure 6.27 is a "what-if" case, it well demonstrates the need of operation evaluation and uncertainty management in order to alleviate risky operating conditions that cannot be corrected by the incorporated power management strategies.

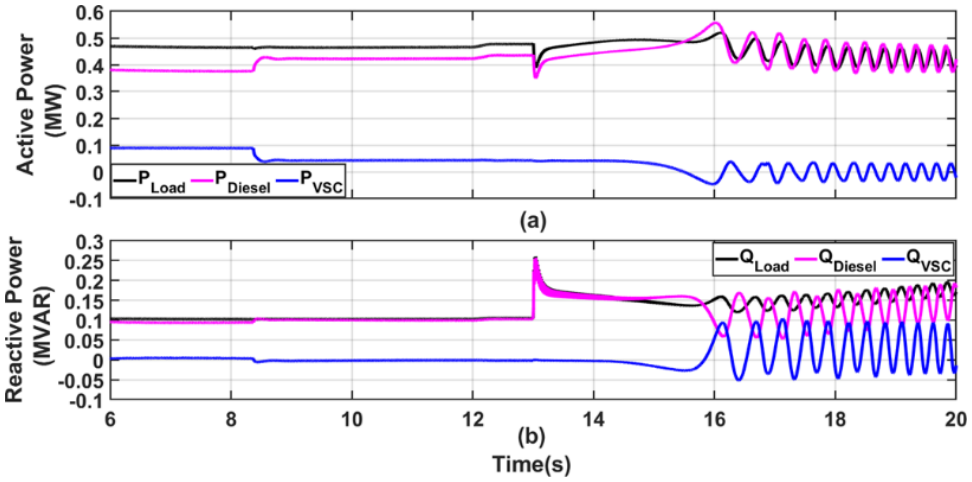

Figure 6.25 Maximum loading case 2: (a) Active power and (b) Reactive power

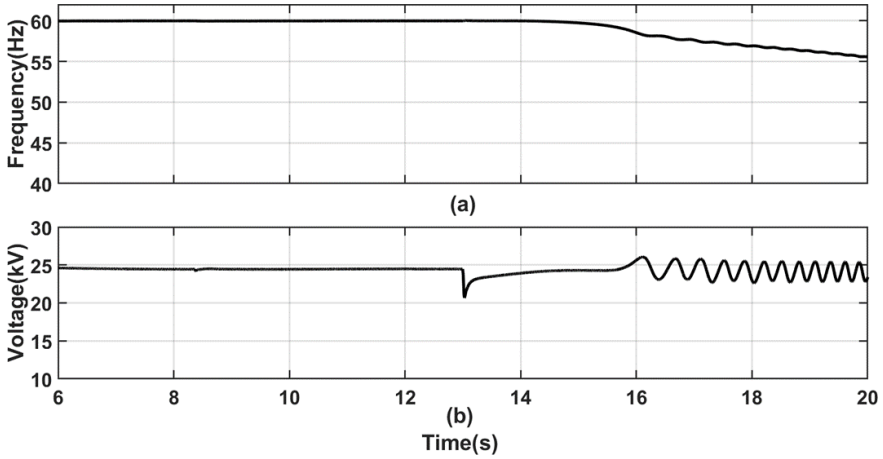

Figure 6.26 Maximum loading case 2: (a) Frequency and (b) Voltage

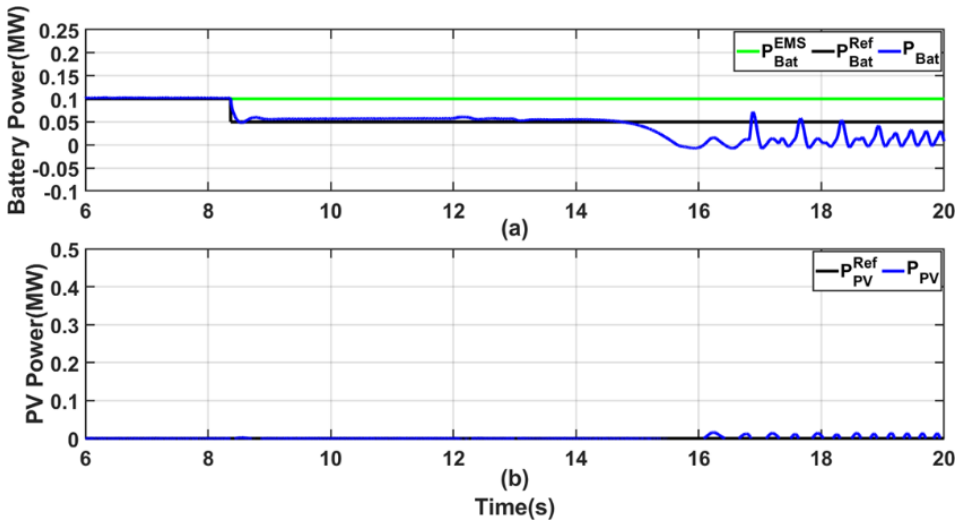

Figure 6.27 Maximum loading case 2: (a) Battery power and (b) PV power

In Figure 6.28, the power system status was analysed for a possible faulty condition by replacing the induction motor starting event of case 1 by a three-phase to ground fault applied at Bus_6 in Figure 6.1.

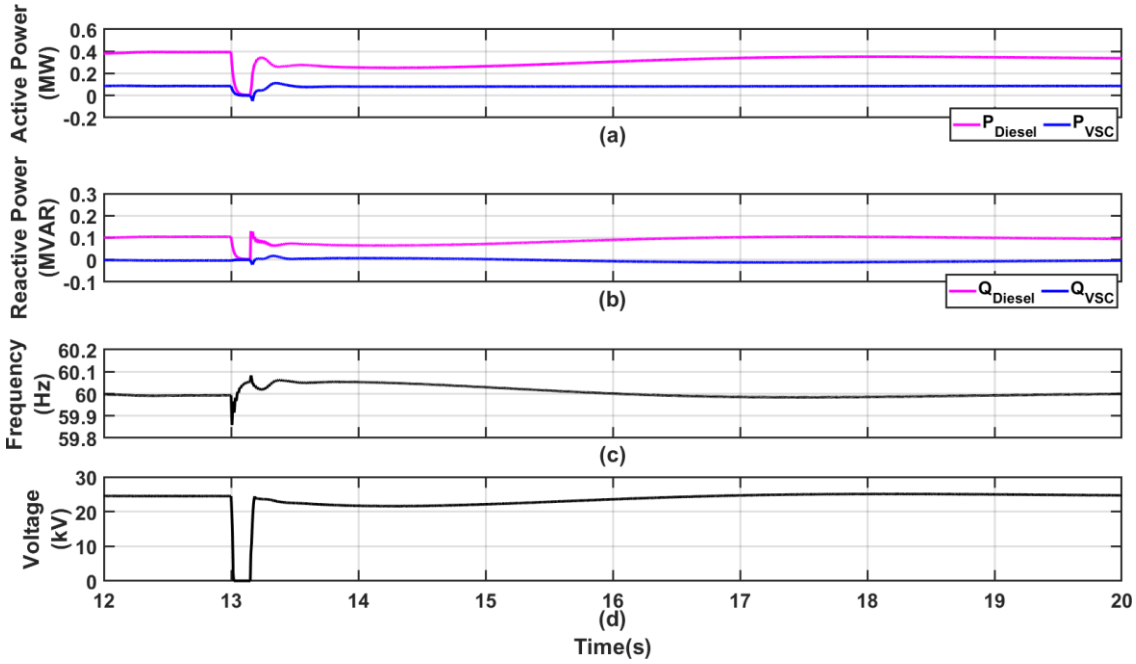

Figure 6.28 Maximum loading case 3: (a) Active power, (b) Reactive power, (c) Frequency, and (d) Voltage at Bus_8

The applied fault was cleared after 0.15 s by taking out the faulty section at Bus_4. Following the fault clearing, the system recovers back to the normal operating conditions within about 7 s. Due to the curtailing of the faulty section, the power demand reduces slightly from the pre-fault conditions, which allows the diesel generator to stably continue the grid-forming task without the assistance from battery unit.

6.7.2.2. Diesel minimum loading scenario

The scenario depicted in Figure 6.29-Figure 6.31 analyses a possible minimum loading violation for DG_1. The system is initially supplying a load close to 0.18 MW in the Gensup mode and DG_1 is operating slightly above its minimum loading limit (0.12 MW). At 8 s time, the irradiance increases and DG_1 reduces its power to balance the grid. As DG_1 goes below 0.12 MW, the secondary controls gradually reduce P_{Bat}^{Ref} from P_{Bat}^{EMS}, allowing the diesel unit to operate at its minimum loading limit. Around 11 s, the load increases and P_{Bat}^{Ref} gets redefined at its initial reference, P_{Bat}^{EMS}. Throughout this scenario the system frequency and voltage show a stable response.

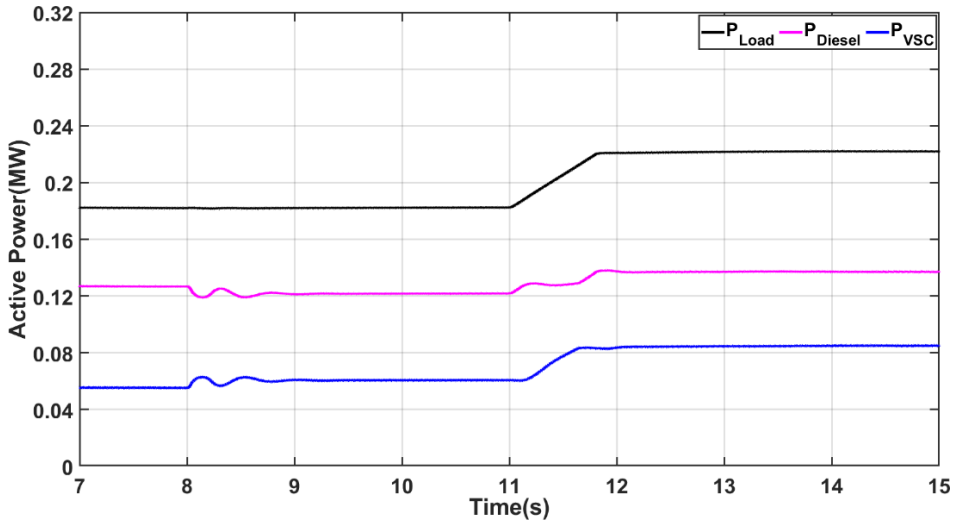

Figure 6.29 Minimum loading case: Active power

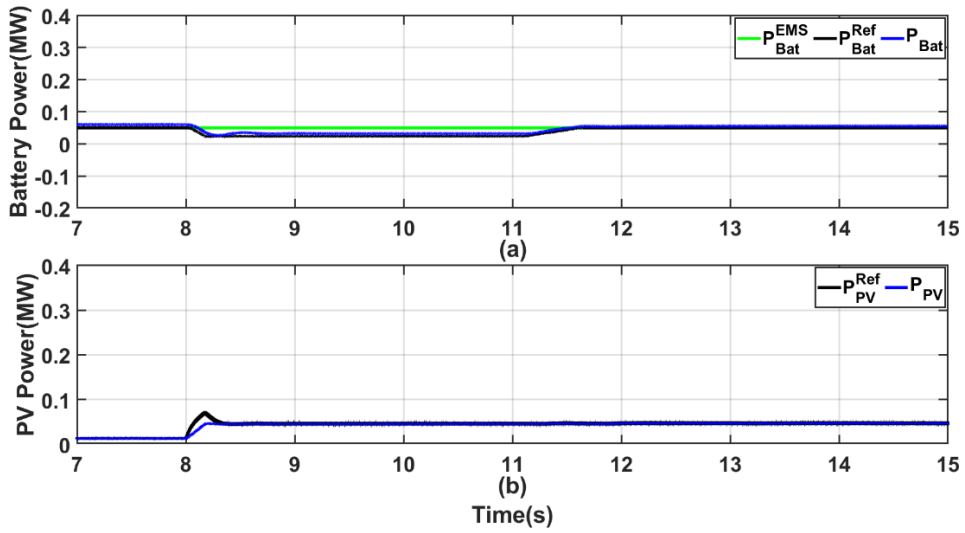

Figure 6.30 Minimum loading case: (a) Battery power and (b) PV power

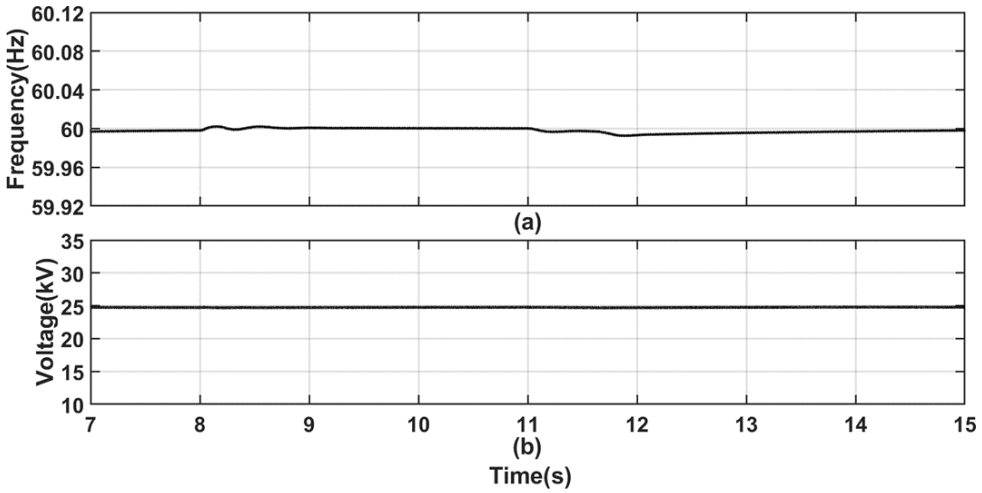

Figure 6.31 Minimum loading case: (a) Frequency and (b) Voltage

6.8 Concluding Remarks

Power management strategies for PV, diesel, and battery units were proposed to logically transition the EMS set-points to the unit-level controls. An operation evaluation mechanism is deployed to assess the applicability of the derived optimum operational routines and the underlying power management controls via integrating a detailed simulation model of the actual power system operation. The results revealed that the proposed performance evaluation mechanism aided in verifying the competence of the power management strategies and identifying risks associated with the initially derived

operation routines. The initially suggested operational routines were appropriately modified by the secondary-level power management strategies to ensure a logical operation with minimal compromise to the operational objectives. The overall study demonstrated the importance of close coordination and performance verification of the quantitative and logical control layers.

Chapter 7

Conclusions, Contributions, and Future Work

7.1 Introduction

This chapter concludes the thesis by summarizing the content and conclusions obtained in each chapter accompanied by the contributions. Recommendations for future research are also discussed.

7.2 Thesis Summary and Conclusions

The required scope of work to attain the research goal was compiled in five chapters. Based on the identified research gaps, necessary models/methodologies were devised while providing deliverables to achieve the research goal as concluded below.

In Chapter 2, a HOMER software-based sizing study was conducted with factful load and resource data to develop a realistic test system configuration to demonstrate the energy and power management functionalities implemented in the following chapters. According to the obtained results, PV-Diesel-Battery topology at high renewable penetration levels was selected as the preferred test system configuration. At a 21% renewable fraction, this configuration showed around 22% CO_2 emission reductions compared to the base-case diesel-only power system. Despite the high capital costs, the extrinsic economic indices showed positive return, although at lower rates, and intrinsic economic indices such as LCOE remained comparable to the base case.

The development of mathematical models and algorithms that form the energy management system was presented in Chapter 3 to Chapter 5.

In Chapter 3, the basic operation optimization framework was developed in a computationally efficient manner with only continuous optimization variables. The observed average computation times showed more than 50% reduction compared to a test case deploying both discrete and continuous optimization variables. This feature allowed it to reduce the computational burden of other decision support systems proposed in Chapter 4 and Chapter 5, where the optimization problem needs to be solved many times with varying input conditions. Also, in Chapter 3, the problem formulation combined several operational requirements related to remote off-grid power systems. Compared to an existing diesel-only operation, the addition of PV and energy storage and integration of operation optimization showed around 59.5% cost reductions and 59.8% emission reductions for a distinct summer day operation. For a representative winter day, the costs and emission reductions were observed to be around 27.7% and 10.5%, respectively. For winter days, it was seen that reductions in peak load can be useful to energize the power system with the lower-rated generator. Also, for summer days with longer energy excess periods, increased correlation between loads and the solar resource was needed to reduce the energy spillage.

In Chapter 4, a DR integrated EMS was developed to further increase the cost and emission reductions achieved in Chapter 3. A DR estimation technique based on PFIS was used in combination with operation optimization to find the best electricity rate structure that would achieve the desired variations in the load profile. The integration of DR estimation model allowed the overall scheme to be implemented with minimum bi-directional interactions and simplified communication architecture, which is useful in the context of remote power systems. Also, within an assessment framework, the proposed method can be used to evaluate the flexibility given by DR to the day-ahead energy management task during a hypothetical trial that would precede an actual implementation in the future. With the load conditions influenced under the DR scheme for the winter day, system operation was optimized while alleviating the need to start a second diesel generator. The cost and emission reductions were estimated to be 4.9% and 0.6%, respectively, compared to that obtained in Chapter 3. The inclusion of DR scheme only

achieved a 73 kWh reduction in the spilled solar energy for the considered summer day. Compared to Chapter 3 results, the cost and emission reductions were estimated to be 4.1% and 2.4%, respectively. Due to the lower availability of shiftable loads, both in variety and magnitude, the benefits achievable with DR was observed to be limited for the considered remote power system, specially during the summer season. However, in comparison to the existing diesel-only operation, the addition of PV and energy storage and optimization of the operation with the DR integrated EMS achieved over 60% cost and emission reductions for the considered summer day operation. The cost and emission reductions achieved for the considered winter day was estimated to be 31% and 11%, respectively.

In Chapter 5, the robustness of the energy management layer developed in Chapter 3 and Chapter 4 for forecast uncertainties was enhanced by integrating an uncertainty management strategy. A hybrid decision making process using deterministic optimization and scenario-based stochastic optimization was proposed to deliver the set-points for the lower-level controls. The proposed method, which is formulated in a MPC framework, deploys two different look-ahead windows for the deterministic and stochastic optimization processes. The applicability of the proposed method was demonstrated for the same PV-Diesel-Battery power system considered in previous chapters and the results were compared with other energy management strategies. In terms of costs, CO_2 emissions, and complying with operation constraints such as component limits, the proposed method functions closer to a scenario where no forecast uncertainty exists in the day-ahead time frame and achieved around 5.8% costs and 4% emission reductions compared to a closely-tracked deterministic uncertainty management approach, for an exemplary summer day operation. Moreover, an analysis conducted on the average computation times shows that the proposed method is computationally efficient.

In Chapter 6, power management strategies were implemented and coordinated with the previously developed energy management functions in a hierarchical architecture. The EMS was integrated to the tertiary-level. Power management strategies for PV, diesel, and battery units were developed and integrated to the secondary-level control layer to achieve a logical system operation while confirming to the limits of individual components and the system as a whole. Also, an operation evaluation framework was developed to provide a set of guidelines to assess the feasibility of the EMS set-points using EMT simulations.

The operation evaluation process was demonstrated in PSCAD/EMTDC^{TM} for several critical operating points detected in typical power system operation plans derived by the EMS. The simulated scenarios show that the developed power management strategies can appropriately modify the optimum set-points when required, to facilitate a stable, secure, and reliable operation while adhering to the system limitations. Also, the system performance under unanticipated scenarios such as higher deviations from predicted forecasts, faults, starting of large induction motors, etc. were analyzed and proper recommendations were suggested to modify the operation plan if deemed appropriate. The overall result verifies the importance of close coordination and performance verification of the energy and power management control layers.

The main goal of the proposed research was to develop appropriate models and methodologies to implement the energy and power management functions to optimize the operation of a remote off-grid HRES in terms of the operating costs and emissions while ensuring logical operation of the power system respecting both steady state and dynamic capabilities of individual equipment and the system as a whole. As detailed in Section 1.6, seven sub-objectives were proposed to achieve the main goal of this thesis. Chapter 2 attained sub-objective (a) to develop a realistic test system configuration. The outcomes of Chapter 3 to Chapter 5 achieved sub-objectives (b)-(e) while delivering a EMS that can generate set-points to achieve a quantitatively optimized operation trajectory while minimizing operating costs and CO_2 emissions within the imposed operation constraints. Also, the devised energy management layer captured several operational requirements related to remote off-grid HRESs as discussed before. Chapter 6 demonstrated the close coordination and operation evaluation of power and energy management phases by achieving sub-objectives (f)-(g). This allowed the EMS set-points to be logically transitioned to the unit-level controls during actual system operation while prioritizing dynamic limitations and system variables such as voltage and frequency.

Overall, the outcomes of the five chapters improved the capabilities of energy and power management systems to ensure a quantitatively optimized and logical power system operation for the remote off-grid HRESs. Therefore, in conclusion, it can be contended that the goal of this thesis has been achieved.

7.3 Major Contributions

The major contributions made while fulfilling the research goal are summarized as follows.

- Development of an operation optimization framework by combining several operational requirements related to remote off-grid power systems such as minimizing operational costs and emissions, achieving optimized schedule for the diesel generators with reduced starts, reducing battery degradation, and minimizing energy spillage.
- Development of a computationally efficient operation optimization problem formulation technique. Due to the simplified structure and fast convergence times, it can be effortlessly integrated with any other supervisory-level decision support system during the day-ahead or intra-day operation planning and evaluation process.
- Development of a DR integrated day-ahead energy management framework that can maximize the benefits for both the utility and the consumers in remote power systems with a simplified communication/control platform with minimal bi-directional utility-consumer interactions. Also, to the best of my knowledge this is the first study integrating stochastic uncertainty to the fuzzy based modelling in the context of DR.
- Development of a hybrid uncertainty management strategy using stochastic and deterministic techniques that resulted in a simplified and computationally efficient problem formulation with reduced dependence on frequently updated forecasts.
- Development of power management controls to integrate the EMS set-points to the unit-level controls in a maximally permissive manner while adapting to limitations of diesel, battery, and PV modules during actual operation.
- Development of an operation evaluation routine to provide a set of guidelines to assess and modify the set-points derived by the EMS considering system dynamics, lower-level control capabilities, and equipment limitations based on EMT simulations.

7.4 Potential Future Research Areas

Directions for future research that arises from the models and methodologies discussed in this thesis are summarised as follows.

- The development of an automated parameter tuning technique would be a useful addition to the proposed DR estimation technique in Chapter 4, to appropriately modify the characterization of the PFIS to accommodate alternative representations of human behaviour influenced by changing user characteristics over time.
- In Chapter 6, the proposed operation evaluation framework can be automated with modern simulation tools and intelligent decision support systems for identifying critical scenarios, risks, and corrective actions. This will alleviate the need of regular supervision and the operation evaluation can be continued during the control horizon as well.
- Also, further studies can be performed to demonstrate the applicability of the proposed methods for other non-dispatchable renewable energy sources (i.e., wind) and dispatchable storage units (i.e., fuel cells, supercapacitors etc.), respectively.

References

[1] M. Arriaga, C. A. Canizares, and M. Kazerani, “Northern lights: Access to electricity in Canada’s northern and remote communities,” *IEEE Power Energy Mag.*, vol. 12, no. 4, pp. 50–59, 2014, doi: 10.1109/MPE.2014.2317963.

[2] D. Lovekin, J. Moorhouse, V. Morales, and B. Salek, “Diesel reduction progress in remote communities: Research summary,” 2020. [Online]. Available: https://www.pembina.org/reports/diesel-reduction-progress-research-summary-pdf.pdf.

[3] P. R. Bhattarai and S. Thompson, “Optimizing an off-grid electrical system in Brochet, Manitoba, Canada,” *Renew. Sustain. Energy Rev.*, vol. 53, pp. 709–719, 2016, doi: 10.1016/j.rser.2015.09.001.

[4] Y. S. Mohammed, M. W. Mustafa, and N. Bashir, “Hybrid renewable energy systems for off-grid electric power: Review of substantial issues,” *Renew. Sustain. Energy Rev.*, vol. 35, pp. 527–539, 2014, doi: 10.1016/j.rser.2014.04.022.

[5] K. Kusakana, “Operation cost minimization of photovoltaic-diesel-battery hybrid systems,” *Energy*, vol. 85, pp. 645–653, 2015, doi: 10.1016/j.energy.2015.04.002.

[6] M. J. Khan and M. T. Iqbal, “Pre-feasibility study of stand-alone hybrid energy systems for applications in Newfoundland,” *Renew. Energy*, vol. 30, no. 6, pp. 835–854, 2005, doi: 10.1016/j.renene.2004.09.001.

[7] Manitoba Hydro, “Recommendations for reducing or eliminating the use of diesel fuel to supply power in off-grid communities,” 2008, [Online]. Available: http://www.hydro.mb.ca/regulatory_affairs/electric/gra_2010_2012/Appendix_13_9.pdf.

[8] R. Tonkoski, L. A. C. Lopes, and D. Turcotte, “Active power curtailment of PV inverters in diesel hybrid mini-grids,” *2009 IEEE Electr. Power Energy Conf. EPEC 2009*, pp. 1–6, 2009, doi: 10.1109/EPEC.2009.5420964.

[9] P. Bajpai and V. Dash, “Hybrid renewable energy systems for power generation in stand-alone applications: A review,” *Renew. Sustain. Energy Rev.*, vol. 16, no. 5, pp. 2926–2939, 2012, doi: 10.1016/j.rser.2012.02.009.

[10] “IEEE Standard for the Specification of Microgrid Controllers,” *IEEE Std 2030.7-*

2017, pp. 1–43, 2018, doi: 10.1109/IEEESTD.2018.8295083.

[11] E. Foruzan, S. Asgarpoor, and J. M. Bradley, "Hybrid system modeling and supervisory control of a microgrid," *NAPS 2016 - 48th North Am. Power Symp. Proc.*, no. 1, pp. 1–6, 2016, doi: 10.1109/NAPS.2016.7747840.

[12] A. Parisio, E. Rikos, and L. Glielmo, "A model predictive control approach to microgrid operation optimization," *IEEE Trans. Control Syst. Technol.*, vol. 22, no. 5, pp. 1813–1827, 2014, doi: 10.1109/TCST.2013.2295737.

[13] A. K. Basu, S. P. Chowdhury, S. Chowdhury, and S. Paul, "Microgrids: Energy management by strategic deployment of DERs - A comprehensive survey," *Renew. Sustain. Energy Rev.*, vol. 15, no. 9, pp. 4348–4356, 2011, doi: 10.1016/j.rser.2011.07.116.

[14] L. Olatomiwa, S. Mekhilef, M. S. Ismail, and M. Moghavvemi, "Energy management strategies in hybrid renewable energy systems: A review," *Renew. Sustain. Energy Rev.*, vol. 62, pp. 821–835, 2016, doi: 10.1016/j.rser.2016.05.040.

[15] X. Wang, A. Palazoglu, and N. H. El-Farra, "Operation of residential hybrid renewable energy systems: Integrating forecasting, optimization and demand response," *Proc. Am. Control Conf.*, pp. 5043–5048, 2014, doi: 10.1109/ACC.2014.6859105.

[16] R. Deng, Z. Yang, M. Y. Chow, and J. Chen, "A survey on demand response in smart grids: Mathematical models and approaches," *IEEE Trans. Ind. Informatics*, vol. 11, no. 3, pp. 570–582, 2015, doi: 10.1109/TII.2015.2414719.

[17] T. Logenthiran, D. Srinivasan, and T. Z. Shun, "Demand side management in smart grid using heuristic optimization," *IEEE Trans. Smart Grid*, vol. 3, no. 3, pp. 1244–1252, 2012, doi: 10.1109/TSG.2012.2195686.

[18] J. Aghaei and M. I. Alizadeh, "Demand response in smart electricity grids equipped with renewable energy sources: A review," *Renew. Sustain. Energy Rev.*, vol. 18, pp. 64–72, 2013, doi: 10.1016/j.rser.2012.09.019.

[19] B. Zhao, X. Zhang, J. Chen, C. Wang, and L. Guo, "Operation optimization of standalone microgrids considering lifetime characteristics of battery energy storage system," *IEEE Trans. Sustain. Energy*, vol. 4, no. 4, pp. 934–943, 2013, doi: 10.1109/TSTE.2013.2248400.

[20] L. K. Gan, J. K. H. Shek, and M. A. Mueller, “Optimised operation of an off-grid hybrid wind-diesel-battery system using genetic algorithm,” *Energy Convers. Manag.*, vol. 126, pp. 446–462, 2016, doi: 10.1016/j.enconman.2016.07.062.

[21] X. Liu, Z. Zhang, W. Wang, H. Zheng, J. Hao, and Y. Chen, “Two-stage Robust Optimal Dispatch Method Considering Wind Power and Load Correlation,” *2nd IEEE Conf. Energy Internet Energy Syst. Integr. EI2 2018 - Proc.*, 2018, doi: 10.1109/EI2.2018.8582205.

[22] E. R. Sanseverino, M. L. Di Silvestre, M. G. Ippolito, A. De Paola, and G. Lo Re, “An execution, monitoring and replanning approach for optimal energy management in microgrids,” *Energy*, vol. 36, no. 5, pp. 3429–3436, 2011, doi: 10.1016/j.energy.2011.03.047.

[23] A. M. Zein Alabedin, E. F. El-Saadany, and M. M. A. Salama, “Generation scheduling in Microgrids under uncertainties in power generation,” *2012 IEEE Electr. Power Energy Conf. EPEC 2012*, pp. 133–138, 2012, doi: 10.1109/EPEC.2012.6474937.

[24] W. Alharbi and K. Bhattacharya, “Accommodating high levels of renewable generation in remote microgrids under uncertainty,” *Proc. - 2014 Electr. Power Energy Conf. EPEC 2014*, pp. 60–64, 2014, doi: 10.1109/EPEC.2014.11.

[25] Y. Li, Z. Yang, G. Li, D. Zhao, and W. Tian, “Optimal Scheduling of an Isolated Microgrid with Battery Storage Considering Load and Renewable Generation Uncertainties,” *IEEE Trans. Ind. Electron.*, vol. 66, no. 2, pp. 1565–1575, 2019, doi: 10.1109/TIE.2018.2840498.

[26] D. E. Olivares, J. D. Lara, C. A. Canizares, and M. Kazerani, “Stochastic-Predictive Energy Management System for Isolated Microgrids,” *IEEE Trans. Smart Grid*, vol. 6, no. 6, pp. 2681–2693, 2015, doi: 10.1109/TSG.2015.2469631.

[27] J. Sachs and O. Sawodny, “A Two-Stage Model Predictive Control Strategy for Economic Diesel-PV-Battery Island Microgrid Operation in Rural Areas,” *IEEE Trans. Sustain. Energy*, vol. 7, no. 3, pp. 903–913, 2016, doi: 10.1109/TSTE.2015.2509031.

[28] Y. Gu and L. Xie, “Stochastic Look-Ahead Economic Dispatch With Variable Generation Resources,” *IEEE Trans. Power Syst.*, vol. 32, no. 1, pp. 17–29, 2017.

[29] S. Bruno, M. Dassisti, M. La Scala, M. Chimienti, C. Cignali, and E. Palmisani, “Predictive dispatch across time of hybrid isolated power systems,” *IEEE Trans. Sustain. Energy*, vol. 5, no. 3, pp. 738–746, 2014, doi: 10.1109/TSTE.2013.2295428.

[30] H. J. Kim, M. K. Kim, and J. W. Lee, “A two-stage stochastic p-robust optimal energy trading management in microgrid operation considering uncertainty with hybrid demand response,” *Int. J. Electr. Power Energy Syst.*, vol. 124, no. August 2020, p. 106422, 2021, doi: 10.1016/j.ijepes.2020.106422.

[31] A. Ghasaei, Z. J. Zhang, W. M. Wonham, and R. Iravani, “A Discrete-Event Supervisory Control for the AC Microgrid,” *IEEE Trans. Power Deliv.*, vol. 8977, no. c, pp. 1–1, 2020, doi: 10.1109/tpwrd.2020.2988687.

[32] B. Singh, G. Pathak, and B. K. Panigrahi, “Seamless Transfer of Renewable-Based Microgrid Between Utility Grid and Diesel Generator,” *IEEE Trans. Power Electron.*, vol. 33, no. 10, pp. 8427–8437, 2018, doi: 10.1109/TPEL.2017.2778104.

[33] Q. Shafiee, J. M. Guerrero, and J. C. Vasquez, “Distributed secondary control for islanded microgrids-a novel approach,” *IEEE Trans. Power Electron.*, vol. 29, no. 2, pp. 1018–1031, 2014, doi: 10.1109/TPEL.2013.2259506.

[34] H. Shi, F. Zhuo, H. Yi, F. Wang, D. Zhang, and Z. Geng, “A novel real-time voltage and frequency compensation strategy for photovoltaic-based microgrid,” *IEEE Trans. Ind. Electron.*, vol. 62, no. 6, pp. 3545–3556, 2015, doi: 10.1109/TIE.2014.2371434.

[35] F. Katiraei, R. Iravani, N. Hatziargyriou, and A. Dimeas, “Microgrids management,” *IEEE Power Energy Mag.*, vol. 6, no. 3, pp. 54–65, May 2008, doi: 10.1109/MPE.2008.918702.

[36] J. A. P. Lopes, C. L. Moreira, and A. G. Madureira, “Defining control strategies for analysing microgrids islanded operation,” *2005 IEEE Russ. Power Tech, PowerTech*, vol. 21, no. 2, pp. 916–924, 2005, doi: 10.1109/PTC.2005.4524548.

[37] R. Luna-Rubio, M. Trejo-Perea, D. Vargas-Vázquez, and G. J. Ríos-Moreno, “Optimal sizing of renewable hybrids energy systems: A review of methodologies,” *Sol. Energy*, vol. 86, no. 4, pp. 1077–1088, 2012, doi: 10.1016/j.solener.2011.10.016.

[38] “IEEE Recommended Practice for the Planning and Design of the Microgrid,” *IEEE Std 2030.9-2019*, pp. 1–46, 2019, doi: 10.1109/IEEESTD.2019.8746836.

[39] D. Connolly, H. Lund, B. V. Mathiesen, and M. Leahy, “A review of computer tools for analysing the integration of renewable energy into various energy systems,” *Appl. Energy*, vol. 87, no. 4, pp. 1059–1082, 2010, doi: 10.1016/j.apenergy.2009.09.026.

[40] A. H. Fathima and K. Palanisamy, “Optimization in microgrids with hybrid energy systems - A review,” *Renew. Sustain. Energy Rev.*, vol. 45, pp. 431–446, 2015, doi: 10.1016/j.rser.2015.01.059.

[41] M. M. Rahman, M. M. U. H. Khan, M. A. Ullah, X. Zhang, and A. Kumar, “A hybrid renewable energy system for a North American off-grid community,” *Energy*, vol. 97, pp. 151–160, 2016, doi: 10.1016/j.energy.2015.12.105.

[42] D. Thomas, O. Deblecker, and C. S. Ioakimidis, “Optimal design and techno-economic analysis of an autonomous small isolated microgrid aiming at high RES penetration,” *Energy*, vol. 116, pp. 364–379, 2016, doi: 10.1016/j.energy.2016.09.119.

[43] A. Kaabeche and R. Ibtiouen, “Techno-economic optimization of hybrid photovoltaic/wind/diesel/battery generation in a stand-alone power system,” *Sol. Energy*, vol. 103, pp. 171–182, 2014, doi: 10.1016/j.solener.2014.02.017.

[44] A. Maleki and A. Askarzadeh, “Optimal sizing of a PV/wind/diesel system with battery storage for electrification to an off-grid remote region: A case study of Rafsanjan, Iran,” *Sustain. Energy Technol. Assessments*, vol. 7, pp. 147–153, 2014, doi: 10.1016/j.seta.2014.04.005.

[45] M. Jamshidi and A. Askarzadeh, “Techno-economic analysis and size optimization of an off-grid hybrid photovoltaic, fuel cell and diesel generator system,” *Sustain. Cities Soc.*, vol. 44, no. August 2018, pp. 310–320, 2019, doi: 10.1016/j.scs.2018.10.021.

[46] S. K. Nandi and H. R. Ghosh, “A wind-PV-battery hybrid power system at Sitakunda in Bangladesh,” *Energy Policy*, vol. 37, no. 9, pp. 3659–3664, 2009, doi: 10.1016/j.enpol.2009.04.039.

[47] T. Ma, H. Yang, and L. Lu, “A feasibility study of a stand-alone hybrid solar-wind-

battery system for a remote island," *Appl. Energy*, vol. 121, pp. 149–158, 2014, doi: 10.1016/j.apenergy.2014.01.090.

[48] V. Balaji and H. Gurgenci, "Search for optimum renewable mix for Australian off-grid power generation," *Energy*, vol. 175, pp. 1234–1245, 2019, doi: 10.1016/j.energy.2019.03.089.

[49] "Power Data access Viewer : NASA solar radiation and meteorological data." https://power.larc.nasa.gov/data-access-viewer/ (accessed Aug. 20, 2020).

[50] R. Kaluthanthrige, A. D. Rajapakse, C. Lamothe, and F. Mosallat, "Optimal Sizing and Performance Evaluation of a Hybrid Renewable Energy System for an Off-Grid Power System in Northern Canada," *Technol. Econ. Smart Grids Sustain. Energy*, vol. 4, no. 1, pp. 24–26, 2019, doi: 10.1007/s40866-019-0061-5.

[51] "Renewable energy discount rate survey results – 2017 | Grant Thornton." https://www.grantthornton.ie/insights/factsheets/renewable-energy-discount-rate-survey-results--2017/ (accessed Aug. 19, 2021).

[52] T. Lambert, P. Gilman, and P. Lilienthal, "Micropower System Modeling," in *Integration of Alternative Sources of Energy*, 2006, pp. 379–418.

[53] L. Meng, E. R. Sanseverino, A. Luna, T. Dragicevic, J. C. Vasquez, and J. M. Guerrero, "Microgrid supervisory controllers and energy management systems: A literature review," *Renew. Sustain. Energy Rev.*, vol. 60, pp. 1263–1273, 2016, doi: 10.1016/j.rser.2016.03.003.

[54] M. Vaccari, G. M. Mancuso, J. Riccardi, M. Cantù, and G. Pannocchia, "A Sequential Linear Programming algorithm for economic optimization of Hybrid Renewable Energy Systems," *J. Process Control*, vol. 74, pp. 189–201, 2019, doi: 10.1016/j.jprocont.2017.08.015.

[55] M. Ashari and C. V. Nayar, "An optimum dispatch strategy using set points for a photovoltaic (PV)-diesel-battery hybrid power system," *Sol. Energy*, vol. 66, no. 1, pp. 1–9, 1999, doi: 10.1016/S0038-092X(99)00016-X.

[56] H. Tazvinga, X. Xia, and J. Zhang, "Minimum cost solution of photovoltaic-diesel-battery hybrid power systems for remote consumers," *Sol. Energy*, vol. 96, pp. 292–299, 2013, doi: 10.1016/j.solener.2013.07.030.

[57] A. T. Eseye, J. Zhang, D. Zheng, and D. Wei, "Optimal energy management strategy

for an isolated industrial microgrid using a modified particle swarm optimization," *2016 IEEE Int. Conf. Power Renew. Energy, ICPRE 2016*, pp. 494–498, 2017, doi: 10.1109/ICPRE.2016.7871126.

[58] A. Mohammed, J. Pasupuleti, T. Khatib, and W. Elmenreich, "A review of process and operational system control of hybrid photovoltaic/diesel generator systems," *Renew. Sustain. Energy Rev.*, vol. 44, pp. 436–446, 2015, doi: 10.1016/j.rser.2014.12.035.

[59] G. M. Masters, *Renewable and efficient electric power systems*. John Wiley & Sons, 2013.

[60] P. Luo, Z. Sun, L. Qiang, S. Zhu, and Q. Chen, "The multi-objective day-ahead optimal dispatch of islanded micro grid," *IECON Proc. (Industrial Electron. Conf.*, pp. 5403–5408, 2016, doi: 10.1109/IECON.2016.7793044.

[61] H. O. Anuta, I. L. Gutierrez, C. Bordin, D. Vigo, A. Crossland, and C. J. Dent, "A linear programming approach for battery degradation analysis and optimization in offgrid power systems with solar energy integration," *Renew. Energy*, vol. 101, pp. 417–430, 2016, doi: 10.1016/j.renene.2016.08.066.

[62] C. Amzallag, J. Gerey, J. Robert, and J. Bahuaud, "Standardization of the rainflow counting method for fatigue analysis," *Int. J. Fatigue*, vol. 16, no. 4, pp. 287–293, 1994, doi: 10.1016/0142-1123(94)90343-3.

[63] B. Xu, J. Zhao, T. Zheng, E. Litvinov, and D. S. Kirschen, "Factoring the Cycle Aging Cost of Batteries Participating in Electricity Markets," *IEEE Trans. Power Syst.*, vol. 33, no. 2, pp. 2248–2259, 2018, doi: 10.1109/TPWRS.2017.2733339.

[64] F. A. Mohamed and H. N. Koivo, "Online management genetic algorithms of microgrid for residential application," *Energy Convers. Manag.*, vol. 64, pp. 562–568, 2012, doi: 10.1016/j.enconman.2012.06.010.

[65] X. Wang, A. Palazoglu, and N. H. El-Farra, "Operational optimization and demand response of hybrid renewable energy systems," *Appl. Energy*, vol. 143, pp. 324–335, 2015, doi: 10.1016/j.apenergy.2015.01.004.

[66] Y. Shi and R. Eberhart, "A modified particle swarm optimizer," in *1998 IEEE International Conference on Evolutionary Computation Proceedings. IEEE World Congress on Computational Intelligence (Cat. No.98TH8360)*, May 1998, pp. 69–

73, doi: 10.1109/ICEC.1998.699146.

[67] Y. del Valle, G. K. Venayagamoorthy, S. Mohagheghi, J. C. Hernandez, and R. G. Harley, “Particle swarm optimization: Basic concepts, variants and applications in power systems,” *IEEE Trans. Evol. Comput.*, vol. 12, no. 2, pp. 171–195, 2008, doi: 10.1109/TEVC.2007.896686.

[68] J. Kennedy and R. C. Eberhart, “A discrete binary version of the particle swarm algorithm,” in *1997 IEEE International Conference on Systems, Man, and Cybernetics. Computational Cybernetics and Simulation*, 1997, vol. 5, pp. 4104–4108 vol.5, doi: 10.1109/ICSMC.1997.637339.

[69] P. Siano, “Demand response and smart grids - A survey,” *Renew. Sustain. Energy Rev.*, vol. 30, pp. 461–478, 2014, doi: 10.1016/j.rser.2013.10.022.

[70] E. Karimi and M. Kazerani, “Impact of demand response management on improving social welfare of remote communities through integrating renewable energy resources,” *Can. Conf. Electr. Comput. Eng.*, pp. 1–6, 2017, doi: 10.1109/CCECE.2017.7946739.

[71] S. Zhang, J. Rong, and B. Wang, “An optimal scheduling scheme for smart home electricity considering demand response and privacy protection,” *Int. J. Electr. Power Energy Syst.*, vol. 132, no. April, p. 107159, 2021, doi: 10.1016/j.ijepes.2021.107159.

[72] P. Samadi, S. Member, H. Mohsenian-rad, and R. Schober, “Advanced Demand Side Management for the Future Smart Grid Using Mechanism Design,” *IEEE Trans. Smart Grid*, vol. 3, no. 3, pp. 1170–1180, 2012.

[73] A.-H. Mohsenian-Rad and A. Leon-garcia, “Optimal Residential Load Control With Price Prediction in Real-Time Electricity Pricing Environments,” *IEEE Trans. Smart Grid*, vol. 1, no. 2, pp. 120–133, 2010.

[74] S. Hatami and M. Pedram, “Minimizing the Electricity Bill of Cooperative Users under a Quasi-Dynamic Pricing Model,” in *2010 First IEEE International Conference on Smart Grid Communications*, 2010, pp. 421–426, doi: 10.1109/smartgrid.2010.5622080.

[75] P. Samadi, A.-H. Mohsenian-Rad, R. Schober, V. W. S. Wong, and J. Jatskevich, “Optimal Real-Time Pricing Algorithm Based on Utility Maximization for Smart

Grid," *2010 First IEEE Int. Conf. Smart Grid Commun.*, pp. 415–420, 2010, doi: 10.1109/smartgrid.2010.5622077.

[76] T. A. Nakabi and P. Toivanen, "An ANN-based model for learning individual customer behavior in response to electricity prices," *Sustain. Energy, Grids Networks*, vol. 18, p. 100212, 2019, doi: 10.1016/j.segan.2019.100212.

[77] D. Fischer *et al.*, "Modeling the Effects of Variable Tariffs on Domestic Electric Load Profiles by Use of Occupant Behavior Submodels," *IEEE Trans. Smart Grid*, vol. 8, no. 6, pp. 2685–2693, 2017, doi: 10.1109/TSG.2016.2544141.

[78] B. J. Johnson, M. R. Starke, O. A. Abdelaziz, R. K. Jackson, and L. M. Tolbert, "A dynamic simulation tool for estimating demand response potential from residential loads," *2015 IEEE Power Energy Soc. Innov. Smart Grid Technol. Conf. ISGT 2015*, no. Dlc, pp. 1–5, 2015, doi: 10.1109/ISGT.2015.7131867.

[79] T. Holtschneider and I. Erlich, "Modeling demand response of consumers to incentives using fuzzy systems," *IEEE Power Energy Soc. Gen. Meet.*, pp. 1–8, 2012, doi: 10.1109/PESGM.2012.6345280.

[80] M. Vallés, A. Bello, J. Reneses, and P. Frías, "Probabilistic characterization of electricity consumer responsiveness to economic incentives," *Appl. Energy*, vol. 216, no. February, pp. 296–310, 2018, doi: 10.1016/j.apenergy.2018.02.058.

[81] A. H. Meghdadi and M.-R. Akbarzadeh-T, "Probabilistic fuzzy logic and probabilistic fuzzy systems," *IEEE Int. Conf. Fuzzy Syst.*, vol. 3, pp. 1127–1130, 2002, doi: 10.1109/fuzz.2001.1008853.

[82] M. R. Akbarzadeh-T and A. Bemani-N, "Probabilistic fuzzy systems, expressions and approaches," *4th Iran. Jt. Congr. Fuzzy Intell. Syst. CFIS 2015*, pp. 1–6, 2016, doi: 10.1109/CFIS.2015.7391682.

[83] D. George, N. S. Pearre, and L. G. Swan, "High resolution measured domestic hot water consumption of Canadian homes," *Energy Build.*, vol. 109, no. July, pp. 304–315, 2015, doi: 10.1016/j.enbuild.2015.09.067.

[84] J. D. Sterman, "Domestic Water Heating and Water Heater Energy Consumption in Canada," *Am. J. Public Health*, vol. 96, no. 3, pp. 505–514, 2006, doi: 10.2105/AJPH.2005.066043.

[85] S. Shao, M. Pipattanasomporn, and S. Rahman, "Development of physical-based

demand response-enabled residential load models," *IEEE Trans. Power Syst.*, vol. 28, no. 2, pp. 607–614, 2013, doi: 10.1109/TPWRS.2012.2208232.

[86] M. M. Rahman, S. Hettiwatte, and S. Gyamfi, "An intelligent approach of achieving demand response by fuzzy logic based domestic load management," *2014 Australas. Univ. Power Eng. Conf. AUPEC 2014 - Proc.*, no. October, pp. 1–6, 2014, doi: 10.1109/AUPEC.2014.6966610.

[87] J. Aghaei, T. Niknam, R. Azizipanah-Abarghooee, and J. M. Arroyo, "Scenario-based dynamic economic emission dispatch considering load and wind power uncertainties," *Int. J. Electr. Power Energy Syst.*, vol. 47, no. 1, pp. 351–367, 2013, doi: 10.1016/j.ijepes.2012.10.069.

[88] S. Mohammadi, S. Soleymani, and B. Mozafari, "Scenario-based stochastic operation management of MicroGrid including Wind, Photovoltaic, Micro-Turbine, Fuel Cell and Energy Storage Devices," *Int. J. Electr. Power Energy Syst.*, vol. 54, pp. 525–535, 2014, doi: 10.1016/j.ijepes.2013.08.004.

[89] A. G. Zamani, A. Zakariazadeh, and S. Jadid, "Day-ahead resource scheduling of a renewable energy based virtual power plant," *Appl. Energy*, vol. 169, pp. 324–340, 2016, doi: 10.1016/j.apenergy.2016.02.011.

[90] W. Su, J. Wang, and J. Roh, "Stochastic energy scheduling in microgrids with intermittent renewable energy resources," *IEEE Trans. Smart Grid*, vol. 5, no. 4, pp. 1876–1883, 2014, doi: 10.1109/TSG.2013.2280645.

[91] A. Baziar and A. Kavousi-Fard, "Considering uncertainty in the optimal energy management of renewable micro-grids including storage devices," *Renew. Energy*, vol. 59, pp. 158–166, 2013, doi: 10.1016/j.renene.2013.03.026.

[92] A. Parisio, E. Rikos, and L. Glielmo, "Stochastic model predictive control for economic/environmental operation management of microgrids: An experimental case study," *J. Process Control*, vol. 43, pp. 24–37, 2016, doi: 10.1016/j.jprocont.2016.04.008.

[93] P. Patrinos, S. Trimboli, and A. Bemporad, "Stochastic MPC for real-time market-based optimal power dispatch," *Proc. IEEE Conf. Decis. Control*, pp. 7111–7116, 2011, doi: 10.1109/CDC.2011.6160798.

[94] D. Zhu and G. Hug, "Decomposed stochastic model predictive control for optimal

dispatch of storage and generation," *IEEE Trans. Smart Grid*, vol. 5, no. 4, pp. 2044–2053, 2014, doi: 10.1109/TSG.2014.2321762.

[95] Q. Wang, Y. Guan, and J. Wang, "A chance-constrained two-stage stochastic program for unit commitment with uncertain wind power output," *IEEE Trans. Power Syst.*, vol. 27, no. 1, pp. 206–215, 2012, doi: 10.1109/TPWRS.2011.2159522.

[96] C. Chen, J. Wang, Y. Heo, and S. Kishore, "MPC-based appliance scheduling for residential building energy management controller," *IEEE Trans. Smart Grid*, vol. 4, no. 3, pp. 1401–1410, 2013, doi: 10.1109/TSG.2013.2265239.

[97] J. P. Torreglosa, P. García, L. M. Fernández, and F. Jurado, "Hierarchical energy management system for stand-alone hybrid system based on generation costs and cascade control," *Energy Convers. Manag.*, vol. 77, pp. 514–526, 2014, doi: 10.1016/j.enconman.2013.10.031.

[98] S. Modes, Q. Jiang, M. Xue, G. Geng, and S. Member, "Energy Management of Microgrid in Grid-Connected and Stand-Alone Modes," *IEEE Trans. Power Syst.*, vol. 28, no. 3, pp. 3380–3389, 2013.

[99] A. Mohamed and O. Mohammed, "Real-time energy management scheme for hybrid renewable energy systems in smart grid applications," *Electr. Power Syst. Res.*, vol. 96, pp. 133–143, 2013, doi: 10.1016/j.epsr.2012.10.015.

[100] M. Jafari, Z. Malekjamshidi, D. D. C. Lu, and J. Zhu, "Development of a Fuzzy-Logic-Based Energy Management System for a Multiport Multioperation Mode Residential Smart Microgrid," *IEEE Trans. Power Electron.*, vol. 34, no. 4, pp. 3283–3301, 2019, doi: 10.1109/TPEL.2018.2850852.

[101] M. Jafari and Z. Malekjamshidi, "Optimal energy management of a residential-based hybrid renewable energy system using rule-based real-time control and 2D dynamic programming optimization method," *Renew. Energy*, vol. 146, pp. 254–266, 2020, doi: 10.1016/j.renene.2019.06.123.

[102] S. Chakraborty, M. D. Weiss, and M. G. Simões, "Distributed Intelligent Energy Management System for a Single-Phase High-Frequency AC Microgrid," *IEEE Trans. Ind. Electron.*, vol. 54, no. 1, pp. 97–109, 2007.

[103] W. C. Clarke, M. J. Brear, and C. Manzie, "Control of an isolated microgrid using hierarchical economic model predictive control," *Appl. Energy*, vol. 280, no.

September, 2020, doi: 10.1016/j.apenergy.2020.115960.

[104] D. E. Olivares, C. A. Canizares, and M. Kazerani, "A centralized energy management system for isolated microgrids," *IEEE Trans. Smart Grid*, vol. 5, no. 4, pp. 1864–1875, 2014, doi: 10.1109/TSG.2013.2294187.

[105] M. Singh, L. A. C. Lopes, and N. A. Ninad, "Grid forming Battery Energy Storage System (BESS) for a highly unbalanced hybrid mini-grid," *Electr. Power Syst. Res.*, vol. 127, pp. 126–133, 2015, doi: 10.1016/j.epsr.2015.05.013.

[106] M. B. Delghavi and A. Yazdani, "A control strategy for islanded operation of a distributed resource (DR) unit," *2009 IEEE Power Energy Soc. Gen. Meet. PES '09*, pp. 1–8, 2009, doi: 10.1109/PES.2009.5275592.

[107] "PSCAD Knowledge Base." https://www.pscad.com/knowledge-base/article/471 (accessed Oct. 27, 2020).

[108] N. W. A. Lidula and A. D. Rajapakse, "Voltage balancing and synchronization of microgrids with highly unbalanced loads," *Renew. Sustain. Energy Rev.*, vol. 31, pp. 907–920, 2014, doi: 10.1016/j.rser.2013.12.045.

[109] D. Shi, Y. Luo, and R. K. Sharma, "Active synchronization control for microgrid reconnection after islanding," *IEEE PES Innov. Smart Grid Technol. Conf. Eur.*, vol. 2015-Janua, no. January, pp. 1–6, 2015, doi: 10.1109/ISGTEurope.2014.7028802.

[110] L. Yu, R. Li, and L. Xu, "Distributed PLL-Based Control of Offshore Wind Turbines Connected with Diode-Rectifier-Based HVDC Systems," *IEEE Trans. Power Deliv.*, vol. 33, no. 3, pp. 1328–1336, 2018, doi: 10.1109/TPWRD.2017.2772342.

Appendices

Appendix A: HOMER Component Data

Specifications for a single PV module

Electrical data @ STC	
Nominal max power at STC (P_{max}) [W]	285
Opt. operating voltage (Vmp) [V]	31.7
Opt. operating current [A]	8.98
Open circuit voltage (Voc) [V]	38.6
Short circuit current (Isc) [A]	9.51
Module efficiency [%]	17.41
Temperature characteristics	
Temperature coefficient for P_{max} [% / °C]	-0.41
Temperature coefficient for V_{oc} [% / °C]	-0.31
Temperature coefficient for I_{sc} [% / °C]	0.053
Nominal operating cell temperature [°C]	45±2
Other	
Cell type	Mono-crystalline
Number of cells	60

STC: Standard test conditions of irradiance of 1000 W/m^2, spectrum AM 1.5, and cell temperature of 25°C.

Site specific inputs for PV

Derating factor [%]	88
Tracking	none
Panel slope [degrees]	58
Panel Azimuth [degrees west of south]	0

Specifications for a single battery unit

Chemistry	Li-ion
Nominal capacity [kWh]	7.6
Throughput [kWh]	45600
Operating voltage range [V]	70.3 – 91.3
Peak power [kW]	5
Roundtrip efficiency [%]	90
Minimum state of charge [%]	10
Maximum state of charge [%]	100

Specifications for the diesel plant

Diesel generators		
Ratings [kW]	DG_1	400
	DG_2	800
Schedule		"Optimized" option in HOMER
Calculation of fuel consumption	DG_1	"straight-line fuel curve" option in HOMER Intercept coefficient [L/hr/kWrated]: 0.0299 Slope [L/hr/kW]: 0.2325
	DG_2	"straight-line fuel curve" option in HOMER Intercept coefficient [L/hr/kWrated]: 0.0271 Slope [L/hr/kW]: 0.2334
Minimum load ratio [%]		30
Diesel fuel		
Carbon content [%]		88
Sulfur content [%]		0.4
Density [kg/m^3]		820

Appendix B: Rainflow Cycle Counting Algorithm [62]

The initial data are the consecutive values S_i ($1 \leq i \leq N$) which represents the peaks and valleys of the SOC profile.

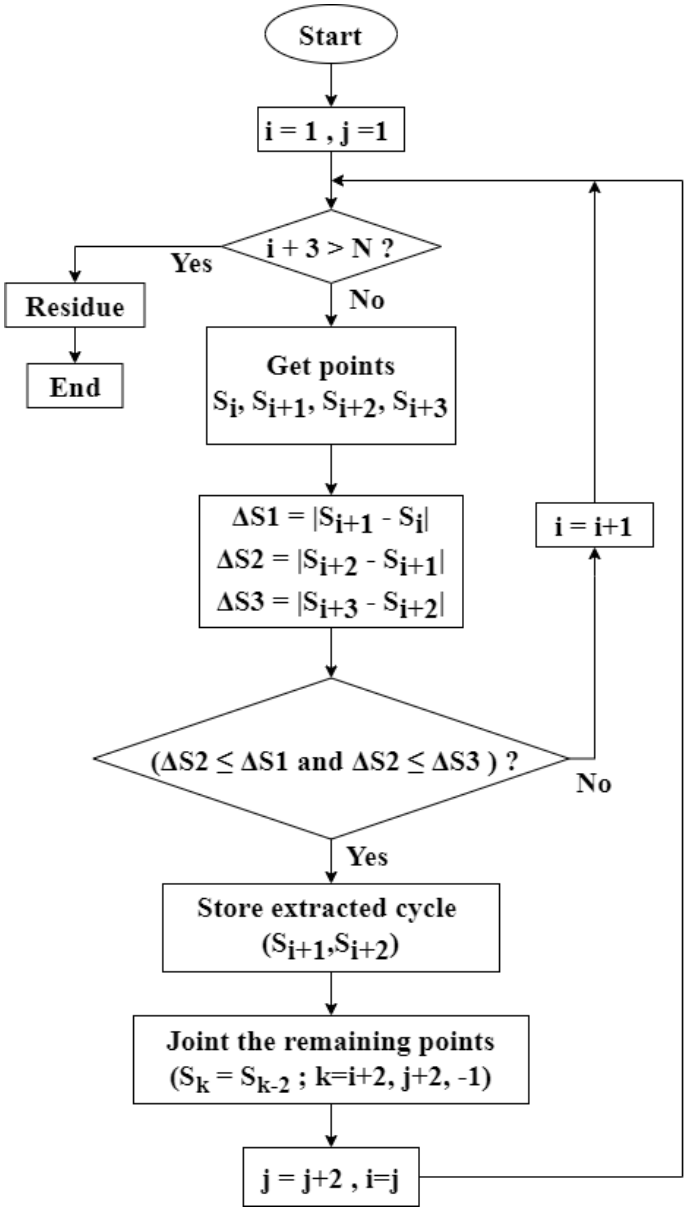

Once the full cycle extraction is completed the remainder of the profile is called the "Residue" and contains only charging and discharging half cycles. A half cycle links each pair of consecutive local extrema in the residue profile.

Appendix C: Demand Response Model Data

C.1 Roulette Wheel Selection Method

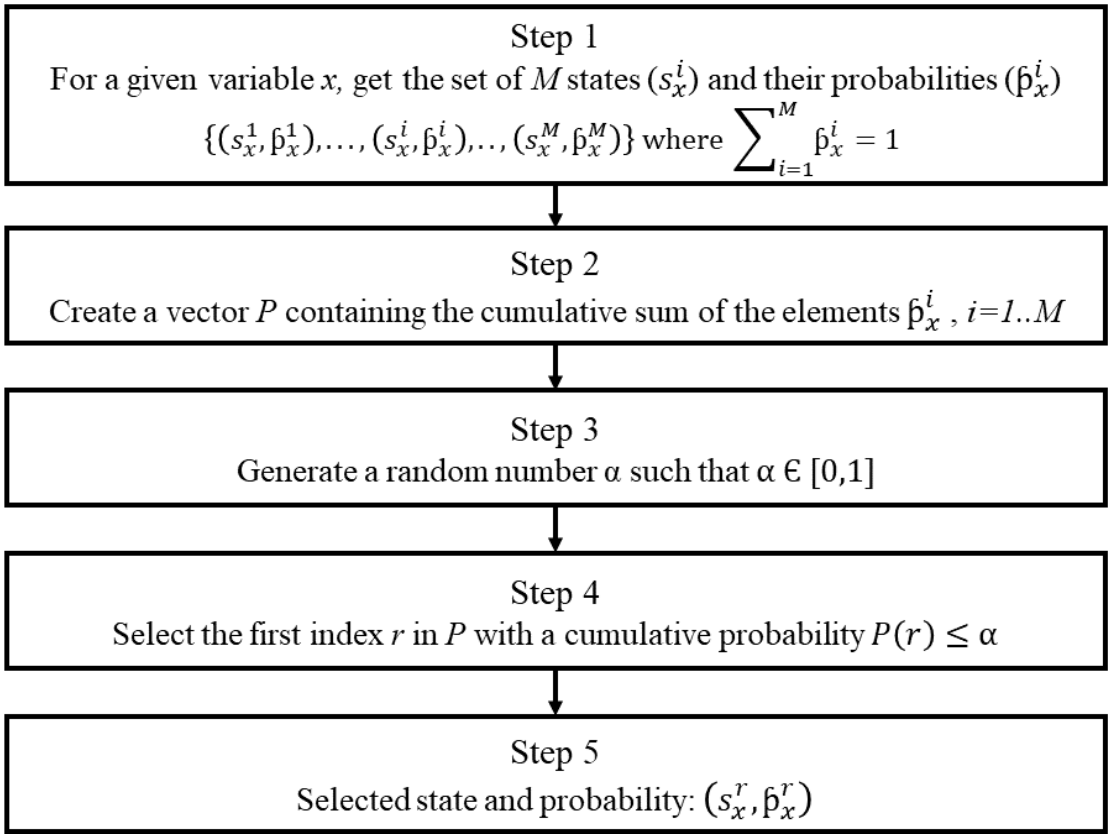

C.2 Scheduling Process of the LCS

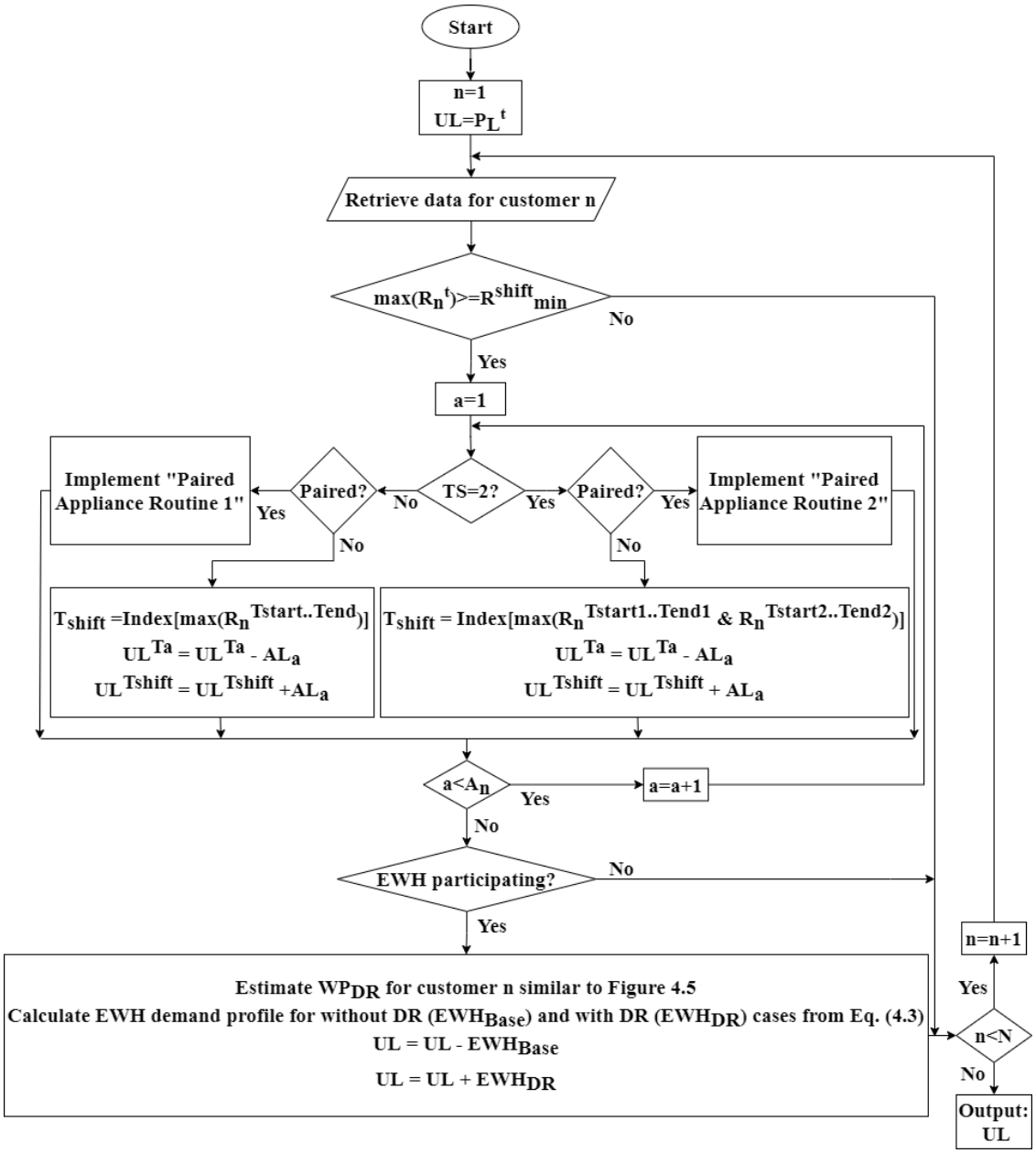

n = Customer ID, a = Load ID, t = Time-step
N = Total customers, A_n= Total shiftable loads of customer n
P_L^t = Forecasted daily load curve
R_n^t = Consumer responsiveness value, R^{shift}_{min}= minimum required responsiveness value
TS= Preferred number of utility-defined timeslots
Ta = Time-step without DR for appliance a, AL_a = Average load of appliance a
Tstart ..Tend = Start and stop time-steps for appliance with TS<2
Tstart1..Tend1 and Tstart2..Tend2 = Start and stop time-steps for appliance with TS=2
Tshift = Time-step with DR

Paired Appliance Routine 1

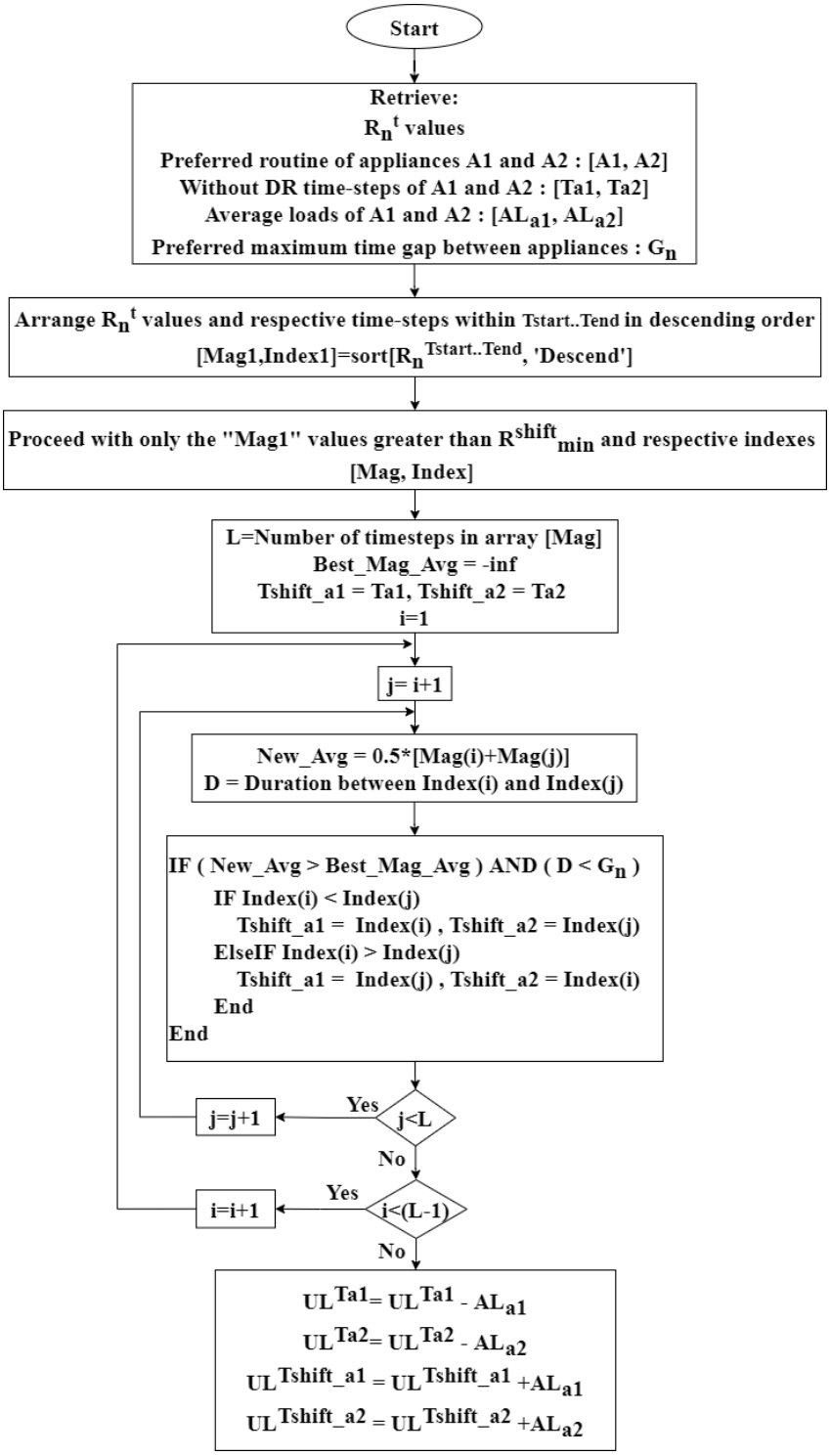

“Paired Appliance Routine 2” was also conducted similar to “Paired Appliance Routine 1” while considering each preferred timeslot of the customer to find the highest responsive time-steps.

C.3 Characterization of Membership Functions

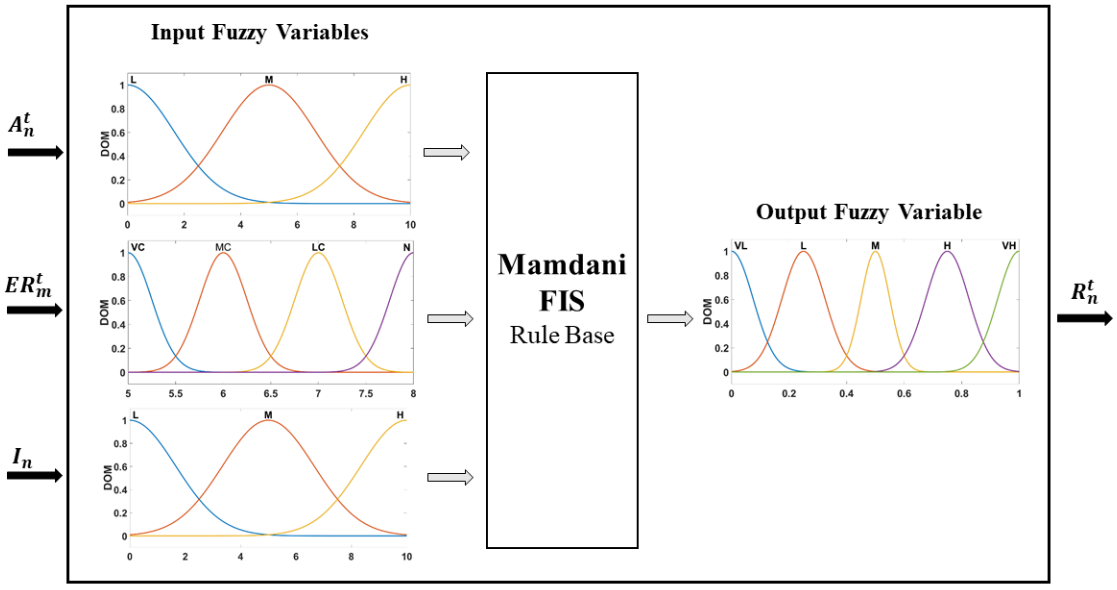

DOM: Degree of Membership

Linguistic interpretation of input and output membership functions is given in Table 4.1.

C.4 Rule Base used in the Probabilistic Fuzzy Inference System

Rule no	Input membership functions			Output membership function probabilities				
	Interest (I_n)	Price (ER_m^t)	Availability (A_n^t)	Customer responsiveness (R_n^t)				
				P_{VL}	P_L	P_M	P_H	P_{VH}
1	H	LC	H	0	0.05	0.8	0.15	0
2	H	LC	M	0.1	0.7	0.15	0.05	0
3	H	LC	L	0.8	0.15	0.05	0	0
4	H	MC	H	0	0	0.05	0.8	0.15
5	H	MC	M	0	0	0.15	0.8	0.05
6	H	MC	L	0.05	0.8	0.15	0	0
7	H	VC	H	0	0	0	0.1	0.9
8	H	VC	M	0	0	0.05	0.15	0.8
9	H	VC	L	0.05	0.75	0.15	0.05	0
10	-	N	-	0.95	0.05	0	0	0
11	M	LC	H	0.05	0.7	0.25	0	0
12	M	LC	M	0.05	0.75	0.2	0	0
13	M	LC	L	0.8	0.15	0.05	0	0
14	M	MC	H	0	0	0.15	0.8	0.05
15	M	MC	M	0	0.05	0.1	0.8	0.05
16	M	MC	L	0.15	0.7	0.15	0	0
17	M	VC	H	0	0	0.05	0.15	0.8
18	M	VC	M	0	0	0.15	0.8	0.05
19	M	VC	L	0.05	0.8	0.15	0	0
20	L	LC	H	0.15	0.8	0.05	0	0
21	L	LC	M	0.8	0.15	0.05	0	0
22	L	LC	L	0.9	0.1	0	0	0
23	L	MC	H	0.05	0.8	0.15	0	0
24	L	MC	M	0.15	0.8	0.05	0	0
25	L	MC	L	0.85	0.15	0	0	0
26	L	VC	H	0	0.05	0.8	0.15	0
27	L	VC	M	0.05	0.85	0.1	0	0
28	L	VC	L	0.15	0.75	0.1	0	0

P_x: Probability of output membership function *x*

For all the rules "AND" connective was used for the input membership functions.

Appendix D: Scenario Reduction Process [87]

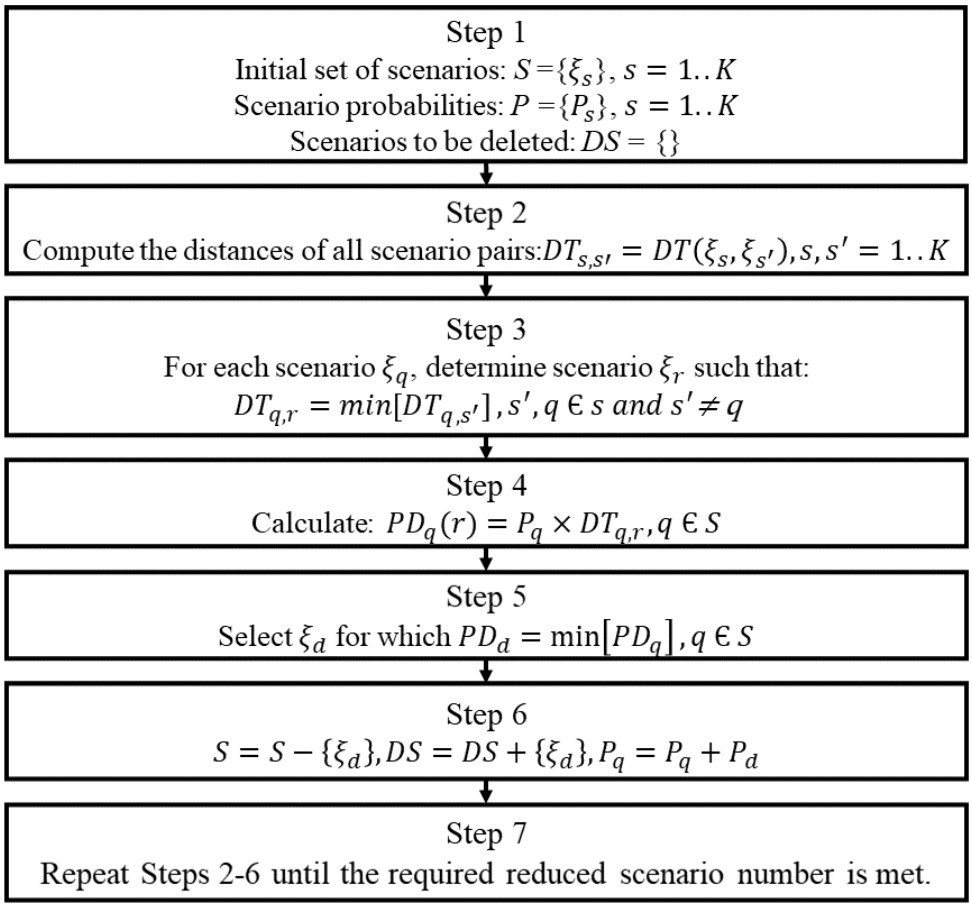

Appendix E: Model Data (referred to Figure 6.1)

Generator data (DG_1)		
Rating [kW]		400
Terminal voltage L-L rms [kV]		0.6
Inertia constant [s]		4.2
Droop [pu]		0.03
Renewable energy system data		
PV unit DC-DC converter rating [kW]		625
Battery unit DC-DC converter rating [kW]		± 600
VSC rating [kW]		± 600
DC link voltage [kV]		1
VSC filter data (LCL filter)	Grid side inductance [μH]	40
	Converter side inductance [μH]	100
	Capacitance [μF]	360
	Resistance [Ω]	0.1
Transformer data		
T_1	Rating [MVA]	2
	Winding voltages L-L rms [kV]	0.6 / 25
	Leakage reactance [pu]	0.1
T_2	Rating [MVA]	1
	Winding voltages L-L rms [kV]	0.48 / 25
	Leakage reactance [pu]	0.1

Transmission line data		
Single line section	Model	π-section
	Positive sequence resistance [Ω/m]	8.76×10^{-4}
	Positive sequence inductive reactance [Ω/m]	5.305×10^{-4}
	Positive sequence capacitive reactance [MΩ×m]	5.588×10^{2}
	Zero sequence resistance [Ω/m]	1.276×10^{-3}
	Zero sequence inductive reactance [Ω/m]	1.557×10^{-3}
	Zero sequence capacitive reactance [MΩ×m]	5.588×10^{2}
Line lengths [m]	TX_{12}	110
	TX_{23}	100
	TX_{24}	375
	TX_{25}	100
	TX_{46}	500
	TX_{47}	350
	TX_{78}	450
	TX_{79}	150